AFOSR-TR-97

REPORT DOCUMENTATION PAGE

0553

1. AGENCY USE ONLY (Leave blank)	2. REPORT DATE	3. REPORT TYPE AND DATES COVERED
		FINAL REPORT 01 Nov 93 - 30 Apr 97

4. TITLE AND SUBTITLE
Studies of Optical Wave Mixing and Phase Conjugation

5. FUNDING NUMBERS
61102F
2301/CS

6. AUTHOR(S)
Professor Yeh

7. PERFORMING ORGANIZATION NAME(S) AND ADDRESS(ES)
Department of Electrical and Computer Engineering
University of California, Santa Barbara
Santa Barbara, CA 93106

8. PERFORMING ORGANIZATION REPORT NUMBER

9. SPONSORING / MONITORING AGENCY NAME(S) AND ADDRESS(ES)
AFOSR/NE
110 Duncan Avenue Suite B115
Bolling AFB DC 20332-8050

10. SPONSORING / MONITORING AGENCY REPORT NUMBER
F49620-94-1-0002

11. SUPPLEMENTARY NOTES

19971103 092

12a. DISTRIBUTION / AVAILABILITY STATEMENT
APPROVED FOR PUBLIC RELEASE: DISTRIBUTION UNLIMITED

12b. DISTRIBUTION CODE

13. The main objective of this research is to carry out theoretical and experimental investigation on optical wave mixing and phase conjugation in various nonlinear media, including photorefractive crystals and optical fibers, as well as novel applications using these nonlinear optical effects. During the research period, we have carried out intensive theoretical and experimental investigation in several important areas in wave mixing and phase conjugation, including the problem of multigrating effects in MPPC, fanning noise reduction by using partially coherent beams, grating enhancement and restoration in photorefractive media, fidelity of image restoration in multimode fibers, reflection-based phase conjugators, cross-talk noise in volume holographic storage, optical phase conjugation and pulse restoration in single mode fibers, photorefractive spatial mode converter for multimode-to-single-mode fiber-optic coupling, energy coupling by partially degenerate four-wave mixing in multichannel lightwave systems, form birefringence of layered media and volume gratings, the effect of beam coherence on mutually pumped phase conjugators (MPPC), polarization-dependent mechanism transformation during self-pumped phase conjugation in Ce:BaTiO3, intensity-dependent absorption and photorefractive properties of some new crystals, including Rb:$KNbO_3$, and Ce:$BaTiO_3$.

14. **OF PAGES**

16. PRICE CODE

17. SECURITY CLASSIFICATION OF REPORT	18. SECURITY CLASSIFICATION OF THIS PAGE	19. SECURITY CLASSIFICATION OF ABSTRACT	20. LIMITATION OF ABSTRACT
UNCLASSIFIED	UNCLASSIFIED	UNCLASSIFIED	

NSN 7540-01-280-5500

Standard Form 298 (Rev. 2-89)
Prescribed by ANSI Std. 239-18

97CC6

Schlossberg

Studies of Optical Wave Mixing and Phase Conjugation

(Grant No. F49620-94-1-0002)

Final Technical Report
(01 Nov 93 to 30 Apr 97)

Prepared for:

Lori L. Chabricky/PKA
Air Force Office of Scientific Research
110 Duncan Avenue, Suite B115
Bolling AFB, Washington, DC 20332-8050

Prepared by:

Pochi Yeh, Principal Investigator
Electrical and Computer Engineering
University of California
Santa Barbara, CA 93106

September 1997

Table of Contents

1.0 Research Description

1.1 Scientific Problem

1.2 Scientific and Technical Approach

1.3 Publications

1.3.1 Papers Published

1.3.2 Conference Papers Presented

2.0 Progress

2.1 Progress Summary

2.2 Progress Details

3.0 Reprints of Selected Published Papers

1.0 Research Description

The main objective of this research is to carry out theoretical and experimental investigation on optical wave mixing and phase conjugation in various nonlinear media, including photorefractive crystals and optical fibers, as well as novel applications using these nonlinear optical effects. During the research period, we have carried out intensive theoretical and experimental investigation in several important areas in wave mixing and phase conjugation, including the problem of multigrating effects in MPPC, fanning noise reduction by using partially coherent beams, grating enhancement and restoration in photorefractive media, fidelity of image restoration in multimode fibers, reflection-based phase conjugators, cross-talk noise in volume holographic storage, optical phase conjugation and pulse restoration in single mode fibers, photorefractive spatial mode converter for multimode-to-single-mode fiber-optic coupling, energy coupling by partially degenerate four-wave mixing in multichannel lightwave systems, form birefringence of layered media and volume gratings, the effect of beam coherence on mutually pumped phase conjugators (MPPC), polarization-dependent mechanism transformation during self-pumped phase conjugation in Ce:BaTiO3, intensity-dependent absorption and photorefractive properties of some new crystals, including Rb:$KNbO_3$, and Ce:$BaTiO_3$.

1.1 Scientific Problem

The unique distortion correction property of optical phase conjugation continues to be extremely attractive in many advanced applications. These include frequency conversion and pulse restoration in fiber optical communication, wavefront correction in free space optical communication, high power lasers, optical image processing, etc. There are many approaches which can be employed to achieve optical phase conjugation. These include optical four-wave mixing, stimulated Brillouin scattering (SBS), self-pumped phase conjugation, etc. In nonlinear media such as photorefractive crystals and Kerr materials, it is possible to achieve mutually pumped phase conjugation (MPPC). Such phase conjugators are ideal for optical communications through scattering media such as atmosphere or sea water. MPPC can also be employed for the phase locking of an array of lasers. It is known that both SPPC and MPPC can involve several index gratings (reflection gratings, transmission gratings and 2k gratings) which may compete for charge carriers resulting in possible instability in the phase conjugation process. In addition, the coherence of the beams plays an important role in the strength of the gratings. In the area of fiber optical communication, it is desirable to have frequency conversion devices which can provide a frequency translation for the signal carrier in WDM systems. Using optical four-wave mixing it is possible to achieve the frequency translation in optical fibers via the Kerr

effect. An important issue is the energy efficiency and the response time of the system (latency). Using optical four-wave mixing, it is also possible to achieve forward phase conjugation which can be utilized for pulse restoration in high speed optical communication system.

1.2 Scientific and Technical Approach:

Mutually-pumped phase conjugation (MPPC) is a nonlinear optical process in which two incoherent laser beams mutually pump each other and generate two phase conjugate beams simultaneously. Most theoretical models for MPPC consider only transmission gratings. In practice, when the laser beams become coherent (e.g. laser phase-locking) or the nonlinear material has fast response time (e.g. Kerr media), the formation of reflection gratings and/or 2k gratings is inevitable. Although there have been several models for MPPC, the effect of reflection and 2k gratings in MPPC has never been investigated. In an effort to understand the dynamic competition between transmission gratings, reflection gratings and 2k gratings, we theoretically investigated the coupling between all the waves by using a set of multi-wave coupled-wave equations. To vary the strength of reflection gratings and 2k gratings, we used a laser with a finite coherence length. By varying the path difference, it is possible to control the mutual coherence between the coupled beams. Experimental investigations using $BaTiO_3$ crystals have also been carried out to validate our theory. In our investigation into the possibility of optical pulse restoration using phase conjugation, we theoretically analyze the coupling between optical waves in an optical fiber via the Kerr effect. By solving the coupled wave equations, we obtained an exact solution for the intensity of all the four waves involved. The solution is useful to provide the energy conversion efficiency as well as the phase conjugation efficiency.

Optical four-wave mixing in nonlinear media such as optical fibers can be employed canbe employed for the compression of optical pulses as well as the restoration of pulse shape due to group velocity dispersion. Holograms and gratings are responsible for wave mixing and phase conjugation in nonlinear media, including photorefractive crystals. The strength of these holograms and gratings depends on the coherence of the writing beams. In SPPC and MPPC, the writing beams may depend on the crystal orientation and the interaction configuration. During this period, we have investigated theoretically and experimentally various models of SPPC in Ce:BaTiO3 crystals. To investigate the effect of 2k-gratings, we used an erasing beam to weaken the 2k-gratings in SPPC. The specific model for SPPC also depends on the fanning pattern. By using various polarization states, we are able to vary the fanning patterns leading to different models of operation. We also investigate the dispersion of form birefringence due to layered structures.

1.3 Publications:

1.3.1 Papers Published:

283. R. F. Nabiev, P. Yeh, and D. Botez, "Spatial gap solitons in periodic nonlinear structures," Opt. Lett., 18, 1612-1614 (1993).

284. S. M. Zhou, Q. B. He, P. Yeh, and H.-K. Liu, "Spatial fidelity in photorefractive image amplification," Opt. Comm, 99, 18-24 (1993).

285. Q. B. He, P. Yeh, L. J. Hu, S. P. Lin, T. S. Yeh, S. L. Tu, S. J. Yang, "Shift-invariant photorefractive joint-transform correlator using Fe:$LiNbO_3$ crystal plates," Appl. Opt., 32, 3113-3115 (1993).

293. Y. Zhu, D. P. Zhang, P. Yeh, and C. Gu, "High Efficiency Photorefractive $BaTiO_3$ Plate for Optical Image Processing," Chinese Science Bulletin, 38, 1424-1427 (1993).

298. Q. B. He and P. Yeh, "Fanning noise reduction in photorefractive amplifiers using incoherent erasures," Appl. Opt., 33, 283-287 (1994).

304. C. Gu and P. Yeh, "Partial Phase Conjugation, Fidelity, and Reciprocity," Opt. Commun., 107, 353-357 (1994).

310. Y. Zhang, S. Campbell, P. Yeh, D. Shen, X. Ma and J. Chen, "Submillisecond photorefractive response time of $KNbO_3:Rb^+$," Opt. Lett., 19, 1397-1399 (1994).

311. X. Yi, P Yeh and C. Gu, "Statistical analysis of cross-talk noise and storage capacity in volume holographic memory," Opt. Lett., 19, 1580-1582 (1994).

314. P. Yeh and A. Chiou, "Optical Phase Conjugation for Interconnection and Image Processing," Chapter 12 of Real-Time Optical Information Processing, Ed. B. Javidi, p. 475-531 (Academic Press, Inc., 1994).

315. Q. B. He, S. Campbell, P. Yeh, X. Y. Ma and D. Shen, "Compact Reflection-grating-based phase conjugator in Fe: $KNbO_3$ crystals," Appl. Opt. 33, 4320-4322 (1994).

318. Q. B. He, H. K. Liu and P. Yeh, "Asymmetric Photorefractive Fabry-Perot Etalons," Appl. Phys. B-Lasers and Optics, 59, 467-470 (1994).

319. W. Wu, P. Yeh and S. Chi, "Phase Conjugation by Four-Wave Mixing in Single-Mode Fibers," Photonics Tech. Lett., 6, 1448-1450 (1994).

324. P. Yeh and C. Gu, "Photorefractive Nonlinear Optics and Applications," Series in Nonlinear Optics and Optical Physics, Vol.2, Chapter 12, 341-388 (1994).

328. C. Yang, Y. Zhang, P. Yeh, Y. Zhu and X. Wu, "Photorefractive properties of Ce:$BaTiO_3$ crystals, " Opt. Comm., 113, 416-420 (1995).

329. S. Campbell, P. Yeh, C. Gu and Q. B. He, "Fidelity of image restoration by partial phase conjugation through multimode fibers, " Opt. Comm., 114, 50-56 (1995).

330. Q. B. He and P. Yeh, "Photorefractive mutually pumped phase conjugation with partially coherent beams," Appl. Phys. B 60, 47-50 (1995).

334. S. Campbell, P. Yeh, C. Gu, S. H. Lin, C-J Cheng, and K. Y Hsu, "Optical Restoration Of Photorefractive Holograms Through Self-Enhanced Diffraction," Opt. Lett., 20, 330-332 (1995).

336. X. Yi, S. Campbell, P. Yeh, and C. Gu, "Statistical Analysis Of Cross-Talk Noise And Storage Capacity In Volume Holographic Memory - Image Plane Holograms," Opt. Lett., 20 779-781 (1995).

338. A. E. T. Chiou, P. Yeh, C. Yang and C. Gu, "Photorefractive spatial mode converter for multimode-to-single-mode fiber-optic coupling," Opt. Lett., 20, 1125-1127 (1995).

341. W. Wu and P. Yeh, " Energy Coupling By Partially Degenerate Four-Wave Mixing In Multichannel Lightwave Systems," IEEE Photonics Technology Letters, Vol. 7, 585-587 (1995).

346. A. Chiou, P. Yeh, C. Yang, C. Gu, "Photorefractive coupler for fault-tolerant coupling," IEEE Photonics Tech. Lett., 7, 789-791 (1995).

348. C. Gu and P. Yeh, "Form birefringence of layered media and volume gratings," J. Opt. Soc. Am., B, 12, 1094-1099 (1995).

351. Y. Lian, S. Lin, S. Campbell, K. Y Hsu, et al, "Polarization-Dependent Mechanism Transformation During Self-Pumped Phase Conjugation In Ce:BaTiO3," Optics Lett. 20, 1683-1685 (1995).

352. P. Yeh, C. Gu, C-J. Cheng, K. Y Hsu, "Hologram Enhancement In Photorefractive Media," Optical Engineering, 34, 2204-2212 (1995).

357. S.C. Delacruz, S. Marcorma, J. Feinberg, Q. B. He, H. K. Liu, and P. Yeh, "Effect of Beam Coherence on Mutually Pumped Phase Conjugators," J. Opt. Soc. Am., B12, 1363-1369 (1995).

358. X. Yi, P. Yeh, and C. Gu,"Cross-Talk Noise In Volume Holographic Memory With Spherical Reference Beams," Optics Lett., 20, 1812-1814 (1995).

359. C. Yang, Y. H. Zhang, X. Yi X, P. Yeh, et al, "Intensity-Dependent Absorption and Photorefractive Properties in Cerium-Doped Batio3 Crystals," Journal Of Applied Physics, 78, 4323-4330 (1995).

361. P. Yeh, C. Gu, C. J. Cheng and K. Y. Hsu, "Optical Restoration of Photorefractive Holograms," Applied Physics B-Lasers and Optics, 61 ,511-514 (1995).

366. C. Gu and P. Yeh,"Form birefringence dispersion in periodic layered media," Opt. Lett., 21, 504-506 (1996).

380. X. Yi, S. H. Lin, P. Yeh and K. Y. Hsu, "Contradirectional Two-Wave Mixing With Partially Coherent Waves In Photorefractive Crystals," Opt. Lett., Vol. 21 No. 15, 1123-1125 (Aug 1, 1996).

381. S. H. Lin, Y. Lian, P. Yeh, K. Y. Hsu et al, "2k-Grating-Assisted Self-Pumped Phase Conjugation - Theoretical And Experimental Studies," J. Opt. Soc. Am. B-Optical Physics, Vol. 13, No. 8, 1772-1779, (Aug 1996).

395. C. Yang and P. Yeh, "Form Birefringence Of Volume Gratings In Photopolymers," Applied Physics Letters, V69 N23:3468-3470 (Dec. 2, 1996)

398. C. Yang and P. Yeh, "Artificial Uniaxial And Biaxial Dielectrics With The Use Of Gratings," J. Appl. Phys., V81 N1:23-29 (Jan. 1997).

1.3.2 Conference Papers:

264. R. F. Nabiev, P. Yeh and D. Botez, "Spatial gap soliton in periodic nonlinear structures," in Integrated Photonics Research Conference Technical Digest, 1993 (Optical Society of America, Washington, DC, 1993), Vol. 10, pp. 312-315.

271. Q. B. He, P. Yeh, X. Ma and D. Shen, "Compact self-pumped phase conjugator in photorefractive Fe:$KNbO_3$," Conference on Lasers and Electro-Optics, 1993 Vol. 11, OSA Technical Digest Series (Optical Society of America, Washington, DC 1993), pp. 526-527.

272. A. Chiou, P. Yeh, and C. Gu, "Spatial mode conversion in photorefractive fibers," in OSA Annual Meeting Technical Digest, 1993 (Optical Society of America, Washington, DC 1993), Vol. 16, p. 7.

278. Q. He, X. Yi, P. Yeh, S. Chi, "Optical pulse compression by means of a single mode fiber and phase conjugation," in OSA Annual Meeting Technical Digest, 1993 (Optical Society of America, Washington, DC 1993), Vol. 16, p. 182.

290. A. Chiou, P. Yeh, C. Gu, and R. Neurgaonkar, "Beam Coupling and Spatial Mode Conversion in Photorefractive Planar Waveguide," Conference Proceedings of IEEE/LEOS Annual Meeting, 319-320 (San Jose, California, 1993).

299. S. Campbell, P. Yeh, Q. B. He, and C. Gu, "Studies of image fidelity during partial phase conjugation," Conference on Lasers and Electro-Optics, Vol. 8, 1994 OSA Technical Digest Series (Optical Society of America, Washington, DC 1994), pp. 12-13.

300. S. Campbell, P. Yeh, and Daofan Zhang, "Photorefractive and thermal fixing properties of 4 mol%-doped lithium niobate," Conference on Lasers and Electro-Optics, Vol. 8, 1994 OSA Technical Digest Series (Optical Society of America, Washington, DC 1994), p. 80.

301. Q. B. He, H.-K. Liu and P. Yeh, "Reflection gratings in the photorefractive mutually pumped phase conjugators," Conference on Lasers and Electro-Optics, Vol. 8, 1994 OSA Technical Digest Series (Optical Society of America, Washington, DC 1994), p. 97.

305. Y. Zhang, S. Campbell, P. Yeh; D. Shen, X. Ma, J. Chen, "Grating response time of photorefractive $KNbO_3:Rb^+$," Proc. 1994 IEEE Conference on Nonlinear Optics, Materials, Fundamentals, and Applications (Waikoloa, Hawaii, July 25-29, 1994), pp. 284-286.

306. W. Wu, P. Yeh, S. Chi, "Frequency conversion by four-wave mixing in single-mode fibers," Proc. 1994 IEEE Conference on Nonlinear Optics, Materials, Fundamentals, and Applications (Waikoloa, Hawaii, July 25-29, 1994), pp. 332-334.

307. P. Yeh, C. Gu, C.-J. Cheng, K. Y. Hsu, "Hologram restoration and enhancement in photorefractive media," (Invited Paper) Proc. 1994 IEEE Conference on Nonlinear Optics, Materials, Fundamentals, and Applications (Waikoloa, Hawaii, July 25-29, 1994), pp. 421-423.

308. S. Campbell, P. Yeh, C. Gu, S. H. Lin, C. -J. Cheng, K. Y. Hsu, "Optical self-enhancement of photorefractive holograms," Proc. 1994 IEEE Conference on Nonlinear Optics, Materials, Fundamentals, and Applications (Waikoloa, Hawaii, July 25-29, 1994), pp. 430-432.

309. X. Yi, P. Yeh, C. Gu, "Cross-talk noise and storage density in holographic memory," Proc. 1994 IEEE Conference on Nonlinear Optics, Materials, Fundamentals, and Applications (Waikoloa, Hawaii, July 25-29, 1994), pp. 436-438.

312. C. Yang, Y. Zhang, P. Yeh and Y. Zhu, "Photorefractive Properties of Ce:BaTiO3," paper MSS3, Annual Meeting of the Optical Society of America (Dallas TX, October 2-7, 1994).

313. P. Yeh, C. Yang, C. Gu and A. Chiou, "Photorefractive Resonators for Fault-Tolerant Coupling," paper ThC3, Annual Meeting of the Optical Society of America (Dallas TX, October 2-7, 1994).

314. P. Yeh and A. Chiou, "Optical Phase Conjugation for Interconnection and Image Processing," Chapter 12 of Real-Time Optical Information Processing, Ed. B. Javidi, p. 475-531 (Academic Press, Inc., 1994).

325. P. Yeh, "Photorefractive Phase Conjugators and Applications," (Invited Paper) The 55th Autumn Meeting of the Japan Society of Applied Physics, September 19-22, Nagoya, Japan (1994), pp. 1181.

331. S. Campbell, Y. Zhang, and P. Yeh, "Material Limitations in Volume Holographic Copying," in Optical Computing, Vol 10, 1995, OSA Technical Digest Series (Optical Society of America, Washington DC, 1995), pp. 77-79.

333. S. Campbell, X. Yi, and P. Yeh, "Sparse-Wavelength Angularly Multiplexed Volume Holographic Memory," in Optical Computing, Vol 10, 1995, OSA Technical Digest Series (Optical Society of America, Washington DC, 1995), pp. 225-227.

339. W. Wu and P. Yeh, "Power coupling by four-wave mixing in single mode fibers," Conference on Lasers and Electro-Optics, Vol. 15, 1995 OSA Technical Digest Series (Optical Society of America, Washington, DC., 1995). pp. 111.

340. S-H. Shin, S. Campbell and P. Yeh, "Photorefractive properties of magnesium-oxide-doped lithium niobate at elevated temperatures," Conference on Lasers and Electro-Optics, Vol. 15, 1995 OSA Technical Digest Series (Optical Society of America, Washington, DC., 1995). pp. 384.

343. S. Campbell, P. Yeh, "Absorption effects in photorefractive volume holographic memory," Technical Digest, Photorefractive Materials, Effects, and Devices, Aspen,

Colorado, June 11-14 (Optical Society of America, Washington, DC 1995) pp. 128-131.

344. A. Chiou, P. Yeh, C. Yang, and C. Gu, "Multimode to singlemode fiber-optic coupling using mutually-pumped phase conjugation," Technical Digest, Photorefractive Materials, Effects, and Devices, Aspen, Colorado, June 11-14 (Optical Society of America, Washington, DC 1995) pp. 439-442.

347. S. Campbell, S.-H Lin, X. Yi and P. Yeh, " Photorefractive volume holographic memory systems: approaches, limitations, and requirements," (Invited Paper) Conference on Photorefractive Fiber and Crystal Devices: Materials, Optical Properties, and Applications, Proc. SPIE - Vol.2529, 134-144, San Diego, CA, USA, July 12-13 (1995).

349. S.-H. Lin, P. Yeh, M.-L. Shieh, K. Y. Hsu, and T.-C. Hsieh, "Optimum conditions for high-fidelity holographic storage in photorefractive crystals," (Invited Paper) Conference on Photorefractive Fiber and Crystal Devices: Materials, Optical Properties, and Applications, Proc. SPIE - Vol.2529, 145-156, San Diego, CA, USA, July 12-13 (1995).

350. P. Yeh, "Recent Advances on Photorefractive Nonlinear Optics and Applications," International Conference on Optical Physics and Applications, (Harbin, China, July 17-21, 1995)

353. C. Gu and P. Yeh, "Dispersion of form birefringence in periodic media," Paper ThHH2, Annual Meeting of the Optical Society of America (Portland OR, September 10-15, 1995), p. 153.

354. Y. Lian, S. H. Lin, S. Campbell, K. Y. Hsu, P. Yeh, "Polarization dependent mechanism transformation in $BaTiO_3$:Ce self-pumped phase conjugators," Paper ThDDD2, Annual Meeting of the Optical Society of America (Portland OR, September 10-15, 1995), p. 170.

355. C. Yang, S. H. Lin, Y. Zhang, P. Yeh, and Y. Zhu, "Dark decay of photorefractive gratings in Ce-doped and undoped $BaTiO_3$, Paper ThWW1, Annual Meeting of the Optical Society of America (Portland OR, September 10-15, 1995), p. 164.

356. C. Yang, S. H. Lin, P. Yeh, and Y. Zhu, "Image resolution and phase conjugation coupling in photorefractive Ce:$BaTiO_3$," Paper ThDDD3, Annual Meeting of the Optical Society of America (Portland OR, September 10-15, 1995), p. 170.

363. P. Yeh, "Hybrid Volume Holographic Memory in Photorefractive Media," (Invited Paper), LEOS'95, Paper NLO10.2, IEEE Laser and Electro-Optics Society Annual Meeting, San Francisco, CA (1995).

364. P. Yeh, "Photorefractive Nonlinear Optics and Neural Networks," The Cecil Conference and Seminar Series on Optical Computing and Neural Networks, (Gothenburg, Sweden, November 13-15, 1995).

370. X. Yi, C. Yang, S. H. Lin, P. Yeh, and C. Gu, "Cross-Talk Noise and Storage Density of Volume Holographic Memory with Spectral Hole Burning Materials," International

Topical Meeting on Optical Computing, Paper OWC18 (Sendai, Japan, 1996).

372. P. Yeh, "Reviving Dying Holograms," International Symposium on Holographic Memories, (Athens, Greece, May 12-14, 1996).

373. P. Yeh, "Photorefractive Nonlinear Optics and Applications," Taipei International Symposium on Recent Development of New Technologies, (Taipei, Taiwan, June 2-5, 1996).

374. X. Yi, S.-H Lin, P. Yeh, and K. Hsu, "Contradirectional two-wave mixing with partially coherent waves in photorefractive crystals, " Technical Digest of CLEO'96 (1996), p. 116-117.

375. P. Yeh and X. Yi, "Cross-talk noise in volume holographic memory," Annual Meeting of The International Society of Optical Engineering, SPIE, Paper No. 2849-11, (Denver, August 5-9, 1996).

376. W. Wu and P. Yeh, "Multiwavelength optical computing using optical wave mixing in photorefractive media, " Nonlinear Optics Topical Meeting, NLO'96, Paper NTuA1, (July 8-12, 1996).

378. X. Yi, C. Yang, S. Lin, P. Yeh, "Spectral-hole-and-angle multiplexed volume holographic memory," Nonlinear Optics Topical Meeting, NLO'96, JTuC5, (July 8-12, 1996).

379. X. Yi, C. Yang, P. Yeh, "Two-wave mixing with partially coherent waves in photorefractive crystals," Nonlinear Optics Topical Meeting, NLO'96, NThA2, (July 8-12, 1996).

386. X. Yi, S.-H. Lin, and P. Yeh, "General solution of contradirectional two-wave mixing with partially coherent waves in photorefractive crystals," 1996 OSA Annual Meeting (Rochester, NY, October 21-25, 1996).

387. X. Yi and P. Yeh, "Co-directional two-wave mixing with partially coherent waves in photorefractive crystals," 1996 OSA Annual Meeting (Rochester, NY, October 21-25, 1996).

388. J-N. Duan, T. Kojima, Y. Sun and P. Yeh, "Dispersion properties of photorefractive gratings," 1996 OSA Annual Meeting (Rochester, NY, October 21-25, 1996)

389. X. Yi, Y. Lian, and P. Yeh, "Diffraction of partially coherent light from fixed 2k-gratings in photorefractive media," 1996 OSA Annual Meeting (Rochester, NY, October 21-25, 1996).

390. Y. Lian, M. Zhao and P. Yeh, "Effect of 2k-gratings in photorefractive phase conjugators," 1996 OSA Annual Meeting (Rochester, NY, October 21-25, 1996).

2.0 Progress:

2.1 Progress Summary:

The following is a list of significant progresses we have made during this period under the support of this program:

- Photorefractive MPPC with partially coherent beams
- Fanning noise reduction in photorefractive amplifiers using incoherent erasures
- Compact Reflection-grating-based phase conjugator in Fe: $KNbO_3$ crystals
- Asymmetric Photorefractive Fabry-Perot Etalons
- Submillisecond photorefractive response time of $KNbO_3:Rb^+$
- Statistical analysis of cross-talk noise and storage capacity in volume holographic memory -both image plane and Fourier plane
- Photorefractive Properties of $Ce:BaTiO_3$
- Phase Conjugation by Four-Wave Mixing in Single-Mode Fibers
- Image restoration by partial phase conjugation through multimode fibers
- Partially Degenerate Four-Wave Mixing in Single-Mode Fibers
- Form birefringence in layered media
- Polarization-Dependent Mechanism Transformation During Self-Pumped Phase Conjugation In Ce:BaTiO3
- Hologram Enhancement and restoration In Photorefractive Media
- Effect of Beam Coherence on Mutually Pumped Phase Conjugators
- Cross-Talk Noise In Volume Holographic Memory With Spherical Reference Beams
- Intensity-Dependent Absorption and Photorefractive Properties in Cerium-Doped Batio3 Crystals
- Form birefringence dispersion in periodic layered media

2.2 Progress details:

Since most of the details of research results have been reported earlier in the annual reports, we only describe the details of the research results during the period between the last annual report and the final report. Detail discussion on some of the important research results for the whole period can be found in Section 3 which contains reprints of these papers.

Self-focusing effects in periodic leaky-wave coupled (antiguided) and evanescent-wave coupled array structures are analyzed for what is to our knowledge the first time. The results obtained can be explained in terms of spatial gap solitons. For infinite-extent arrays of antiguides

it is found that (for interelement-spacing values), below the inphase-mode resonance, self-focusing occurs with increasing light intensity even when the medium is intrinsically self-defocusing (i.e., negative nonlinearity). If the medium has positive nonlinearity the analysis shows that antiguided arrays possess either self-focusing or self-defocusing properties depending on the parameters of the structure, whereas evanescent-wave in-phase coupled arrays always have self-focusing properties. (Opt. Lett., 18, 1612-1614 (1993))

The spatial fidelity of amplified images in photorefractive materials due to spatial gain variations with computation and experiment based on $BaTiO_3$ is investigated. The results indicate how the spatial fidelity of the amplified images decreases as the relative aperture of the Fourier transform lens used in the system increases, and varies with the angle between the pump beam and the axis of the signal converging wave. (Opt. Comm, 99, 18-24 (1993))

The authors report the results of their experimental investigation on a shift-invariant photorefractive image correlator that uses a thin crystal plate of Fe:LiNbO/sub 3/, which operates in the Raman-Nath regime of diffraction. (Appl. Opt., 32, 3113-3115 (1993))

We propose and demonstrate a new scheme of beam fanning reduction in photorefractive amplifiers by using incoherent erasure. This simple and effective approach employs a pump beam with a mixed polarization state or introduces a third incoherent beam for selective erasure. The approach is analyzed, and the experimental results are presented and discussed. (Appl. Opt., 33, 283-287 (1994))

The fidelity of partially phase conjugated images is considered taking into account the finite aperture of phase conjugate mirrors. The analysis is based on the conservation of energy and the reciprocity theorems. In the absence of absorption, the conservation of energy leads to a simple relationship between the image-to-background ratio (I/B) and the aperture of the phase conjugator. In the presence of absorption, the reciprocity theorem leads to an expression of the image-to-background ratio (I/B) that depends on the fraction of power intercepted by the phase conjugator. The results are presented and discussed. (Opt. Commun., 107, 353-357 (1994))

We investigate the photorefractive response time of diffraction gratings in Rb/sup +/- doped KNbO/sub 3/ crystals. Two components of charge carriers, with different response times, are found to contribute to the photoinduced index gratings. One component, which contributes to approximately 70% of the index grating, shows a submillisecond rise time when the total intensity of the writing beams is larger than 5 W/cm/sup2/. The dependence of the response time

on the light intensity and the grating wave vector is also investigated. (Opt. Lett., 19, 1397-1399 (1994))

We present a statistical analysis of cross-talk noise and consider the cross-talk-limited storage capacity of volume holographic memory. Random-walk approximation is employed to estimate the intrapage interpixel cross-talk noise and the signal-to-noise ratio. We obtain simple expressions of the storage capacity in terms of number of bits per volume for a given signal-to-noise ratio or bit-error rate. The results indicate that the storage density is reduced from the ultimate density of lambda/sup -3/ by a factor related to the signal-to-noise ratio. (Opt. Lett., 19, 1580-1582 (1994))

A brief review of phase conjugators that use photorefractive materials as the nonlinear media is presented. An introduction to phase conjugation is followed by a description of the photorefractive effect and wave mixing in these media. Various applications using photorefractive phase conjugators, especially optical interconnection and real-time imaging processing are discussed. (Chapter 12 of Real-Time Optical Information Processing, Ed. B. Javidi, p. 475-531 (Academic Press, Inc., 1994))

We present the design and the results of experimental investigations of a self-pumped phase conjugator through a reflection grating in a special-cut photorefractive KNbO3:Fe crystal. High reflectivity, good phase-conjugate fidelity, and fast response time are obtained. (Appl. Opt. 33, 4320-4322 (1994))

We theoretically analyze the properties of Fabry-Perot etalons which consist of photorefractive-crystal plates with asymmetric mirror reflectance. Peak transmissions and non-reciprocities are enhanced significantly compared with the symmetric photorefractive etalons. The effect of material absorption is also considered. (Appl. Phys. B-Lasers and Optics, 59, 467-470 (1994))

We present an exact solution to the coupled-mode equations, governing four-wave mixing in single-mode fibers, under the perfect phase-matching condition. The solution accounts for pump depletion and fiber absorption. Optimum length of fiber is derived and phase conjugation efficiency is calculated and discussed. The calculated results are in good agreement with the reported experimental results. (Photonics Tech. Lett., 6, 1448-1450 (1994))

We investigate the absorption and photorefractive properties of Ce:BaTiO3 (cerium doped

barium titanate) crystals. The absorption coefficient, electro-optic gain coefficient, and total effective trap density at wavelength 514.5 nm increase systematically with cerium doping concentration. The absorption and the electro-optic gain coefficients exhibit a dependence on the optical intensity. This indicates that there are at least two active photorefractive species. One of these crystals has the highest beam-coupling gain coefficient reported to date, gamma =8.06 cm^{-1} for ordinarily polarized light. The response time of as-grown Ce:$BaTiO_3$ with 15 ppm cerium is 220 ms at an intensity of 800 mW/cm^2. (Opt. Comm., 113, 416-420 (1995)).

We investigate the fidelity of image restoration under conditions of partial phase conjugation through a random medium. For the first time, the conjugated image-to-background ratio is experimentally measured as an evaluation of the phase conjugate mirror's fidelity. Output signal-to-noise ratio and information throughput are also considered as functions of aperture limitations at the various planes of the optical system. (Opt. Comm., 114, 50-56 (1995))

We investigate the mutually pumped phase-conjugation process in photorefractive media with partially coherent pump beams. We consider the effects of transmission, reflection, and 2k-reflection gratings as well as the depletion of both pump beams. The theoretical results can be employed to qualitatively explain the experimental observations. (Appl. Phys. B 60, 47-50 (1995))

For the first time to our knowledge, we demonstrate the use of self-enhanced diffraction to optically restore weak dynamic volume holograms. This restoration process is achieved through the use of a novel beam-toggling scheme that significantly enhances the steady-state diffraction efficiency of volume index gratings stored in photorefractive media. Experiments demonstrating and confirming theory are presented and discussed. (Opt. Lett., 20, 330-332 (1995))

We investigate the cross-talk noise in optical storage based on angle-multiplexed image plane volume holograms. Simple expressions for the signal-to-noise ratio and the storage density are obtained. The cross-talk noise is found to limit the size of the pixels and the number of recorded holograms. The cross-talk-limited storage density of image plane holographic storage is found to be close to that of Fourier plane holographic storage. (Opt. Lett., 20 779-781 (1995))

We report what is to our knowledge the first experimental demonstration of a photorefractive spatial mode converter (based on mutually pumped phase conjugation) that couples light efficiently from a multimode fiber into a single-mode fiber with an extremely large

degree of tolerance to misalignment. Using an argon laser (514.5 nm) and a barium titanate crystal, we have demonstrated that the laser light can be coupled from a multimode fiber (core diameter 100 mu m, numerical aperture 0.37) into a single-mode fiber (core diameter 2.9 mu m, numerical aperture 0.11), with an efficiency of approximately 15% and an alignment tolerance of approximately 100 mu m. The coupling efficiency is more than two orders of magnitude, and the tolerance to misalignments is more than 30 times better than the corresponding values achievable by conventional techniques. (Opt. Lett., 20, 1125-1127 (1995))

We investigate the energy coupling among different frequency carriers by partially degenerate four-wave mixing in single-mode fibers. We show that for a multichannel lightwave system operated near the zero-dispersion frequency of the single-mode fiber, four-wave mixing may cause significant signal depletion in a channel whose power acts as a pump in the four-wave mixing process. Analytical solutions are derived and the signal depletion due to four-wave mixing is obtained. (IEEE Photonics Technology Letters, Vol. 7, 585-587 (1995))

We report the first experimental demonstration of a fault-tolerant laser-to-fiber coupler that is insensitive to both angular and lateral misalignments. Fault-tolerance is achieved by sending a laser beam into a photorefractive crystal that automatically senses and tracks the location of the fiber facet, and diffracts the input beam (via self-generated adaptive dynamic holograms) into the fiber. Using an argon laser (514.5 nm), a barium titanate crystal, and a multimode fiber (core diameter=400 um m, NA=0.16), we have achieved a coupling efficiency of 58% and a tolerance of more than 0.5 mm of lateral misalignment. Techniques to improve the coupling efficiency and the degree of fault tolerance, and to extend this method for the coupling of a laser diode output into a single-mode fiber are discussed. (IEEE Photonics Tech. Lett., 7, 789-791 (1995))

We analyze the form birefringence dispersion of periodic dielectric layered media. We investigate the shape of the normal surface and its dependence on wavelength. Approximation gives an explicit expression for the additional dispersion of the form birefringence that is due to the finite layer thickness. (J. Opt. Soc. Am., B, 12, 1094-1099 (1995))

We report the results of experimental investigations of the mechanism transformation from four-wave mixing and stimulated photorefractive backscattering to four-wave mixing and total internal reflection during self-pumped phase conjugation in a photorefractive crystal by varying the plane of polarization of the input beam. The use of a mixed-polarization input beam can change the fanning pattern, which leads to the mechanism transformation and an

enhancement of the phase-conjugation reflectivity. The temporal dynamics of the buildup process indicate that such an enhancement is due to the presence of both types of mechanism during phase conjugation. In addition, we compare the contributions of 2k gratings with the phase conjugation during both mechanisms. (Optics Lett. 20, 1683-1685 (1995))

We consider the possibility of restoration and/or enhancement of decaying holograms in photorefractive media by using a simple optical readout in conjunction with a phase conjugator. The results indicate that extremely weak holograms can be enhanced provided that the two-beam coupling is sufficiently strong. Steady-state photorefractive holograms can be maintained continuously without decay by using a properly designed readout scheme. The result also provides an explanation for the formation of mutually pumped phase conjugation in terms of the amplification of initial noise gratings. (Optical Engineering, 34, 2204-2212 (1995))

The performance of four different mutually pumped phase conjugators in barium titanate depends on the mutual coherence of the two input beams. In three of the conjugators the use of fully mutually coherent input beams enhances the overall phase-conjugate reflectivity. The authors find that back-scattering and transmission gratings in the photorefractive crystal both contribute to the phase-conjugate signal and that their relative strength depends on the relative coherence of the two input beams. We numerically solve coupled-wave equations that include all gratings and find reasonable agreement between our theory and our experimental data. (J. Opt. Soc. Am., B12, 1363-1369 (1995))

We investigate angle-multiplexed volume holographic memory with spherical reference beams, for which the spherical approximation is made to model the wave-front distortion in general. We find that the angular selectivity and the cross-talk noise with spherical reference beams are close to those with planar reference beams. The results indicate that angle-multiplexed volume holographic memory can be realized in compact systems for which large wave-front distortion is expected. (Optics Lett., 20, 1812-1814 (1995))

We report the optical absorption and photorefractive properties of a series of cerium-doped barium titanate crystals. The light-induced absorption and the intensity-dependent two-beam coupling gain coefficient indicate that there are at least two active trap levels in cerium-doped $BaTiO_3$ crystals. The total effective trap density, the Debye screening wave vector, and the intensity-dependent factor increase with cerium-doping concentration as well as the pump beam intensity. The positive light-induced absorption and the negative absorption gain coefficient as the grating wave vector approaches zero indicate that the excitation cross section of shallow

traps is larger than that of deep traps. One of these crystals exhibits a two-beam coupling coefficient of 8.06 cm^{-1} for ordinarily polarized beams, which is the highest ever reported to date. Both electro-optic index grating and absorption grating are contributing to the coupling coefficient. The response time of as-grown cerium-doped $BaTiO_3$, with 15 ppm cerium is 220 ms at an intensityof 800 mW/cm^2. (Journal Of Applied Physics, 78, 4323-4330 (1995))

We consider the possibility of restoration and/or enhancement of decaying holograms in photorefractive media by using a simple optical readout in conjunction with a phase conjugator. The results indicate that extremely weak holograms can be enhanced provided that the two-beam coupling is sufficiently strong. Steady-state photorefractive holograms can be maintained continuously without decay by using a properly designed readout scheme. The result also provides an explanation for the formation of mutually pumped phase conjugation in terms of the amplification of initial noise gratings. (Applied Physics B-Lasers and Optics, 61 ,511-514 (1995))

We analyze the form birefringence dispersion of periodic dielectric layered media. We investigate the shape of the normal surface and its dependence on wavelength. Approximation gives an explicit expression for the additional dispersion of the form birefringence that is due to the
finite layer thickness. (Opt. Lett., 21, 504-506 (1996))

We investigate contradirectional two-wave mixing with partially coherent waves in photorefractive crystals in the nondepleted pump regime. Equations governing the propagation of the self-coherence function and the mutual-coherence function of the signal wave and the pump wave are derived and simulated numerically. Numerical solutions of these equations are in excellent agreement with the experimental measurements. (Opt. Lett., Vol. 21 No. 15, 1123-1125 (Aug 1, 1996))

We investigated 2k-grating-assisted self-pumped phase conjugation in photorefractive Ce:BaTiO/sub 3/ crystals. The phase-conjugation process involves a combination of four-wave mixing and stimulated photorefractive backscattering. An approximation involving separate interaction regions is used to theoretically calculate the reflectivity of phase conjugation as a function of the coupling strength of four-wave mixing and stimulated photorefractive backscattering. In our experiments, grating-erasure techniques are employed at the interaction regions to investigate the dependence of phase-conjugate reflectivity on the coupling strength of four-wave mixing and stimulated photorefractive backscattering. The experimental results are in

good agreement with the theoretical prediction. (J. Opt. Soc. Am. B-Optical Physics, Vol. 13, No. 8, 1772-1779, (Aug 1996))

We investigate experimentally the form birefringence due to photoinduced one- and two-dimensional volume index gratings in DuPont photopolymers. Experimental results on the dispersion of the form birefringence versus the illumination wavelength and the grating period for one-dimensional gratings are presented. We also investigate the form birefringence due to two-dimensional volume gratings. Positive form birefringence and biaxial form birefringence can be obtained by recording two volume gratings with different grating wave vectors. (Applied Physics Letters, V69 N23:3468-3470 (Dec. 2, 1996))

We investigate the form birefringence due to photoinduced one- and two-dimensional volume index gratings in DuPont photopolymers. The effective medium theory has been applied to the continuous volume subwavelength gratings. With the presence of a one-dimensional volume subwavelength grating, the originally isotropic photopolymer exhibits a negative form birefringence and behaves like a uniaxial dielectric. A form birefringence of $-1.2*10^{-3}$ at λ=632.8 nm is measured at a grating period of Λ=447 nm. Experimental results on the dispersion of the form birefringence versus the illumination wavelength and the grating period are presented. With the presence of a two-dimensional grating, in general, the originally isotropic photopolymer exhibits a biaxial form birefringence and behaves like a biaxial dielectric. Positive form birefringence can also be obtained by recording two volume gratings with different grating wave vectors. By recording two photoinduced volume gratings we can synthesize biaxial dielectrics with the principal axes along any desired directions. We also report the measured principal refractive indices of the medium due to the presence of two-dimensional volume gratings in DuPont photopolymer. (J. Appl. Phys., V81 N1:23-29 (Jan. 1997))

Two-wave mixing in photorefractive crystals is a very useful nonlinear optical phenomenon in many applications, such as image amplification, laser beam cleanup, spatial light modulators, thresholding and power limiting devices. Most of the theoretical works in this area are on the two wave interaction with monochromatic beams. Two wave mixing with partially coherent beams has been studied recently for the case of transmission grating interaction. In our publications (e.g. Optics Letters, 1 Aug. 1996, vol.21, (no.15):1123-5), we present the theoretical analysis and experimental investigation for the case of reflection grating interaction.

In the case of contradirectional two wave mixing with purely diffusive photorefractive medium, the coupled-wave equations for the slowly varying amplitudes $\mathbf{E}_1(\mathbf{t},\mathbf{z})$ and $\mathbf{E}_2(\mathbf{t},\mathbf{z})$ can

be written as

$$\frac{\partial \mathbf{E}_1}{\partial \mathbf{z}} + \frac{1}{\mathbf{v}}\frac{\partial \mathbf{E}_1}{\partial \mathbf{t}} = \frac{\gamma}{2}\frac{\mathbf{Q}\cdot\mathbf{E}_2}{\mathbf{I}_1+\mathbf{I}_2} - \frac{\alpha}{2}\mathbf{E}_1 \tag{1}$$

$$\frac{\partial \mathbf{E}_2}{\partial \mathbf{z}} - \frac{1}{\mathbf{v}}\frac{\partial \mathbf{E}_2}{\partial \mathbf{t}} = \frac{\gamma}{2}\frac{\mathbf{Q}^*\cdot\mathbf{E}_1}{\mathbf{I}_1+\mathbf{I}_2} + \frac{\alpha}{2}\mathbf{E}_2 \tag{2}$$

where γ is the intensity coupling constant, α is the intensity absorption coefficient, $\mathbf{v}$ is the group velocity, $\mathbf{E}_1\exp(-\mathbf{i}\omega\mathbf{t}+\mathbf{ikz})$ and $\mathbf{E}_2\exp(-\mathbf{i}\omega\mathbf{t}-\mathbf{ikz})$ are the coupled quasi-monochromatic waves which interact through a dynamic photorefractive grating $\delta\mathbf{n}(\mathbf{z},\mathbf{t}) \propto \mathbf{Q}\exp[2\mathbf{ikz}]+\mathbf{c.c.}$. The dynamics of the photorefractive grating can be written as

$$\tau\frac{\partial \mathbf{Q}}{\partial \mathbf{t}} + \mathbf{Q} = \mathbf{E}_1\mathbf{E}_2^* \tag{3}$$

where τ is the relaxation time constant determined by the average total intensity, $\tau \sim \left(\langle E_1\rangle^2 + \langle E_2\rangle^2\right)^{-1}$

Consider that the temporal behavior of each wave's complex amplitude is a stationary random process, with coherentce time $\delta\omega^{-1}$ being substantially less than relaxation time of the material $\delta\omega\tau >> 1$. When the optical path difference of the two beams is smaller than the coherence length of the laser, a dynamic photorefractive grating is recorded in the medium. Its position and profile are nearly temporally constant. Then, as an approximatioin, we can replace the dynamic grating amplitude $\mathbf{Q}$ in Eqs.(1) and (2) with its ensemble average as $\mathbf{Q} \approx \langle \mathbf{E}_1\mathbf{E}_2^* \rangle$.

Since the complex amplitudes $\mathbf{E}_1(\mathbf{t},\mathbf{z})$ and $\mathbf{E}_2(\mathbf{t},\mathbf{z})$ are stationary random processes, we can define some of their ensemble averages as $\Gamma_{12}(\mathbf{z},\Delta\mathbf{t}) \equiv \langle \mathbf{E}_1(\mathbf{z},\mathbf{t}_1)\mathbf{E}_2^*(\mathbf{z},\mathbf{t}_2)\rangle$, $\Gamma_{11}(\mathbf{z},\Delta\mathbf{t}) \equiv \langle \mathbf{E}_1(\mathbf{z},\mathbf{t}_1)\mathbf{E}_1^*(\mathbf{z},\mathbf{t}_2)\rangle$, and $\Gamma_{22}(\mathbf{z},\Delta\mathbf{t}) \equiv \langle \mathbf{E}_2(\mathbf{z},\mathbf{t}_1)\mathbf{E}_2^*(\mathbf{z},\mathbf{t}_2)\rangle$ where $\Delta\mathbf{t} = \mathbf{t}_1 - \mathbf{t}_2$. We refer to Γ_{11} and Γ_{22} as the self coherence of the pump beam $\mathbf{E}_1(\mathbf{t},\mathbf{z})$ and the signal beam $\mathbf{E}_2(\mathbf{t},\mathbf{z})$ respectively, and Γ_{12} as the mutual coherence between the signal beam and the pump beam. With these notations, we can immediately write down $\mathbf{Q} \approx \Gamma_{12}(\mathbf{z},0)$, $\mathbf{I}_1(\mathbf{z}) = \Gamma_{11}(\mathbf{z},0)$ and $\mathbf{I}_2(\mathbf{z}) = \Gamma_{22}(\mathbf{z},0)$. Eqs.(1) and (2) can therefore be reduced to a system for these average values as

$$\frac{\partial \Gamma_{12}(\mathbf{z},\Delta\mathbf{t})}{\partial \mathbf{z}} = -\frac{2}{\mathbf{v}}\frac{\partial \Gamma_{12}(\mathbf{z},\Delta\mathbf{t})}{\partial \Delta\mathbf{t}} + \frac{\gamma}{2}\frac{\Gamma_{12}(\mathbf{z},0)}{\mathbf{I}_1+\mathbf{I}_2}\left[\Gamma_{11}(\mathbf{z},\Delta\mathbf{t}) + \Gamma_{22}(\mathbf{z},\Delta\mathbf{t})\right] \tag{4}$$

$$\frac{\partial \Gamma_{11}(z,\Delta t)}{\partial z} = \frac{\gamma}{2}\frac{\Gamma_{12}(z,0)}{I_1+I_2}\Gamma_{12}^{*}(z,-\Delta t)+\frac{\gamma}{2}\frac{\Gamma_{12}^{*}(z,0)}{I_1+I_2}\Gamma_{12}(z,\Delta t)-\alpha\Gamma_{11}(z,\Delta t) \tag{5}$$

$$\frac{\partial \Gamma_{22}(z,\Delta t)}{\partial z} = \frac{\gamma}{2}\frac{\Gamma_{12}(z,0)}{I_1+I_2}\Gamma_{12}^{*}(z,-\Delta t)+\frac{\gamma}{2}\frac{\Gamma_{12}^{*}(z,0)}{I_1+I_2}\Gamma_{12}(z,\Delta t)+\alpha\Gamma_{22}(z,\Delta t) \tag{6}$$

Note that Eqs.(4)-(6) represent the propagation of the mutual conherence and self coherence functions of the two beams. When there is no coupling (i.e. $\gamma = 0$), Eqs.(4)-(6) can be solved analytically as

$$\Gamma_{12}(z,\Delta t) = \Gamma_{12}\left(0,\Delta t+\frac{2z}{v}\right) \tag{7}$$

$$\Gamma_{11}(z,\Delta t) = \Gamma_{11}(z,\Delta t)\exp(-\alpha z) \tag{8}$$

$$\Gamma_{22}(z,\Delta t) = \Gamma_{22}(z,\Delta t)\exp(\alpha z) \tag{9}$$

These solutions are consistent with the classical theory on optical wave interference in linear medium. The mutual coherence function is presented as a propagation wave with the boundary conditions at z=o plane. The self coherence decrease along the z axis due to absorption. When there is coupling, the photorefractive grating implies that the both beam are rescattered by the grating into each other. As a result, part of pump wave branches off in the direction of the signal waves. It causes that the mutual and self conherence functions of the two waves are not the same as simple propagation of the boundary condition. However, we note that Eqs.(4)-(6) are self-consistent. They can be solved numerically if we have the proper boundary conditions. In the presence of pump depletion, we can not obtain sufficient boundary conditions for typical situations. Therefore, although Eqs.(4)-(6) are general, we can not use them to solve the case of pump depletion. For the case of nondepleted pump, sufficient boundary conditions can be easily obtained.

Consider a two wave mixing configuration shown in Fig.1. Both the signal beam and the pump beam come from the same laser source. If the laser source is assumed to have a Gaussian lineshape (fit from the experimental data) with a linewidth of $\Delta\nu$, then the normalized self coherence of the laser source can be written as

$$\Gamma_s(\delta t) = \exp\left[-\left(\frac{\pi\Delta\nu\delta t}{2\sqrt{\ln 2}}\right)^2\right] \tag{10}$$

At the signal beam input plane z=0, the intensity ratio between the signal beam and the pump beam is assumed to be β, and the time delay between the signal beam and the pump beam is assumed to be δt. In our simulation, the intensity of the pump beam is taken to be unit one. Then the boundary conditions at z=0 can be written as

$$\Gamma_{12}(z=0,\Delta t) \equiv \sqrt{\beta}\,\Gamma_s(\Delta t+\delta t) \tag{11}$$

$$\Gamma_{11}(z=0,\Delta t) \equiv \Gamma_s(\Delta t) \tag{12}$$

$$\Gamma_{22}(z=0,\Delta t) \equiv \beta\Gamma_s(\Delta t) \tag{13}$$

With these boundary conditions, Eqs.(4)-(6) become an initial value problem, under the approximation of nondepleted pump.

The results of our calculations are show in Figs. 2, in which we have plotted the mutual coherence function of the two beams and the self coherence function of the signal beam as a function of distance for various coupling constant γ of 1, 3, 5, and 10. The initial optical path difference is taken to be 8 cm at the signal incident plane z=0, the linewidth of the laser $\Delta\nu$ is assumed to be 1.83 GHz, and the input intensity ratio β is assumed to be 10^3. For a small coupling constant, the mutual coherence function is hardly affedted by the presence of the coupling. The curve is almost the same as the propagation of wave equation using Eqs.(7) and (11). For a lager coupling constant, as a result of the coupling, part of the pump wave branches off in the direction of the signal beam. When the weak beam is amplified, it gains substantially by the instantaneous convergence of the temporal profile of the strong pump beam, increasing the strong beam's coherence with weak beam. In other, the increase of the mutual coherence of the two waves also enhances the amplitude of the grating. The interaction length of the two beams could therefore become longer than the coherent legth of the laser source. It leads also to a sharp increase of the gain of the signal beam when the coupling constant is large ($\gamma \geq 5$, as shown in Fig. 2(b)).

Our experimental arrangement for this study is shown in Fig.1. Two partially coherent beams, obtained by splitting an argon laser beam with linewidth of 1.83 Ghz, passed through the signal beam and the pump brenches of the system respectively and then were contradirectionally incident into a $KNbO_3$:Co crystal ($\gamma \approx 3.3\text{cm}^{-1}$, $\alpha \approx 0.5\text{cm}^{-1}$ and thickness L=0.72 cm). The optical path difference of the two beams at the signal incident plane (i.e. z=0) was set to be $\Delta L = \ell_2 - \ell_1$. To monitor the mutual coherence between the signal beam and the pump beam at the output plane z=L, another reference beam (E_{2ref}) was splitted from the pump

beam E_2. The optical path difference of E_1 and E_{2ref} beams was adjusted to be the same as that of E_1 and E_2 beams at the output plane z=L. The visibility of interference fringes generated by E_1 and E_{2ref} beams was observed by a CCD camera at the output plane P1. Therefore the mutual conherence Γ_{12} can be etsimated in terms of the visibility as $(I_{max} - I_{min})/(4\sqrt{I_1 I_2})$, where $(I_{max} - I_{min})$ is the amplitude of the fringes. In the experiment we monitor the interference pattern with and without pump beam E_2. Fig.3 shows pictures with an initial mutual coherence $\Gamma_{12}(0,0) \approx 0.43$ (i.e. $\Delta L = 4$ cm) and intensity ratio $\beta = 664$. Notice the increase of fringes visibility due to the coupling. The measured mutual coherence $\Gamma_{12}(L,0)$ increases from 0.19 to 0.7. To futher verify the theoretical prediction of the increase of the mutual coherence, we then measure the mutual coherence $\Gamma_{12}(L,0)$ as a function of the artifical optical path difference ΔL. Fig. 4 shows a complete family of data obtained in this measurement (dots) and the theoretical curve for the same parameters. Owing to the reflected wave by the grating being completely coherent with the pump wave at the reflected face, it leads to an significant increase in the mutual coherence. The curve shows this effect which makes the mutual conherence increase very sharply as the optical path difference decreases.

Another effect on the increase of the mutual coherence is the enhancement of the amplitude of the grating and interaction length of the two beams inside crystal. This enhancement influences the achievable intensity gain of the signal wave. Fig. 5 shows the measurement of the two-wave-mixing gain (dots) of the signal wave at z=L plane as a function of the path difference ΔL. Along with the datas is the theoretical curve for the same parameters. The curve shows asymmetric with respect to the maximum point of the intensity gain and the shift of the point inside crystal due to the different tails of the decrease of the coherence function. The experimental results are excellent agreement with the theoretical prediction.

In conclusion we have demonstrated that the contradirectional two wave mixing of partial coherent beams inside a photrefractive crystal with an inertial nonlinear response leads to a increase of the mutual coherence subatantially and the interaction legth of the two beams. A set of the coupled equation has been derived to describe the propagation of the mutual coherence and the self coherence functions of the two beams. The experimental results have demonstrated the increase of the mutual coherence and the enhancement of the two-wave-mixing gain of the signal beam due to the coupling.

Figures:

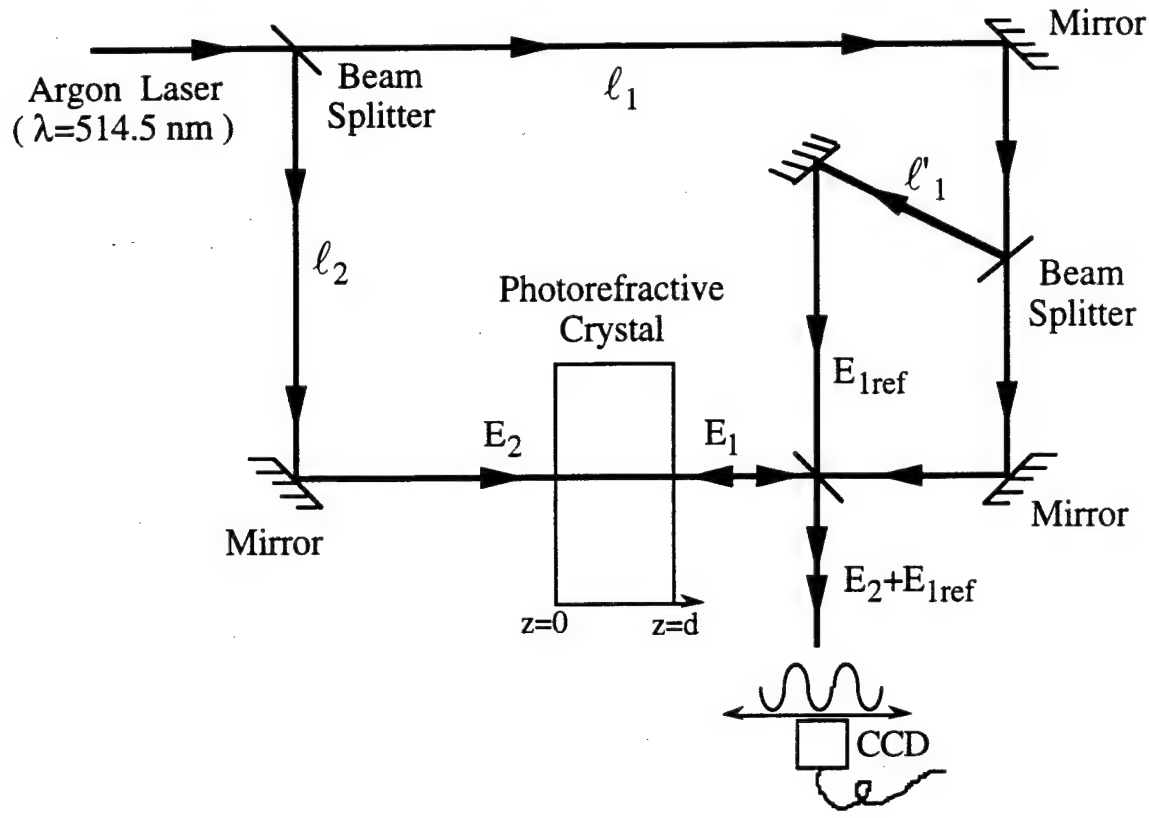

Fig. 1. Schematic of the two-wave-mixing configuration used in our calculations and experiments. The distance ℓ_1 and ℓ_2 are the optical path length of the signal beam and pump beam from laser source to the signal beam incident plane z=0, respectively. The ℓ_{2ref} is the optical path length of reference beam E_{2ref} from laser source to the signal output plane z=L.

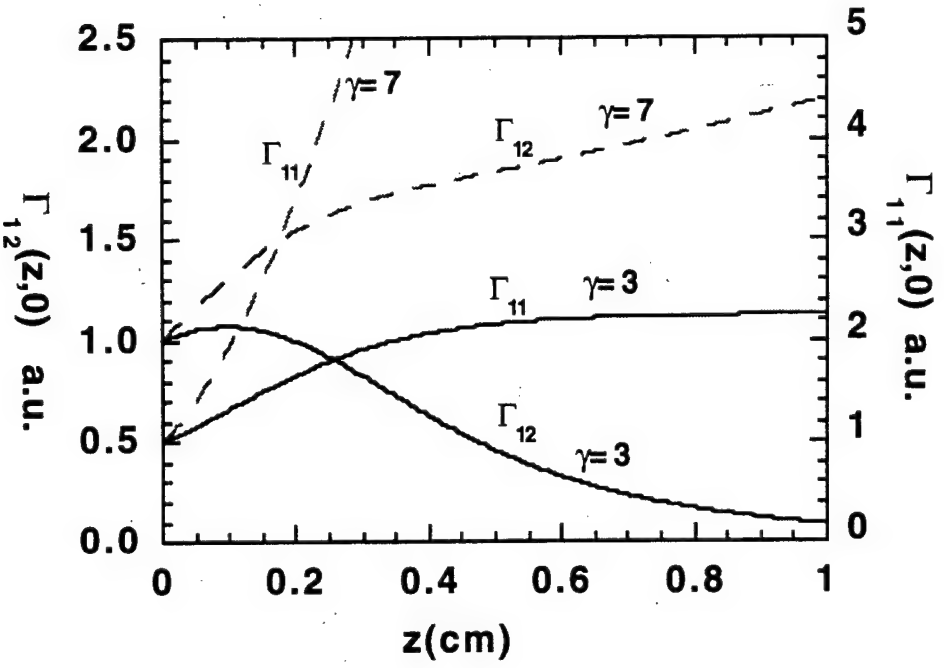

Fig.2. (a) The mutual coherence function $\Gamma_{12}(\mathbf{z},0)$ and (b) the self coherence function of the signal beam $\Gamma_{11}(\mathbf{z},0)$ as a function of z for various coupling constant γ of 1, 3, 5, and 10.

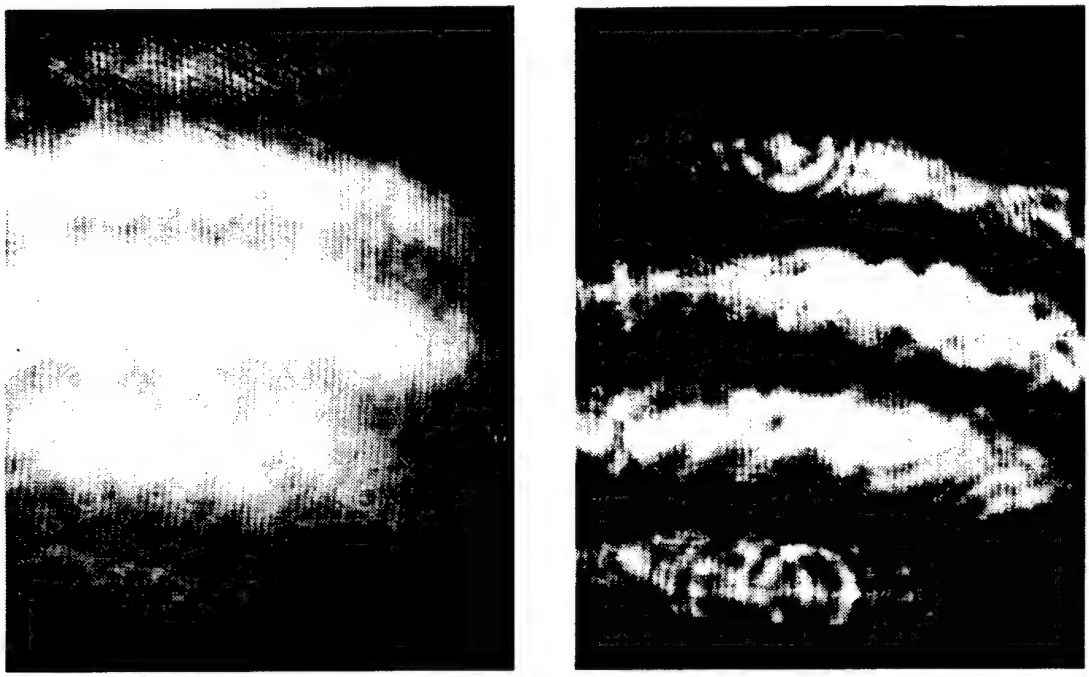

Fig. 3. Interference pattern of the signal beam and the reference beam at the output plane P1 (a) without (b) with coupling. Notice the increase of fringe visibility due to the coupling.

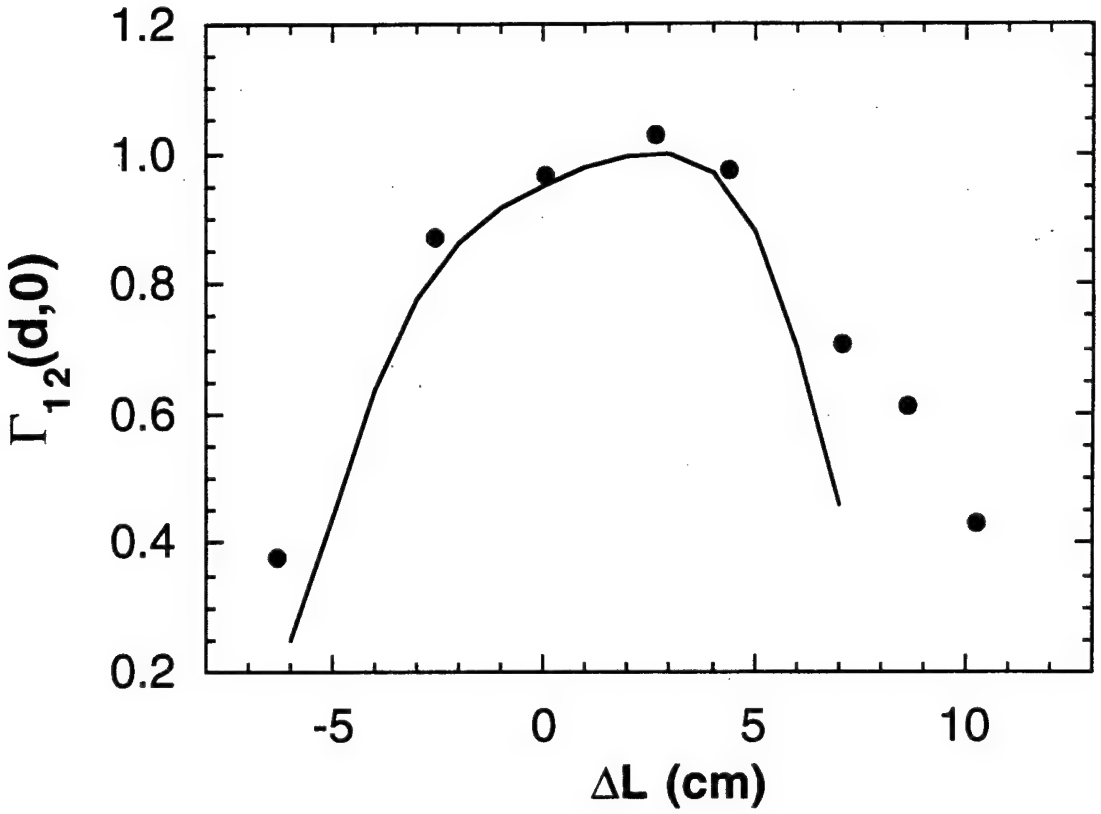

Fig. 4. The mutual coherence $\Gamma_{12}(\mathbf{L},0)$ as a function of the optical path difference $\Delta\mathbf{L}$ of the two beams.

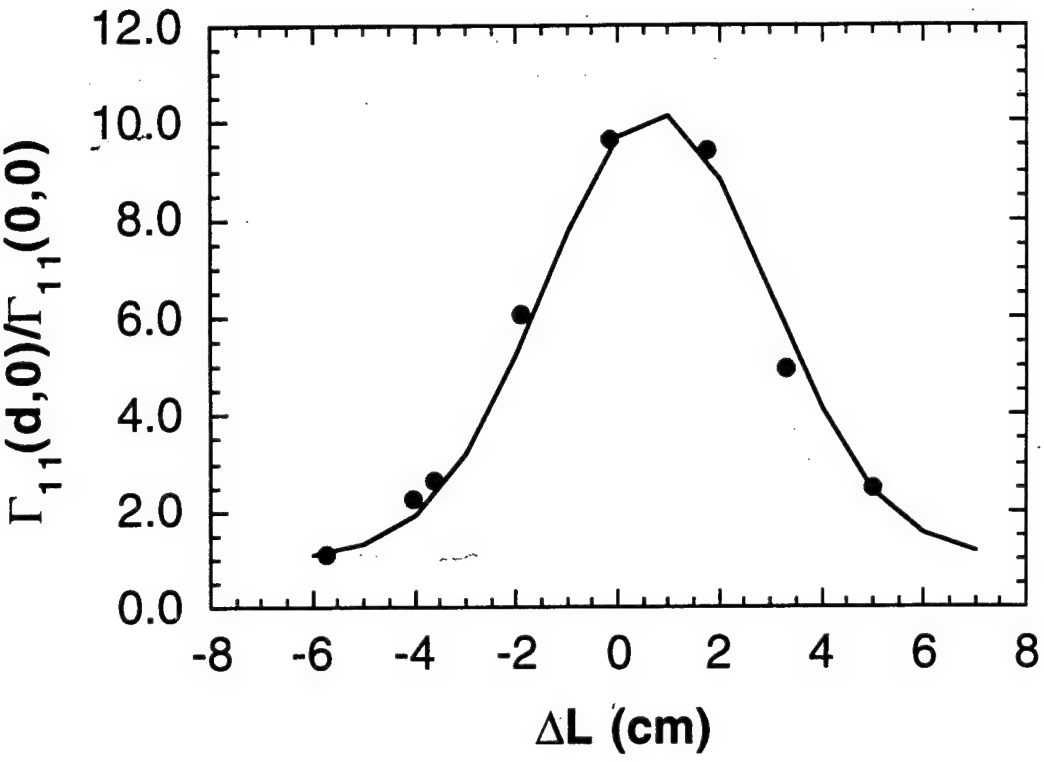

Fig. 5. The measurement of the two-wave-mixing gain of the signal wave at z=L plane as a function of the path difference **ΔL** of the two beams.

3.0 Reprints of Selected Papers

Energy Coupling by Partially Degenerate Four-Wave Mixing in Multichannel Lightwave Systems

Weishu Wu and Pochi Yeh, *Fellow, IEEE*

***Abstract*—We investigate the energy coupling among different frequency carriers by partially degenerate four-wave mixing in single-mode fibers. We show that for a multichannel lightwave system operated near the zero-dispersion frequency of the single-mode fiber, four-wave mixing may cause significant signal depletion in a channel whose power acts as a pump in the four-wave mixing process. Analytical solutions are derived and the signal depletion due to four-wave mixing is obtained.**

FOUR-WAVE MIXING (FWM) is an important nonlinear process for optical fiber communication systems [1]–[3]. Applications of four-wave mixing such as frequency conversion [4] and phase conjugation [5], [6] have been analyzed and demonstrated. On the other hand, FWM can degrade the performance of a multichannel lightwave system [7]. One problem related to FWM is the cross talk resulting from the generation of new frequency components for channels supposed to be zero. Another problem associated with FWM is the signal depletion due to energy coupling between different channels. Although the effects of cross talk can be, to some extent, alleviated by designing a system composed of unequally spaced frequency channels [7], signal depletion is inevitable for both systems with equal and unequal frequency spacings if the input powers are sufficiently large.

FWM in single-mode fibers has been extensively studied under the assumption of pump nondepletion [1]–[4], [8]. Analytical solutions taking into account of pump depletion has been obtained only for cases where fiber absorption [2], [9] and/or group velocity dispersion [8] can be neglected. However, these assumptions are not valid for cases in which long interaction length of the fiber is utilized to obtain efficient FWM [5]–[7]. In this paper, we present analytical solutions to partially degenerate four-wave mixing (PDFWM) in single-mode fibers near the zero-dispersion frequency. These solutions are then used to analyze the energy coupling in both systems with unequal and equal frequency spacings.

To describe the energy coupling, we start from the coupled-mode equations for PDFWM,

$$\frac{dA_1}{dz} = -i2\gamma A_1^* A_2 A_3 \exp(i\Delta k z) - \frac{\alpha}{2}A_1$$

$$\frac{dA_2}{dz} = -i\gamma A_1 A_1 A_3^* \exp(-i\Delta k z) - \frac{\alpha}{2}A_2$$

$$\frac{dA_3}{dz} = -i\gamma A_1 A_1 A_2^* \exp(-i\Delta k z) - \frac{\alpha}{2}A_3 \tag{1}$$

where α is the absorption coefficient of the fiber, γ is the nonlinearity coefficient [1] of the fiber, $\Delta k = 2k_1 - k_2 - k_3$ is the propagation constant difference describing the phase mismatch of the PDFWM process, and A_1,A_2, and A_3 are the amplitudes for the center frequency component and two side components, respectively. In arriving at (1), we assumed that the intensity-dependent phase shift is small enough to be neglected. The phase matching condition for PDFWM, $\Delta k = 0$, can be satisfied if the central frequency, $f_1 = (f_2 + f_3)/2$, is set to the zero-dispersion frequency, f_0, as well as all the frequencies are near f_0 so that the higher order dispersion terms can be neglected [10]. Under the phase matching condition, the above equations can be rewritten, by substituting $A_j = \sqrt{P_j}\exp(i\phi_j) = \sqrt{Q_j}\exp(-\alpha z/2)\exp(i\phi_j)$, as

$$\frac{dQ_1}{dz} = -4\gamma\sqrt{Q_1Q_1Q_2Q_3}\exp(-\alpha z)\sin\ \Delta\phi$$

$$\frac{dQ_2}{dz} = +2\gamma\sqrt{Q_1Q_1Q_2Q_3}\exp(-\alpha z)\sin\ \Delta\phi$$

$$\frac{dQ_3}{dz} = +2\gamma\sqrt{Q_1Q_1Q_2Q_3}\exp(-\alpha z)\sin\ \Delta\phi \tag{2}$$

$$\frac{d\Delta\phi}{dz} = \gamma\left(\frac{1}{Q_2} + \frac{1}{Q_3} - \frac{4}{Q_1}\right)\sqrt{Q_1Q_1Q_2Q_3} \cdot \exp(-\alpha z)\cos\ \Delta\phi. \tag{3}$$

where $\Delta\phi = 2\phi_1 - \phi_2 - \phi_3$ is the relative phase of the three waves.

It can be easily seen that the direction of energy coupling is determined by the sign of the relative phase, $\Delta\phi$. In cases when $P_2(0)$ or $P_3(0)$ is absent, the FWM process will result in a relative phase such that energy will be transferred to P_2 or P_3. If the energy is coupled from P_1 to P_2 and P_3, the solution to (2) can be written as

$$\begin{aligned} Q_1 &= P_1(0)y \\ Q_2 &= 0.5P_1(0)(1-y) + P_2(0) \\ Q_3 &= 0.5P_1(0)(1-y) + P_3(0) \end{aligned} \tag{4}$$

where y is a function of z to be determined.

Analytical expression for y has been derived for initial condition $P_3(0) = 0$ [6]. When $P_3(0) = 0$, it has been shown that the relative phase is always $\pi/2$ due to the fact that $\sqrt{Q_1Q_1Q_2Q_3}\cos\ \Delta\phi$ is a constant. In that case, y is given by

$$y = \frac{r+1}{r\cosh^2(\sqrt{r+1}f) + 1} \tag{5}$$

where $r \equiv 2P_2(0)/P_1(0)$ and $f = \gamma P_1(0)[1 - \exp(-\alpha z)]/\alpha$.

Manuscript received September 30, 1994; revised January 18, 1995. This work is supported in part by grants from the US Air Force Office of Scientific Research and Office of Naval Research.

The authors are with the Department of Electrical and Computer Engineering, University of California, Santa Barbara, CA 93106 USA.

IEEE Log Number 9410468.

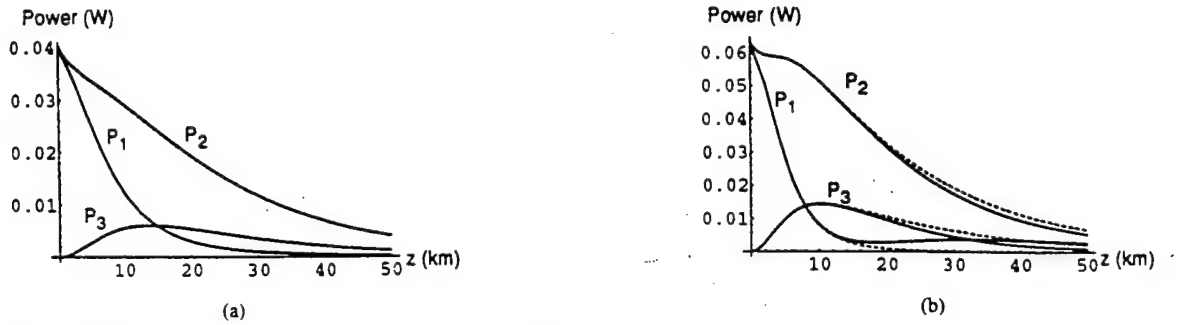

Fig. 1. Power coupling by PDFWM as a function of fiber length z. The dashed lines are the results obtained using the analytical solution without the effects of SPM/XPM, while the solid lines are the results obtained using numerical methods taking into account the effect of SPM/XPM for input powers of (a) 16 dBm and (b) 18 dBm. The nonlinear coefficient γ is 1.853×10^{-5} cm^{-1} W^{-1}, and fiber absorption coefficient is 0.23 dB/km for a fiber with effective area of 70 μm^2 and nonlinear refractive index n_2 of 3.2×10^{-20} m^2/W at $\lambda = 1.55$ mm.

Fig. 1 shows the energy coupling by PDFWM in a 50 km long fiber. The dashed lines are the results obtained using the analytical solution derived above, while the solid lines are the results obtained using numerical methods taking into account the phase shift caused by the intensity-dependent refractive index. The input powers are 16 dBm and 18 dBm in Fig. 1(a) and (b), respectively. It shows that for moderate input powers, the effect of the intensity-dependent phase shift can be reasonably neglected.

It is worth noticing that although (5) was derived under the boundary condition $P_3(0) = 0$, it is still valid for cases where a small $P_3(0)$ is present. Although the presence of $P_3(0)$ may result in an arbitrary value for the initial relative phase $\Delta\phi$, the relative phase will quickly approach $\pi/2$ before any significant energy coupling occurs because $d\Delta\phi/dz$ is very large (roughly proportional to $1/\sqrt{P_3}$). When $P_3(0)$ can not be ignored compared with the other two inputs, which is the case for multichannel lightwave systems with equal frequency spacings and with all input powers present, the energy coupling depends on $\Delta\phi$, which determines the interference between the input signals and the newly generated FWM components. By inspecting (2) and (3), we find out that maximum energy coupling occurs when $\Delta\phi(0) = \pm\pi/2$. For these two limiting cases, analytical solutions can be derived. By examining (3), we can easily find that $\Delta\phi = \pm\pi/2$ are solutions to (3). The function y can be solved by substituting (4) back to the first equation of (2) and is given by

$$y = \frac{4\bar{r}^2 \exp(2\bar{r}f)}{r_0^2 \exp(4\bar{r}f) + 2(2 + r_2 + r_3) \exp(2\bar{r}f) + r_0^{-2}(r_3 - r_2)^2} \tag{6}$$

where f is the same as in (5), $r_2 \equiv 2P_2(0)/P_1(0)$, $r_3 \equiv 2P_3(0)/P_1(0)$, $\bar{r} = \sqrt{(1 + r_2)(1 + r_3)}$, and $r_0 = \sqrt{r_3(r_2 + 1)} + \sqrt{r_2(r_3 + 1)}$. When $r_2 = r_3 = r$, (6) reduces to

$$y = \frac{r + 1}{r \exp[2(1 + r)f] + 1}. \tag{7}$$

In this case ($\Delta\phi = \pi/2$), P_1 is a decreasing function of z, and P_2, P_3 are increasing functions of z, according to (2). In other words, the energy is transferred from P_1 to P_2 and P_3.

When $\Delta\phi(0) = -\pi/2$, analytical solution can be similarly obtained. In this case, the energy is transferred from P_2 and P_3 to P_1. The energy transfer will cease if either P_2 or P_3 is depleted. If we assume, without loss of generality, that $P_2(0) < P_3(0)$, then the solution is in form of

$$\begin{aligned} Q_1 &= 2P_2(0)u + P_1(0) \\ Q_2 &= -P_2(0)u + P_2(0), \\ Q_3 &= -P_2(0)u + P_3(0) \end{aligned} \tag{8}$$

with u given by (9) below, where $r_{12} = P_1(0)/2P_2(0)$, $r_{32} = P_3(0)/P_2(0)$, $f_2 = 2\gamma P_2(0)[1 - \exp(-\alpha z)]/\alpha$, $c = (1 + r_{12})(r_{32} + r_{12})$, and $a = 2\sqrt{cr_{32}} + r_{12} + r_{12}r_{32} + 2r_{32}$. It is interesting to note that when $P_1(0) = 0$, $u \equiv 0$, which means that only amplification, instead of generation, of the center component is possible.

Equation (9) can also be simplified when $P_2(0) = P_3(0)$. In this case, $r_{32} = 1$, and (9) reduces to

$$u = \frac{1 - \exp[-2(1 + r_{12})f_2]}{\exp[-2(1 + r_{12})f_2] + r_{12}} r_{12}. \tag{10}$$

For $\Delta\phi(0)$ other than $\pm\pi/2$, exact analytical solutions in simple form are not available. The interference between the input signals and the newly generated FWM components may result in a complicated energy coupling, i.e., periodic energy transfer. However, when $P_3(0) \ll P_1(0)$, we expect that the energy coupling can be well described by (4) and (5), as pointed out earlier. In addition, if $\Delta\phi$ does not change significantly over the fiber length, an approximate analytical solution can be easily obtained. The presence of sin $\Delta\phi$ in (2) is equivalent to a simple modification of the nonlinear coefficient γ.

The analytical solutions can be used to investigate energy coupling and depletion in fiber communications systems. For a

$$\frac{4cr_{12} \exp(-2\sqrt{c}f_2)}{a \exp(-4\sqrt{c}f_2) - 2a(1 + 2r_{12} + r_{32})r_{12} \exp(-2\sqrt{c}f_2) + r_{12}^2(r_{32} - 1)^2/a} - r_{12}. \tag{9}$$

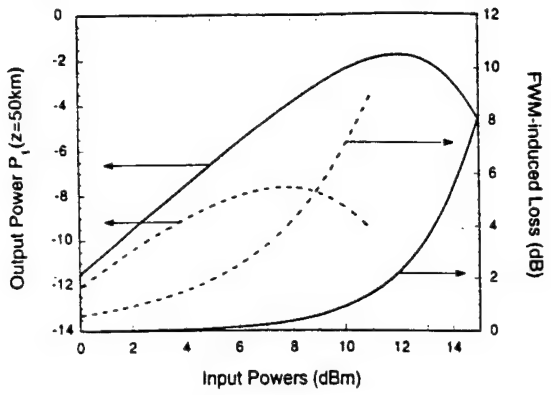

Fig. 2. Output powers and the FWM-induced losses due to PDFWM in channel f_1 as functions of input power for multichannel lightwave systems. The solid lines are for systems with unequal frequency spacings, and dashed lines are for systems with equal frequency spacings. Equal input powers for all channels are assumed for both cases.

multichannel lightwave system with unequal frequency spacings, energy coupling can be described by (4) and (5). The coupling will lead to a significant energy depletion for signal in channel f_1, thus imposing an upper limit on the input power. Further increase of input power will result in a smaller output power in channel f_1 due to the FWM process. To see this, let us study the signal evolution after transmission through a 50 km long fiber. For simplicity, we assume that all channels have the same input power. We plot the output power $P_1(L)$ as a function of $P_1(0)$ in Fig. 2 (solid lines). We note that for input power greater than 12 dBm, the output power at $z = 50$ km begins to drop. Furthermore, even in regions where output power does increase with the increase of input power, the FWM-induced loss of P_1 (defined as $10\log[P_1^{\text{no FWM}}(L)/P_1^{\text{FWM}}(L)]$) is considerable. For fibers with larger nonlinearity, the FWM-induced loss will be even more significant.

For multichannel lightwave systems with equal frequency spacings, we can use (6)–(10) to describe energy coupling if each channel has a finite power at its input port. For the purpose of comparing systems with unequal frequency spacings, we limit our attention to the case of $\Delta\phi = \pi/2$, which corresponds to cases of maximum energy coupling. The dashed lines in Fig. 2 shows the output power $P_1(L)$ and the FWM-induced loss as functions of input power $P_1(0)$ for a fiber length of $L = 50$ km. By examining the figure we note that the signal depletion is more severe compared with systems with unequal frequency spacings (solid lines). In this case, the upper limit of input power is about 8 dBm. Furthermore, the FWM-induced loss is much larger due to a stronger signal depletion in this case. This verifies again the conclusion that multichannel lightwave systems with unequal frequency spacings are preferable to those with equal frequency spacings [7]. To further reduce the impact of FWM on the system performance, all input powers should be kept below a certain value. In addition, no channel frequency should be the same as (or even too close to) the zero-dispersion frequency of the fiber so that phase matching condition for PDFWM is not satisfied. For a given channel spacing $\Delta\lambda$ and effective fiber length L, the minimum separation $f_1 - f_0$ should be such that $\Delta kL \geq \pi$. For systems operated near the zero-dispersion frequency, Δk is given by $2\pi(dD_c/d\lambda)(\Delta\lambda)^2(f_1 - f_0)$, where D_c is the fiber chromatic dispersion [10]. $f_1 - f_0$ can be roughly estimated as 20 GHz if the effective fiber length is 20 km. In this way, the effect of FWM can be minimized due to phase mismatching.

In conclusion, we have studied PDFWM with pump depletion from the physical point of view. Analytical solutions for PDFWM with all inputs present have been derived for multichannel systems operated near the zero-dispersion frequency. It has been shown that energy can be coupled from either the center component or the side components as a result of interference of inputs and FWM-generated components in multichannel systems with equal frequency spacing. It has also been shown that for input power beyond a certain value, power in the pump channel will be considerably depleted over a relative short distance. To ensure good system performance, effective suppression of FWM is critical.

REFERENCES

[1] G. P. Agrawal, *Nonlinear Fiber Optics.* London: Academic Press Inc., 1989.
[2] G. Cappellini and S. Trillo, "Third-order three-wave mixing in single-mode fibers: Exact solutions and spatial instability effects," *J. Opt. Soc. Am. B*, vol. 8, pp. 824–832, 1991.
[3] K. O. Hill, D.C. Johnson, B. S. Kawasaki, and R. I. MacDonald, "CW three-wave mixing in single mode fibers," *J. Appl. Phys.*, vol. 49, pp. 5098–5106, 1978.
[4] K. Inoue and H. Toba, "Wavelength conversion experiment using fiber four-wave mixing," *IEEE Photon. Technol. Lett.*, vol. 40, pp. 69–72, 1992.
[5] S. Watanabe, T. Naito, and T. Chikama, "Compensation of chromatic dispersion in a single-mode fiber by optical phase conjugation," *IEEE Photon. Technol. Lett.*, vol. 5, pp. 92–95, 1993.
[6] W. Wu, P. Yeh, and S. Chi, "Phase conjugation by four-wave mixing in single-mode fibers," to appear in *IEEE Photon. Technol. Lett.*, 1994.
[7] F. Forghieri, R. W. Tkach, and A. R. Chraplyvy, "Performance of WDM systems with unequal channel spacing to suppress four-wave mixing," *ECOE'94 Tech. Dig.*, 1994, pp. 741–744.
[8] N. Shibata, R. P. Braun, and R. G. Waarts, "Phase-mismatched dependence of efficiency of wave generation through four-wave mixing in a single-mode fiber," *J. Quantum Electron.*, vol. 23, pp. 1205–1210, 1987.
[9] E. Lichtman, A. A. Friesem, R. G. Waarts, and H. H. Yaffe, "Exact solution of four-wave mixing of copropagating light beams in a Kerr medium," *J. Opt. Soc. Am. B*, vol. 4, pp. 1801–1805, 1987.
[10] K. Inoue, "Four-wave mixing in an optical fiber in the zero-dispersion wavelength region," *J. Lightwave Technol.*, vol. 10, pp. 1553–1561, 1992.

Effect of beam coherence on mutually pumped phase conjugators

San-Ching De La Cruz, Stuart MacCormack, and Jack Feinberg

Departments of Physics and Electrical Engineering, University of Southern California, Los Angeles, California 90089-0484

Q. Byron He* and Hua-Kuang Liu

Jet Propulsion Laboratory, California Institute of Technology, 4800 Oak Grove Drive, Pasadena, California 91109

Pochi Yeh

Department of Electrical and Computer Engineering, University of California, Santa Barbara, Santa Barbara, California 93106

The performance of four different mutually pumped phase conjugators in barium titanate depends on the mutual coherence of the two input beams. In three of the conjugators the use of fully mutually coherent input beams enhances the overall phase-conjugate reflectivity. We find that backscattering and transmission gratings in the photorefractive crystal both contribute to the phase-conjugate signal and that their relative strength depends on the relative coherence of the two input beams. We numerically solve coupled-wave equations that include all gratings and find reasonable agreement between our theory and our experimental data.

1. INTRODUCTION

Imagine trying to inject light into the gain regions of a present-day laser-diode array. Such a laser-diode array might measure 1 cm across, but its 20 or so gain regions are each only 200 μm across $\times$ 1 μm high. Injecting light precisely into these lasing regions is like trying to thread 20 needles in a haystack simultaneously. However, if the output from the laser array is sent into a photorefractive crystal, and if a separate light beam is also directed into the same crystal, then the crystal could, in principle, connect the two light beams, sending each beam back down the path of the other. Acting as a mutually pumped phase conjugator, the crystal would transform each light beam into the phase-conjugate replica of the other light beam. In the above application the crystal would direct the injected light beam precisely into the lasing regions of the array. The two incident light beams need not be coherent with each other, although they should have the same nominal wavelength.

Using the double phase-conjugate mirror (DPCM),[1] a number of authors have demonstrated short-lived injection locking of a laser.[2,3] MacCormack *et al.*[4] used a bird-wing[5] conjugator and obtained stable locking between two laser diodes.

When two lasers are connected by a phase conjugator and the lasers become phase locked, their light beams become mutually coherent. Can the crystal continue to act as a mutually pumped phase conjugator with mutually coherent light beams? We show below that the answer depends on the particular geometry of the mutually pumped phase conjugator.

First we give a heuristic explanation of how mutually pumped phase conjugators work.[5,6] Let the two input beams be labeled 2 and 4. (We use this counterintuitive beam-numbering scheme to stick to the convention of Ref. 7.) Light randomly scattered from beam 2 travels across beam 2 and writes a multitude of different beam-fanning gratings. Beam 4 tends to erase most of these gratings. However, beam 4 will be incident at the Bragg angle for some small set of these fanning gratings, and it will efficiently deflect from them. The deflected beam 4 interferes with the incident beam 4 to reinforce selectively only the deflecting gratings. Simultaneously the same process occurs with beams 2 and 4 switched. The result is that the shared fanning gratings grow in strength, whereas the unshared fanning gratings collapse. The shared fanning gratings make up a volume hologram that converts beam 2 into the phase-conjugate replica of beam 4, and vice versa. The above description applies to the DPCM. The bridge,[8] the bird-wing, and the British (also known as the mutual incoherent beam coupler)[9] conjugators, all shown in Fig. 1, are somewhat more complicated; they have more than one interaction region, and in the latter two devices the light beams are also internally reflected at one or more crystal faces.

Let the two input beams have wave vectors $\mathbf{k}_2$ and $\mathbf{k}_4$, respectively. If these two beams are at least partially coherent with each other, then they will create gratings in addition to the shared transmission grating described above. These additional gratings affect the performance of the conjugator. Figure 2 shows that input beam 2 can write a backscattering grating, with wave vector $\mathbf{k} = 2\mathbf{k}_2$, with the counterpropagating conjugate beam that comes

0740-3224/95/071363-07$06.00

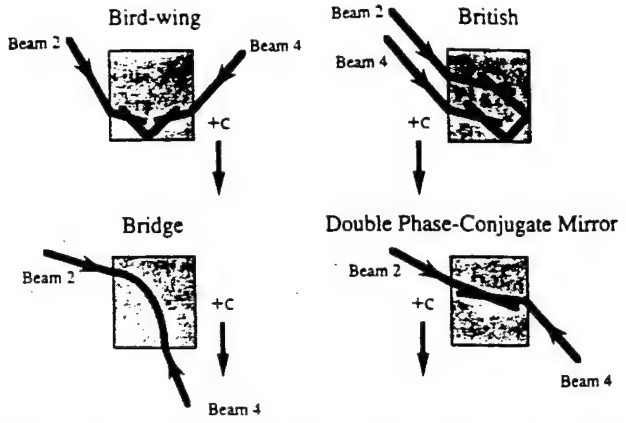

Fig. 1. Four different mutually pumped phase conjugators. The British and the bird-wing conjugators use internal reflections to guide the beams.

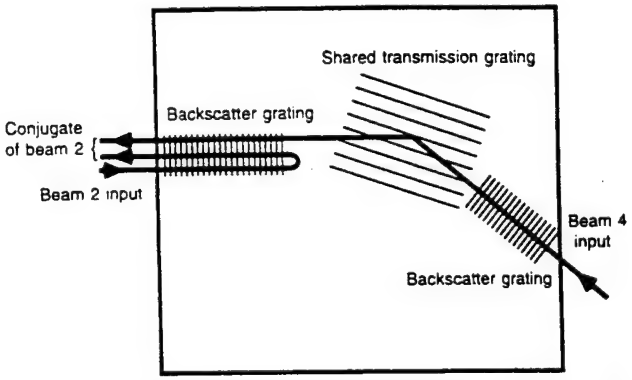

Fig. 2. Two contributions to the phase-conjugate signal: the shared transmission grating deflects each input beam into the conjugate of the other beam, whereas the backscattering gratings deflect each input beam into its own phase conjugate. Backscattering gratings form only if the two input beams are at least partially mutually coherent.

from beam 4. Similarly, along the path of beam 4 will be a backscattering grating with wave vector $\mathbf{k} = 2\mathbf{k}_4$. We note that if the input beams are mutually coherent they will also write a reflection grating of wave vector $\mathbf{k} = \mathbf{k}_2 - \mathbf{k}_4$. This reflection grating contributes only weakly and indirectly to the phase-conjugate signal, and its principal effect is to deflect a portion of the input beams out of the interaction region.

In general there are two primary contributions to the phase-conjugate signal: (1) the beam deflected from the shared transmission grating and (2) the beam reflected from backscattering gratings. The strength of only the backscattering gratings depends on the degree of mutual coherence between the input beams. In this paper we measure how these two contributions to the phase-conjugate signal vary as we alter the mutual coherence of the two incident light beams. Our measurement techniques are similar to those employed by Gruneisen *et al.*, who measured the total phase-conjugate signal in the DPCM.[10] We also present theoretical fits to our data, using a recently developed theory of four-wave mixing of partially coherent beams in such conjugators.[11]

2. EXPERIMENT

We operated our argon-ion laser at $\lambda = 514.5$ nm with an étalon to increase its coherence length to a few meters. A beam splitter (shown in Fig. 3) generated the two extraordinary-polarized input beams. We matched the optical paths of the two beams from the laser to the conjugator to within 10 cm. We equalized the beam powers incident at the entrance to the conjugator with a half-wave plate and polarizer. For all our measurements the input beam powers were typically ~14 mW/beam. At the conjugator the beams' diameters (1/*e* intensity) were 0.75 mm. We monitored the input beam power and the phase-conjugate signal for both input beams, using reflections from uncoated optical wedges. We positioned an aperture in front of each detector to ensure that we measured only the phase-conjugate beam. A Faraday isolator reduced any feedback into the argon-ion laser by at least 30 dB.

We used nominally undoped photorefractive crystals of $BaTiO_3$ to form the different conjugators. Unable to find one $BaTiO_3$ crystal that could support all four conjugators, we used two crystals that exhibited good beam fanning: a crystal named Hua [6.05 mm × 4.58 mm × 5.89 mm (parallel to the *c* axis)], for the bridge and the bird-wing conjugators, and a crystal named Twin [5.39 mm × 5.19 mm × 5.40 mm (*c* axis)] for the DPCM and the British conjugators.

We controlled the mutual coherence of the two input beams as follows. We placed a piezoelectric transducer up against a mirror mount to give beam 4 a controllable-amplitude, triangle-wave phase jitter. We set the jitter frequency at 870 Hz to take advantage of a mechanical resonance in the mirror mount. The resulting phase jitter caused any optical interference pattern written between the two input beams to oscillate spatially at 870 Hz. This frequency was an order of magnitude faster than the measured response rate of our crystals at the optical intensities used in our experiment, so the crystal effectively time averaged the phase jitter and thereby reduced the effective mutual coherence of the two input beams. Changing the amplitude of the voltage on the piezoelectric transducer varied the mutual coherence of the two input beams. We observed that imparting a phase jitter to an input beam had no effect on that beam's fanning in the crystal. This result was expected because in beam

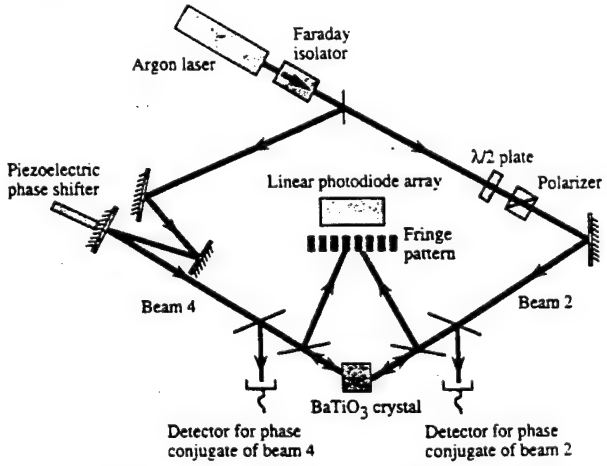

Fig. 3. Experimental setup. The piezoelectric pusher imparts a phase jitter to cause input beams 2 and 4 to be partially mutually incoherent, as measured by the linear photodiode array. The half-wave plate and the polarizer form a variable attenuator to equalize the powers of the two input beams at the crystal.

fanning all the rays originate from the same beam, so the same phase jitter was present on all these rays and canceled out.

We measured the effective mutual coherence of the two input beams by interfering them and measuring their fringe visibility $\nu \equiv (I_{max} - I_{min})/(I_{max} + I_{min})$. This fringe visibility ranges from $\nu = 0$ with mutually incoherent input beams to $\nu = 1$ with fully mutually coherent input beams. We monitored the interference fringes generated by overlapping equal intensities of both input beams on a 512-element linear photodiode array whose 20-ms readout time was comparable with the crystal's response time. We determined ν by dividing the output from the linear photodiode array by the output produced with mutually incoherent beams ($\nu = 0$) and fitting the resulting curve to a sine wave to determine its visibility, as shown in Fig. 4. We could vary the fringe visibility over almost its full range, from $\nu = 0.05$ to $\nu = 0.95$.

We initially set up four different mutually pumped conjugators, using mutually incoherent beams at angles similar to those described in Refs. 1, 5, 8, and 9. We then adjusted the beam angles and positions to optimize the stability and the power reflectivity of the phase-conjugate signals for both beams.

Starting from fully incoherent beams, we decreased the voltage applied to the piezoelectric transducer, measured the corresponding fringe visibility, and then allowed the conjugator to stabilize and to adapt to the change in mutual coherence. At each coherence point we measured six quantities:

(i) the total cw phase-conjugate reflectivity of beam 2;
(ii) the total cw phase-conjugate reflectivity of beam 4;
(iii) the phase-conjugate transmission of beam 4 (we blocked beam 2 and within a few milliseconds measured any signal that was phase conjugate to beam 2; this was a measure of the fraction of beam 4 converted into the phase conjugate of beam 2 because the shutter momentarily blocked any contribution to the phase-conjugate signal from the backscattering of beam 2);
(iv) the phase-conjugate transmission of beam 2, detected similarly to the measurement of (iii) above;
(v) the purely backscattered contribution to the phase conjugate of beam 2 (we momentarily blocked beam 4 and measured any signal that was phase conjugate to beam 2);
(vi) the purely backscattered contribution to the phase conjugate of beam 4, detected similarly to the measurement of (v) above.

We usually found no difference if we approached a particular value of ν from below or above; however, for a small number of cases (not shown in Figs. 5–9 below), we observed bistable operation, with the extreme case that some conjugators would not self-start with fully coherent input beams.

When using fully coherent input beams, we found that tapping one of the beam-steering mirrors caused the phase-conjugate signal either to drop immediately from a maximum value or to increase from a minimum value, but never to oscillate about an intermediate value. This effect implies that the phase shift between the transmitted and the backscattered beams was always 0° or 180°, as expected for a backscattering grating in $BaTiO_3$ with purely diffusive charge transport and no applied dc electric field.[12]

Figures 5–9 show the dependence of both the total phase-conjugate reflectivity and the transmission on the mutual coherence of the two input beams. Both quantities are the ratio of powers, with no corrections for Fresnel loss. The reflectivity data include both the transmitted and the backscattered contributions to the conjugate signals, whereas the transmission data reveal only the transmitted signal. The solid curves are fits to the total reflectivity, as detailed in Section 3. The phase-conjugate reflectivities and transmissions of the different conjugators depended on the particular angles and alignment of the two incident beams. Our data show behavior typical for each geometry, given that we optimized the reflectivity of the conjugators.

With mutually coherent input beams the stability of the conjugate signals depended critically on the stability of the setup, and we eventually used smaller and more stable 38.1-cm-high pedestal mounts to reduce fluctuations greatly.[13] Such reduced fluctuations can be seen by comparison of the British I and the British II conjugators shown in Figs. 8 and 9, respectively. These fluctuations are likely caused by small drifts external to the crystal. If the reflectivity fluctuated (usually on a time scale of seconds), we plotted its maximum value, and we represent these fluctuations by vertical bars on a few data points. The horizontal error bars represent the uncertainty in the relative coherence values. This uncertainty was most noticeable at the higher coherence values, where slight air currents and vibrations became

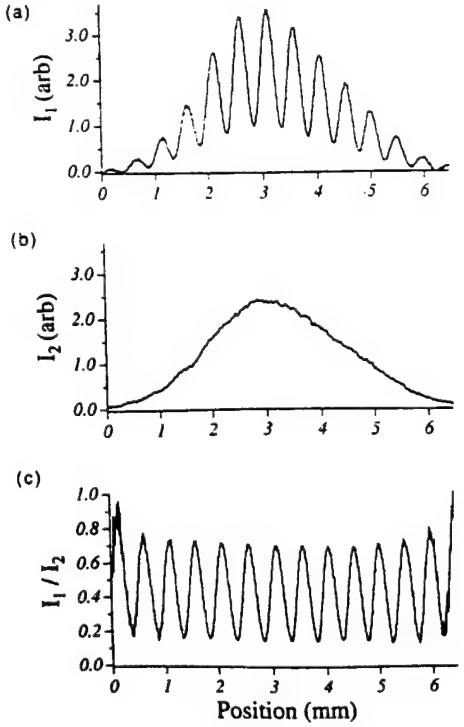

Fig. 4. Measurement of the mutual coherence ν of the two input beams. (a) Interference fringes produced by two partially mutually coherent beams with a background offset subtracted. (b) No fringes produced by two completely incoherent beams, with the same offset subtracted. Division of trace (a) by trace (b) produces the sinusoidal fringe pattern (c), which in this case has a measured visibility $\nu = 0.54$.

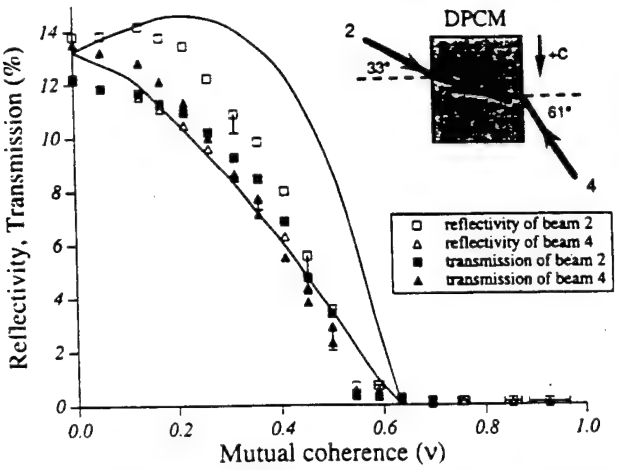

Fig. 5. Behavior of the DPCM mutually pumped phase conjugator as we alter the mutual coherence of the input beams from mutually incoherent ($\nu = 0$) to mutually coherent ($\nu = 1$). The reflectivity data include contributions from both transmission and backscattering gratings, whereas the transmission data come only from the transmission grating. The solid curves are our theoretical fits to the two total reflectivities. The horizontal and the vertical bars on a few representative data points show the uncertainty in the measured coherence values and the fluctuations in the measured signals. Note that the DPCM conjugator turns off when the input beams become too coherent with each other.

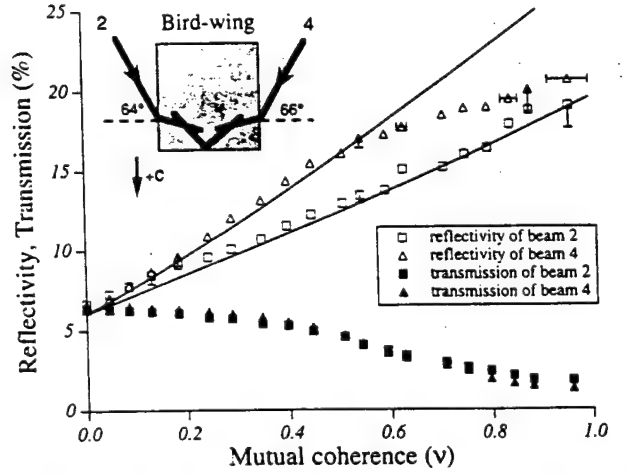

Fig. 6. Bird-wing conjugator. The symmetry of the beam paths inside the crystal ensures similar data for the two input beams. The fits are to the reflectivity data.

important and limited the fringe visibility $\nu < 0.95$. All the phase-conjugate signals were stable, with mutually incoherent input beams. Table 1 lists our subjective comparison of all four conjugators.

The British conjugator exhibited different behaviors according to the position and the angle of the input beams. Figure 8 shows data for British I, in which we positioned both input beams close to the $+c$ face of the crystal. The resulting coupling channel was short, and the curvature of the two input beams had a pronounced asymmetry inside the crystal, with beam 2 fanning more strongly than beam 4. In contrast, Fig. 9 shows data for British II, in which we positioned both input beams slighter further from the $+c$ face and at smaller angles of incidence. This conjugator developed a longer coupling channel, with both beams now having similar curvatures inside the crystal.

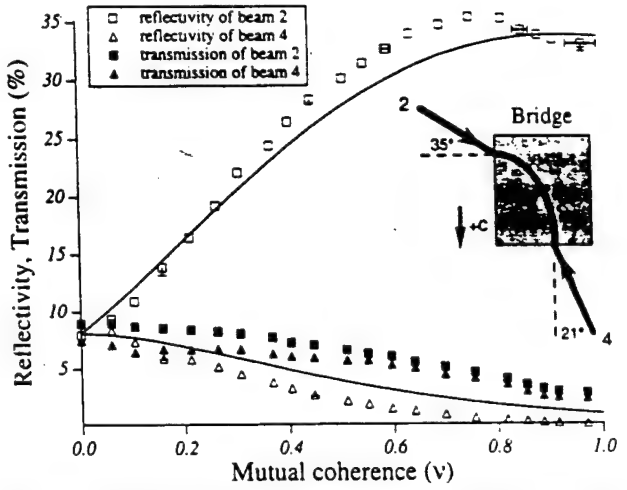

Fig. 7. Bridge conjugator. The asymmetry shown in the reflectivities of the bridge conjugator is caused by the difference in the sign of the backscattering coupling strength for the two input beams. The fits are to the reflectivity data.

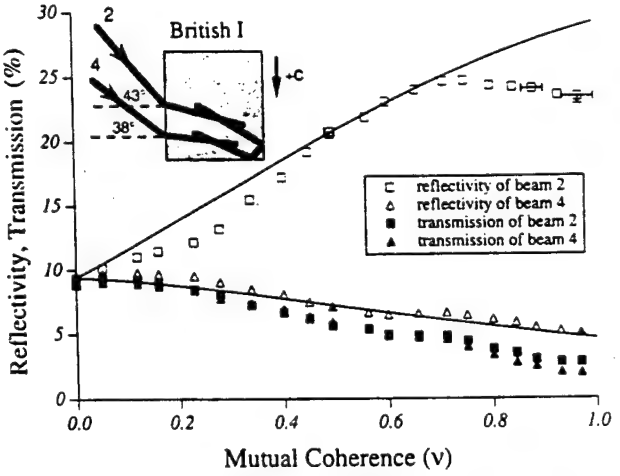

Fig. 8. British I conjugator has a small loop in the crystal. The fits are to the reflectivity data.

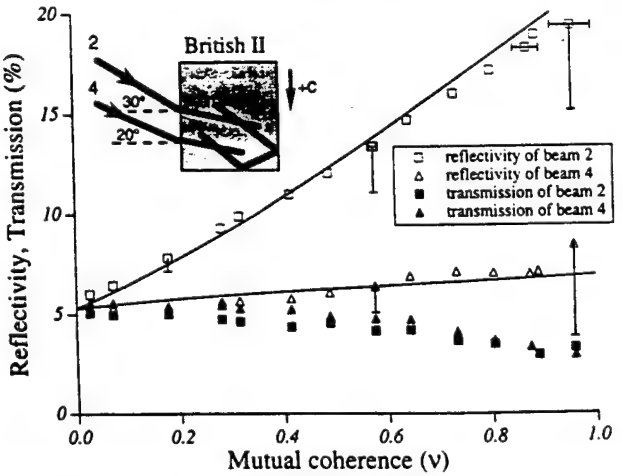

Fig. 9. British II conjugator has a larger loop in the crystal. The large signal fluctuations shown in these data were caused by a less stable optical setup. When we switched to a more stable setup the British conjugator was the least noisy of the four types of conjugator investigated. The fits are to the reflectivity data.

Table 1. Ease-of-Use and Signal Fluctuations of the Mutually Pumped Phase Conjugators

Conjugator	Ease of Setup	Signal Fluctuations
DPCM	Easy	Moderate
Bird wing	Somewhat easy	Small
Bridge	Somewhat difficult	Small
British	Difficult	Very small

In general, as we increased the mutual coherence of the two input beams at least one conjugate signal increased, whereas both transmissions decreased. The exception was the DPCM shown in Fig. 5, which usually ceased to operate when the input beams became coherent with each other ($\nu = 1$). We could obtain phase-conjugate signals from the DPCM with fully coherent input beams, but only after tedious alignment. Both phase-conjugate outputs in the bird-wing conjugator and the British II conjugator increased as $\nu \rightarrow 1$, whereas in the bridge and the British I conjugators one conjugate signal grew, but the other diminished in power. At $\nu \sim 1$, we checked that the bridge, the bird-wing, and the British conjugators were not acting as self-pumped conjugators by confirming that both input beams were required for sustained conjugation.

In the DPCM we occasionally observed that the phase-conjugate reflectivity of beam 2 increased steadily as ν increased from 0 to 0.25, where the reflectivity then dropped abruptly, as predicted by our theoretical plots. However, most of the time the reflectivity of beam 2 in the DPCM began to collapse at $\nu \approx 0.1$, as shown in Fig. 5. The DPCM data presented here agree in general with those reported by Gruneisen *et al.*,[10] with the exception that their DPCM conjugated weakly even with high mutual coherence. We note that our theory does not take into account the effects of conical scattering, which can cause significant loss.[14] Also, unequal fanning losses experienced by beams 2 and 4 can cause the different reflectivities observed for the two beams at $\nu = 0$.

As the mutual coherence of the two input beams is increased, backscattering gratings increase in strength and affect the performance of the conjugators in three ways. First, each input beam can now exchange energy with its own phase-conjugate beam through two-beam coupling, with the direction of energy transfer being determined by the orientation of the beams with respect to the crystal's c axis. Second, this two-beam coupling can create an imbalance in the two input beams' intensities inside the crystal; this imbalance reduces the cross-erasure efficiency, which weakens the transmission grating. Third, backscattering gratings can decrease the overall transmission of a conjugator by simply reflecting energy away from the transmitted phase-conjugate beam.

Figure 10 shows how the computed amplitude coupling coefficient γ_b of a backscattering grating varies as a function of the angle θ between the beams' propagation directions inside the crystal and the c axis.[15] For this calculation we use recent values for the effective Pockels coefficients, which include the small influence of elastic stiffness, piezoelectric stress, and the elasto-optic effect.[16] We find that input beams traveling at angles $6° < \theta < 90°$ are depleted by backscattering gratings. We estimate that, in the bird-wing and the British conjugators, the angles of both conjugate beams with respect to the c axis lie in the range $95° < \theta < 150°$, so, according to Fig. 10, in these conjugators both conjugate beams gain from backscattering gratings at the expense of the input beams. To estimate the contribution of backscattering gratings to the phase-conjugate signal we use the relation

$$\text{backscatter reflectivity} = (\sqrt{\text{total reflectivity}} \pm \sqrt{\text{transmission}})^2,$$

where the terms are added if the components are out of phase or are subtracted if they are in phase, and we neglect the contribution of reflection grating to the conjugate signal. For example, for the bridge conjugator the computed backscattering power reflectivity for beam 2 with fully mutually coherent beams ($\nu = 1$) is $(\sqrt{33\%} - \sqrt{2.4\%})^2 = 17.6\%$. This result agrees with our measured backscattered power reflectivity of 18%. We performed such calculations for all the data shown and found good agreement between the calculated and the measured backscattered contributions. This finding confirms that the conjugate signals are due to transmission and backscattering gratings and that reflection gratings can be neglected in the analysis of these experiments.

Backscattering gratings affect the different conjugators differently. The effect of backscattering gratings is seen most clearly in the data of Fig. 7 for the bridge conjugator. Here one conjugate beam travels somewhat opposite the c axis at $\theta \sim 130°$ and so gains from its backscattering grating, whereas the other conjugate beam is at $\theta \sim 70°$ and so is depleted by its backscattering grating. This effect causes the asymmetry seen in the reflectivity data. In contrast, in the bird-wing conjugator the path of the two beams are symmetric about the c axis, and both conjugate beams gain equally by backscattering. Figure 6 confirms that making the input beams coherent has little effect on the transmission grating, inasmuch as the strength of this grating depends only on the rela-

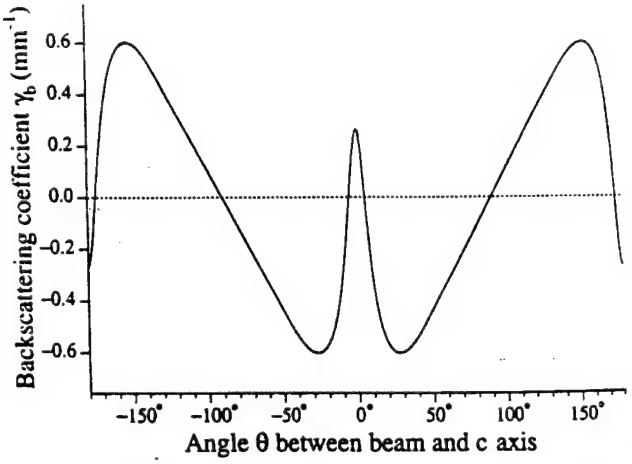

Fig. 10. Amplitude two-beam coupling efficient γ_b for a beam and its counterpropagating beam as a function of the internal angle between the beam and the $BaTiO_3$ crystal's c axis. A positive coupling coefficient means that the beam is gaining energy from its counterpropagating beam. For example, a beam propagating between 6.7° and 90° to the $+c$ axis is depleted by its counterpropagating beam. This calculation uses recent values for the electro-optic coefficients[12] and assumes an effective charge-carrier density of $N = 5 \times 10^{16}$ cm^{-3} and e-polarized rays at $\lambda = 514.5$ nm.

tive intensity of the two input beams and not on their mutual coherence. For the DPCM, as the input beams are made more coherent with each other, the resulting backscattering gratings amplify input beam 4 and deplete input beam 2, and the resulting intensity imbalance so weakens the primary transmission grating that it collapses, as shown in Fig. 5. We confirmed this effect by increasing the power of input beam 2 in the DPCM while keeping the power of beam 4 constant. We found that conjugation would then persist even with fully coherent beams because now the intensities of the input beams were more closely matched inside the crystal. In contrast, conjugation ceased when we decreased the power of beam 2. Evidently the bridge and the British conjugators fall somewhere between the bird wing and the DPCM. These conjugators experience an intensity imbalance with mutually coherent input beams, but not enough to cause the transmission grating to collapse.

3. THEORY

We write coupled-wave equations that include transmission, reflection, and backscattering gratings,[7] and we also include the mutual coherence parameter β_{ij} between beams i and j.[17] For a single interaction region we obtain

$$\frac{dA_1}{dz} = \gamma_t \frac{A_1A_4^* + A_2^*A_3}{I_0} A_4 + \gamma_r \frac{|\beta_{13}|A_1A_3^* + |\beta_{24}|A_2^*A_4}{I_0} A_3 + \gamma_b \frac{|\beta_{12}|A_1A_2^*}{I_0} A_2 - \alpha A_1,$$

$$\frac{dA_2^*}{dz} = \gamma_t \frac{A_1A_4^* + A_2^*A_3}{I_0} A_3^* + \gamma_r \frac{|\beta_{13}|A_1A_3^* + |\beta_{24}|A_2^*A_4}{I_0} A_4^* + \gamma_b \frac{|\beta_{12}|A_1A_2^*}{I_0} A_1^* + \alpha A_2^*,$$

$$\frac{dA_3}{dz} = \gamma_t \frac{A_1A_4^* + A_2^*A_3}{I_0} A_2 + \gamma_r \frac{|\beta_{13}|A_1^*A_3 + |\beta_{24}|A_2A_4^*}{I_0} A_1 - \gamma_{b'} \frac{|\beta_{34}|A_3A_4^*}{I_0} A_4 + \alpha A_3,$$

$$\frac{dA_4^*}{dz} = -\gamma_t \frac{A_1A_4^* + A_2^*A_3}{I_0} A_1^* + \gamma_r \frac{|\beta_{13}|A_1^*A_3 + |\beta_{24}|A_2A_4^*}{I_0} A_2^* - \gamma_{b'} \frac{|\beta_{34}|A_3A_4^*}{I_0} A_3 - \alpha A_4^*.$$

The boundary conditions are

$$A_1(0) = A_3(L) = 0,$$

$$\frac{|A_4(0)|^2}{|A_2(L)|^2} = q,$$

where A_2 and A_4 are amplitudes of the input beams and A_1 and A_3 are their respective conjugates; $I_0 = |A_1|^2 + |A_2|^2 + |A_3|^2 + |A_4|^2$ is the total intensity; and γ_t, γ_r, γ_b, $\gamma_{b'}$ are the coupling coefficients for the transmission, the reflection, and the two backscattering gratings, respectively. The backscattering gratings for the two input beams can have different strengths in general. L is the interaction length, and z is the direction of propagation for beams 1 and 4. Also, α is the bulk absorption coefficient, and q is the power ratio of the two incident input pump beams just inside their respective crystal faces. When the two input beams are mutually incoherent, i.e., when $|\beta_{24}| = |\beta_{13}| = |\beta_{12}| = |\beta_{34}| = 0$, the coupled-wave equations reduce to the conventional equations, where only the transmission grating is present.[6] Because the photorefractive effect in $BaTiO_3$ crystals is dominated by diffusive charge transport, here the coupling coefficients are all real numbers. We simplify the coupled equations by approximating $|\beta_{24}| = |\beta_{13}| = |\beta_{13}| = |\beta_{34}| = |\beta|$ because we calculate that under experimental conditions the differences between the $|\beta_{ij}|$ values are less than ~5%. Although our theory is based on a one-interaction-region model, the equations can be extended to multiple regions with different coupling strengths.[18]

We solve the coupled-wave equations with standard fourth-order Runge–Kutta and shooting algorithms. The mutual coherence is equal to the measured fringe visibility, $|\beta| = \nu$, because the two beams that we interfere in our visibility measurements had equal intensity.[17] We use our measured values for the bulk absorption of the $BaTiO_3$ crystal ($\alpha = 2.6\ cm^{-1}$ in Hua and $\alpha = 1.5\ cm^{-1}$ in Twin). For each conjugator we calculate the ratio q of the input beam powers just inside the entrance face of the crystal from our measured incident beam power and the measured Fresnel loss at the crystal surface.

We fit our experimental data with four coupling-strength parameters ($\gamma_t \cdot L$, $\gamma_r \cdot L$, $\gamma_b \cdot L$, $\gamma_{b'} \cdot L$). We first choose $\gamma_t \cdot L$ to make the computed reflectivities match the experimental values measured with mutually incoherent beams ($\nu = 0$). We then adjust the values of the remaining parameters to best fit the measured phase-conjugate reflectivities with $\nu \neq 0$, as shown by the solid curves in Figs. 5–9. For DPCM, where the input beams are nearly counterpropagating, we impose the additional restriction $\gamma_b = -\gamma_{b'}$. Table 2 shows that the resulting gain–length products are well within the range expected for $BaTiO_3$ and have the correct sign for the given beam directions in the crystal. For example, from the measured angles of incidence of the input beams and the calculated backscattering coefficient of Fig. 10

Table 2. Values of the Fitting Parameters[a]

Conjugator	$\gamma_t \cdot L$	$\gamma_r \cdot L$	$\gamma_b \cdot L$	$\gamma_{b'} \cdot L$	$\alpha \cdot L$	L (mm)
DPCM	2.8	2.2	1.1	−1.1	0.5	6.0
Bridge	2.9	1.0	4.1	−0.4	0.65	4.5
Bird wing	3.3	0.5	2.3	2.4	0.9	8.0
British I	3.9	0.7	2.4	1.2	1.1	11.0
British II	3.3	1.1	2.1	0.6	0.76	11.5

[a]Amplitude gain times length for the transmission, the reflection, the two backscattering gratings, and the intensity absorption used in our theoretical fits. A negative value for the backscattering coefficient corresponds to a depletion of the conjugate signal. Although not required for the fits, our estimate of the interaction length (±1 mm) inside each crystal, obtained by observation of the actual beam paths, is also provided.

we expect that, in the DPCM and in the bridge conjugator, backscattering gratings will decrease the conjugate of beam 4, and not of beam 2. In these two conjugators the phase-conjugate to beam 4 travels at angles $6° < \theta < 90°$ with respect to the positive c axis, which makes $\gamma_{b'} < 0$. For all other cases $\gamma_b > 0$ and $\gamma_{b'} > 0$, and the backscattering gratings couple energy from each input beam into its respective phase-conjugate beam. We noticed that increasing the value of γ_r always decreases the strength of the conjugate signal for all four conjugators.

4. CONCLUSION

With two mutually incoherent light beams incident upon a mutually pumped phase conjugator, each phase-conjugate signal comes exclusively from the other light source. However, when the two incident light beams are mutually coherent, each phase-conjugate signal is made up of a mixture of the light from both light sources. From the viewpoint of locking lasers with such conjugators, both the transmitted and the backscattered components are useful for injection locking because both are at the same frequency and are phase conjugate to the output of the slave laser. However, because the backscattering grating cannot respond to any light modulations faster than the grating's response time, only the transmitted component can phase lock or phase modulate a laser.

Of the four mutually pumped phase conjugators investigated here, only the bird-wing and the British conjugators provide two conjugate output beams when the two input beams are fully mutually coherent. The bridge conjugator produces only one output beam of significant intensity when the beams are coherent. This result might be advantageous in laser-locking schemes in which feedback into the injecting laser is undesirable. The DPCM ceases operation with fully mutually coherent beams. A one-region, one-dimensional numerical model was able to fit the main trends of our data with reasonable values for all the fitting parameters.

ACKNOWLEDGMENTS

Research at the University of Southern California was supported by U.S. Air Force Office of Scientific Research grant F49620-92-J-0022.

*Present address, Energy Power Group, 900 South Shackleford Road, Little Rock, Arizona 72211.

REFERENCES AND NOTES

1. S. Weiss, S. Sternklar, and B. Fischer, "Double phase-conjugate mirror: analysis, demonstration, and applications," Opt. Lett. **12,** 114 (1987). Note that the orientation of the c axis of our DPCM differs from that shown in Fig. 1 of this reference.
2. S. Sternklar, S. Weiss, M. Segev, and B. Fischer, "Beam coupling and locking of lasers using photorefractive four-wave mixing," Opt. Lett. **11,** 528 (1986).
3. M. W. Wright and J. G. McInerney, "Injection locking semiconductor lasers with phase conjugate feedback," Opt. Commun. **110,** 689 (1994).
4. S. MacCormack, J. Feinberg, and M. H. Garrett, "Injection locking a laser-diode array with a phase-conjugate beam," Opt. Lett. **19,** 120 (1994).
5. M. D. Ewbank, "Mechanism for photorefractive phase conjugation using incoherent beams," Opt. Lett. **13,** 47 (1988).
6. P. Yeh, "Coupled-mode theory of hologram sharing in mutually pumped phase conjugators," Appl. Opt. **28,** 1961 (1989).
7. M. Cronin-Golomb, B. Fischer, J. O. White, and A. Yariv, "Theory and applications of four-wave mixing in photorefractive media," IEEE J. Quantum Electron. **QE-20,** 12 (1984).
8. D. Wang, Z. Zhang, Y. Zhu, S. Zhang, and P. Ye, "Observations on the coupling channel of two mutually incoherent beams without internal reflections in $BaTiO_3$," Opt. Commun. **73,** 495 (1989).
9. A. M. C. Smout and R. W. Eason, "Analysis of mutually incoherent beam coupling in $BaTiO_3$," Opt. Lett. **12,** 498 (1987).
10. M. T. Gruneisen, E. D. Seeberger, J. F. Mileski, and K. Koch, "Effects of laser coherence on coupling efficiency for the double phase-conjugate mirror," Opt. Lett. **16,** 596 (1991).
11. Q. B. He and P. Yeh, "Photorefractive mutually-pumped phase conjugation with partially coherent beams," Appl. Phys. B **60,** 47 (1994).
12. R. S. Cudney, R. M. Pierce, G. D. Bacher, and J. Feinberg, "Absorption gratings in photorefractive crystals with multiple levels," J. Opt. Am. B **8,** 1326 (1991).
13. These mounts were provided by New Focus, Inc., 1275 Reamwood Avenue, Sunnyvale, Calif. 94089-2256.
14. D. Statman and B. Liby, "Two-beam cross coupling from mutually incoherent lasers," J. Opt. Soc. Am. B **6,** 1884 (1989).
15. K. R. MacDonald, J. Feinberg, M. Z. Zha, and P. Günter, "Asymmetric transmission through a photorefractive crystal of barium titanate," Opt. Commun. **50,** 146 (1984).
16. M. Zgonik, P. Bernasconi, M. Duelli, P. Schlesser, P. Günter, M. H. Garrett, D. Rytz, Y. Zhu, and X. Wu, "Dielectric, elastic, piezoelectric, electro-optic and elasto-optic, tensors of $BaTiO_3$ crystals," Phys. Rev. B **50,** 5941 (1994).
17. See, e.g., M. Born and E. Wolf, *Principles of Optics*, 6th ed. (Pergamon, New York, 1980), Chap. 10. Note that the symbol for mutual coherence is often γ.
18. Q. C. He, "Theory of photorefractive phase conjugators with mutually incoherent beams," IEEE J. Quantum Electron. **24,** 2507 (1988).

Polarization-dependent mechanism transformation during self-pumped phase conjugation in $BaTiO_3$:Ce

Yingwu Lian, S. H. Lin,* Scott Campbell, Ken Y. Hsu,* and Pochi Yeh

Department of Electrical and Computer Engineering, University of California, Santa Barbara, Santa Barbara, California 93106

Yong Zhu

Institute of Physics, Chinese Academy of Sciences, Beijing 100080, China

Received April 25, 1995

We report the results of experimental investigations of the mechanism transformation from four-wave mixing and stimulated photorefractive backscattering to four-wave mixing and total internal reflection during self-pumped phase conjugation in a photorefractive crystal by varying the plane of polarization of the input beam. The use of a mixed-polarization input beam can change the fanning pattern, which leads to the mechanism transformation and an enhancement of the phase-conjugation reflectivity. The temporal dynamics of the buildup process indicate that such an enhancement is due to the presence of both types of mechanism during phase conjugation. In addition, we compare the contributions of $2k$ gratings with the phase conjugation during both mechanisms. © 1995 Optical Society of America

The phenomenon of self-pumped phase conjugation (SPPC) has received a great deal of attention because of its important potential applications. In 1982, Feinberg[1] demonstrated a SPPC mirror by using a single crystal without any external mirrors. Since then, there has been much interest in trying to understand the physical mechanisms. In 1983, MacDonald and Feinberg[2] proposed a model in which the phase-conjugate wave was generated by means of four-wave mixing (FWM) in two separate interaction regions. These two interaction regions were coupled by total internal reflections within the crystal. This is known as the four-wave mixing and total internal reflection (FWM-TIR), or Cat, model. Recently we[3,4] proposed an alternative model [four-wave mixing and stimulated photorefractive backscattering (FWM-SPB), in which the SPB is produced by the formation of $2k$ gratings] to explain the origin of the SPPC observed in $KTaNbO_3$ and $BaTiO_3$:Ce crystals. In both FWM-TIR and FWM-SPB conjugators the SPPC is established through FWM interactions when the fanning beam is retroreflected by TIR or SPB. In the FWM-TIR phase conjugator, the retroreflection of the fanned beam is due to two successive total internal reflections from one of the crystal's corners. Thus a feedback optical loop with two FWM interaction regions inside the crystal can usually be seen. In the FWM-SPB phase conjugator the retroreflection of the fanned beam is generated by SPB, which may be seeded by random scattering centers in the crystal or on the crystal's surfaces or even by an external retroreflector. As a result, individual filaments that contain counterpropagating beams can often be seen.

In a typical SPPC experimental configuration an extraordinarily polarized input beam is incident upon the a face of a regular-cut $BaTiO_3$ photorefractive crystal. The SPPC formation mechanism is usually determined by the fanning pattern and the boundary conditions. Generally, SPPC is generated by the FWM-SPB mechanism in some doped crystals but by the FWM-TIR mechanism in undoped crystals. This is due to stronger fanning and larger coupling coefficients for $2k$ gratings in doped crystals. Recently we observed that the formation mechanism of SPPC was transformed from FWM-SPB to FWM-TIR when the wavelength of the input beam was increased.[4] In this Letter we report, for the first time to our knowledge, the mechanism transformation during SPPC in a given crystal and at a fixed wavelength that is due to the variation of the polarization state of the input beam. We also show that the phase-conjugation (PC) reflectivity can be increased by changing the plane of polarization of the input beam. In this regime of high reflectivity, both mechanisms are responsible for the PC. In addition, we compare the contributions of $2k$ gratings to PC during both mechanisms by using an ordinarily polarized erasure beam.

In our experimental demonstration we used a Ce-doped $BaTiO_3$ crystal that had a red-orange color and a dopant concentration of approximately 30 parts in 10^6. The crystal was poled and 0° cut with dimensions 6.15 mm × 5.20 mm × 8.2 mm ($a \times b \times c$). In all our SPPC experiments, we utilized the output from an Ar^+ laser at 514.5 nm, extraordinarily polarized, directly incident upon the a face of our crystal at an external angle of $\theta = 60°$. The experimental setup is shown in Fig. 1. With an input intensity of approximately 1 W/cm^2, the plane of polarization of the input beam could be rotated by a half-wave plate.

In $BaTiO_3$:Ce crystals, extraordinarily polarized beams produce the strongest fanning effects. In our experiment we were able to change the fanning pattern by varying the plane of polarization of the input beam. Figure 2 shows the images of these different fanning patterns at various polarization states before the phase conjugation reaches its steady state. It is known that the coupling coefficient in $BaTiO_3$:Ce crystals for an ordinarily polarized beam is much less than that of an extraordinarily polarized beam, and the cross coupling is negligible.[5] Thus the

0146-9592/95/161683-03$6.00/0

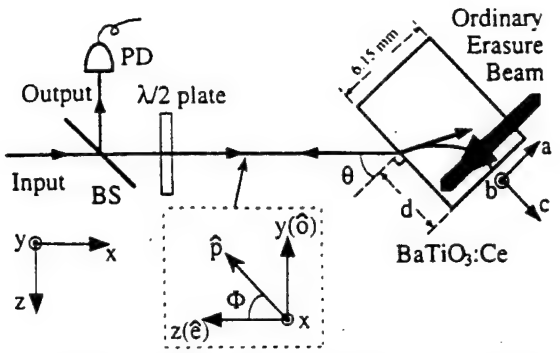

Fig. 1. Experimental setup utilized for studying the polarization-dependent mechanism transformation during SPPC. The external incident angle was $\theta = 60°$, and the incident position d was 4 mm. As shown in the inset, the polarization state Φ of the input beam is defined as the angle of the polarization $\hat{p}$ measured from yz plane. PD, photodetector; BS, beam splitter.

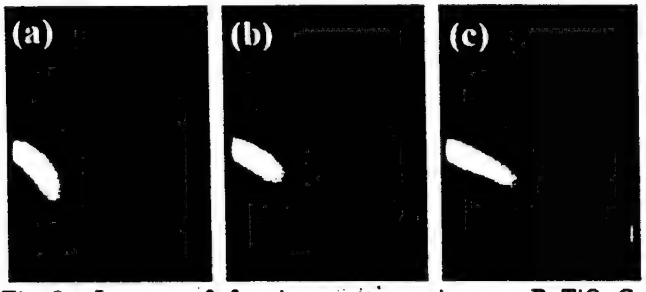

Fig. 2. Images of fanning patterns in our $BaTiO_3$:Ce crystal at different polarization angles of the incident beam before SPPC reaches its steady state: (a) $\Phi = 0°$, (b) $\Phi = 20°$, (c) $\Phi = 60°$. The c axis of the crystal is directed from the top to the bottom of the image, and the input beam is propogating from left to right.

extraordinarily polarized component will contribute significantly to the fanning, whereas the ordinarily polarized component, not being phase matched to the gratings written by the extraordinary component, will only serve to erase some of the index gratings and to reduce the effective coupling constant. From Fig. 2, we also note that the fanning patterns move to the corner of the crystal as Φ increases. This means that the fanning (or the fanning coupling constant) can be effectively controlled by use of a mixed-polarization beam. We believe that these changes of the fanning pattern and the effective coupling constant are responsible for the mechanism transformation during SPPC in $BaTiO_3$:Ce crystals.

Figure 3(a) shows the beam path in the crystal at $\Phi = 0°$ when the PC signal reached steady state, demonstrating a typical FWM-SPB mechanism. The input beam was depleted completely after propagating through a short distance and bent toward the bottom surface of crystal because of strong fanning. The beam pattern at steady state is characterized by many filaments that are produced through the SPB process by $2k$ gratings. This SPPC formation is significantly different from the traditional FWM-TIR mechanism. There is no closed optical path involving the corner of the crystal. The mechanism of this kind of phase conjugation was previously modeled and explained in Ref. 3.

Figure 3(b) shows a typical beam path in the crystal at $\Phi = 20°$, when two types of mechanism exist simultaneously. The time response of the self-pumped phase-conjugate reflectivity was found to consist of a two-plateau structure (Fig. 4). When the input beam was turned on, an initial quasi-steady-state SPPC reflectivity was reached, and two filaments appeared. This looked like a FWM-SPB phase conjugator. After this stage a weak loop started to appear and the SPPC reflectivity gradually reached

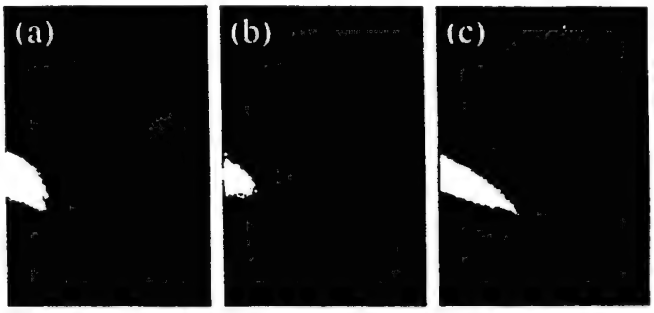

Fig. 3. Images of steady-state beam paths during SPPC at three different polarization angles of the incident beam: (a) $\Phi = 0°$, (b) $\Phi = 20°$, (c) $\Phi = 60°$.

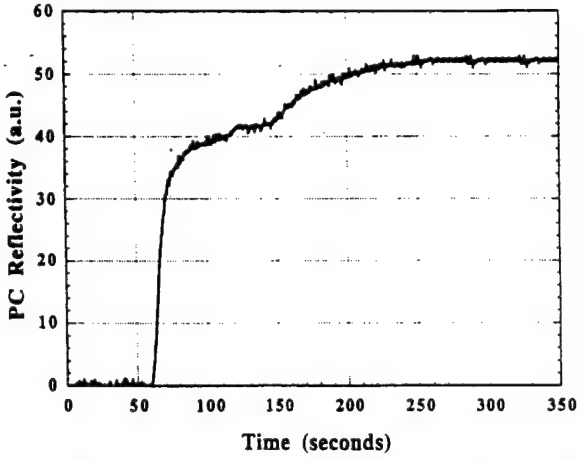

Fig. 4. Time evolution of the phase-conjugate signal. The pump intensity was approximately 1 W/cm^2.

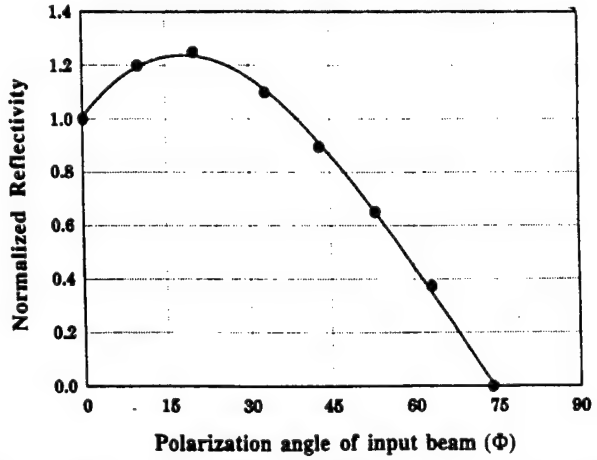

Fig. 5. Normalized PC reflectivity as a function of the polarization angle Φ of the input beam. These data are not corrected for Fresnel reflections.

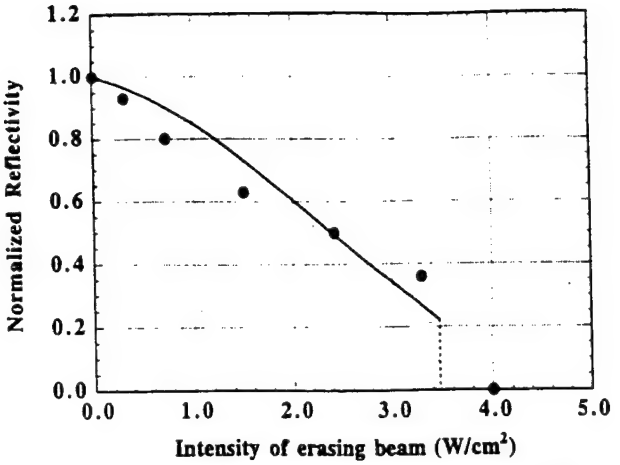

Fig. 6. PC reflectivity as a function the intensity of the ordinarily polarized erase beam. Note the phase-conjugate threshold at an erase intensity of ≈4 W/cm². The solid curve is from a theoretical calculation for the FWM-SPB case.

a second steady state. This means that the FWM-SPB mechanism was mainly responsible for the SPPC formation at first, and then the FWM-TIR mechanism gradually settled in. When the ordinarily polarized component of the input beam was increased by rotation of the input plane of polarization, the filaments gradually moved to the corner of the crystal. The optical beam paths supporting SPPC were gradually transformed into a FWM-TIR arrangement. Figure 3(c) shows the case with $\Phi = 60°$, in which the optical path loop at the bottom-right-hand corner is clearly shown.

The PC reflectivity as a function of the plane of polarization Φ of the input beam is shown in Fig. 5. Here the reflectivity is defined as I^*/I_e, where I^* is the PC output and I_e is the intensity of the extraordinary component of the input beam. We note that the phase-conjugate output is always extraordinarily polarized regardless of the input polarization state. The reflectivity is normalized to that of a totally extraordinarily polarized state of input beam ($\Phi = 0°$). We observed that there was a reflectivity enhancement of ≈20% for $\Phi = 20°$ when the two SPPC mechanisms existed simultaneously. This leads to the conclusion that optimal SPPC output is produced by utilization of both types of mechanism. The phenomena of mechanism transformation during SPPC and the enhancement of phase-conjugate reflectivity are due to the presence of an ordinarily polarized component in the input beam that reduces the strength of the fanning pattern. Thus the energy loss that is due to fanning can be limited.

To illustrate further the difference between the FWM-SPB and FWM-TIR mechanisms, we uniformly illuminated the filaments by using a second erasure beam incident from the right-hand side of the crystal (see Fig. 1). The erasure beam was incoherent with the input beam and was ordinarily polarized. The erasure beam reduced the modulation depth of the index grating and the coupling coefficients throughout the region of the filaments (or the loop). We measured the PC reflectivity as a function of the intensity of the erasure beam, I_0, to compare the effect of $2k$ gratings in both FWM-SPB and FWM-TIR. The backscattering coupling coefficient γ_{2k} may be rewritten as $\gamma_{2k}(I_0) = \gamma_{2k}^0/(1 + I_0/I)$, where I_0 is the intensity of the erasure beam, I is the total intensity of the forward-propagating beam (fanning beam) and the backward-propagating beam in the filament (or the loop), and γ_{2k}^0 is the coupling coefficient at $I_0 = 0$. Figure 6 shows the phase-conjugate reflectivity as a function of I_0 with an interaction length of $L = 3$ mm for the $2k$ gratings. We note that the PC reflectivity decreased as the intensity of erasure beam increased and exhibited a sharp threshold at $I_0 \approx 4$ W/cm² in the FWM-SPB model [shown in Fig. 3(a)]. In our experiment, I was approximately 2 W/cm², and the average coupling coefficient γ_{2k}^0 for the case shown in Fig. 3(a) was approximately 10 cm^{-1}. In the FWM-TIR model of SPPC, the decrease in reflectivity (which is the ratio of the PC signal with and without the erase beam) is approximately 10% when the intensity of the erasure beam is $I_0 \approx 4$ W/cm². We conclude therefore that the $2k$ gratings in the loop make very little contribution to the phase conjugation. This result is in agreement with the research of Ref. 6. In FWM-SPB, the initial retroreflections from crystal surface imperfections are very weak. Thus the presence of $2k$ gratings is essential for enhancement of the retroreflection. In the case of FWM-TIR, the corner cube is already providing nearly a 100% retroreflection regardless of the presence of $2k$ gratings.

In summary, we have demonstrated a polarization-dependent mechanism transformation during SPPC in a photorefractive $BaTiO_3$:Ce crystal. We have also shown that the introduction of an ordinarily polarized component in the input beam can modify the fanning pattern and enhance the PC reflectivity. In addition, we have compared the contribution of the $2k$ gratings with the phase conjugation for both mechanisms.

This research was supported in part by the U.S. Office of Naval Research and the U.S. Air Force Office of Scientific Research. Pochi Yeh is also a principal technical advisor at Rockwell International Science Center, Thousand Oaks, California.

*Permanent address, Institute of Electro-Optical Engineering, National Chiao Tung University, Hsinchu, Taiwan.

References

1. J. Feinberg, Opt. Lett. **7,** 486 (1982).
2. K. R. MacDonald and J. Feinberg, J. Opt. Soc. Am. **73,** 548 (1983).
3. Y. W. Lian, H. Gao, P. Ye, Q. Guan, and J. Wang, Appl. Phys. Lett. **63,** 1754 (1993).
4. Y. W. Lian, S. X. Dou, H. Gao, Y. Zhu, X. Wu, C. Yang, and P. Ye, Opt. Lett. **19,** 610 (1994).
5. Q. B. He and P. Yeh, Appl. Opt. **33,** 283 (1994).
6. G. L. Wood, E. J. Sharp, and G. J. Salamo, Proc. Soc. Photo-Opt. Instrum. Eng. **1626,** 21 (1992).

Appl. Phys. B 60, 47–50 (1995)

Applied Physics B Lasers and Optics

Photorefractive mutually pumped phase conjugation with partially coherent beams

Q. B. He[1], P. Yeh[2,] *

[1] Jet Propulsion Laboratory, MS 303-310, California Institute of Technology, 4800 Oak Grove Drive, Pasadena, CA 91109-8099, USA (Fax: + 1-818/393-5013, E-mail: QHE@telerobotics.jpl.nasa.gov)
[2] Department of Electrical and Computer Engineering, University of California at Santa Barbara, Santa Barbara, CA 93106, USA

Received: 5 May 1994/Accepted: 5 June 1994

Abstract. We investigate the mutually pumped phase-conjugation process in photorefractive media with partially coherent pump beams. We consider the effects of transmission, reflection, and $2k$-reflection gratings as well as the depletion of both pump beams. The theoretical results can be employed to qualitatively explain the experimental observations.

PACS: 42.65.Hw; 42.80; 42.70

The Mutually Pumped Phase-conjugation (MPPC) process is one of the most important discoveries in the field of photorefractive nonlinear optics over the past fifteen years [1–3]. Since it does not require mutual coherence of the two pump beams, the mutually pumped phase conjugator has great potentials in many applications including optical communication, laser phase locking, optical interconnect, optical computing, etc. [3–6]. Experimentally, it has been observed that the mutual coherence of the two pump beams changes the performance of the mutually pumped phase conjugator considerably. This is critical in applications such as laser phase locking, and coherent optical communication. For example, in the phase-locking applications the two free-runing lasers are mutually incoherent before they are phase locked. These two laser beams are incident into a photorefractive mutually pumped phase conjugator as the pump beams. Once the phase conjugation process occurs and if the frequency of the lasers are colse to each other, these two lasers tend to be phase locked, i.e., they become partially or fully coherent. It would be desirable to maintain an efficient coupling through the mutually pumped phase-conjugation process with partially or fully coherent laser beams so that lasers can be stably phase locked. However, it has been observed experimentally that the performance of some configurations of the photorefractive MPPCs is quite sensitive to the degree of mutual coherence of the pump beams [7]. In previous theoretical models, the pump beams are assumed mutually incoherent and only the transmission gratings are considered. In fact, when the two pump beams are partially coherent, reflection and $2k$-reflection gratings must be taken into account. Although multiple grating effects in the conventional four-wave mixing geometry have been investigated theoretically, the results are unable to explain the experimental observations due to the geometry differences and various limitations [8, 9]. In this paper, we present theoretical studies of the mutually pumped phase-conjugation process with partially

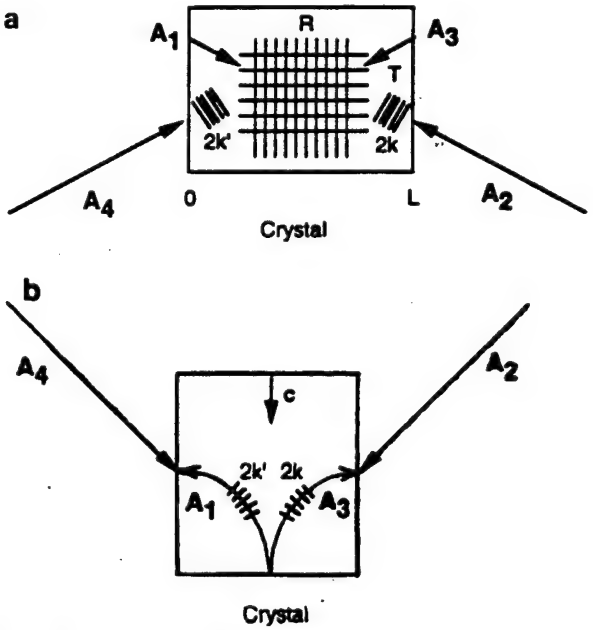

Fig. 1. a Schematic of a photorefractive mutually pumped phase conjugator with the presence of transmission (T), reflection (R) and $2k$ reflection ($2k$, $2k'$) gratings. **b** Schematic drawing of a bird wing MPPC

* P. Yeh is also a Principal Technical Advisor at Rockwell International Science Center

coherent beams. The model takes into account transmission, reflection, and $2k$-reflection gratings as well as the depletion of the pump beams. The results are in quanlitative agreement with the experimental results [7, 10].

It is well known that the transmission gratings are responsible for the mutually pumped phase-conjugation process in most of the configurations [11]. For simplicity, we consider the case of one interactive region in the mutually pumped phase-conjugation process, also known as Double-Phase Conjugate Mirror (DPCM). We assume the diffusion-dominated photorefractive effect, i.e., with real coupling constants. Referring to Fig. 1a, we consider two plane waves of amplitude of A_2 and A_4 with a degree of mutual coherence of $v(0 \le v \le 1)$ incident in a photorefractive crystal. When the pump beams are partially coherent, besides the transmission grating $A_1 A_4^* + A_2^* A_3$, reflection grating $A_1 A_3^* + A_2^* A_4$, $2k$ gratings $A_1 A_2^*$, and $A_3 A_4^*$ are all present in the photorefractive medium. The nonlinear coupled wave equations are written as:

$$\frac{dA_1}{dz} = \gamma_t \frac{A_1 A_4^* + A_2^* A_3}{I_0} A_4 + v\left(\gamma_r \frac{A_1 A_3^* + A_2^* A_4}{I_0} A_3 + \gamma_{2k} \frac{A_1 A_2^*}{I_0} A_2\right),$$

$$\frac{dA_2^*}{dz} = \gamma_t \frac{A_1 A_4^* + A_2^* A_3}{I_0} A_3^* + v\left(\gamma_r \frac{A_1 A_3^* + A_2^* A_4}{I_0} A_4^* + \gamma_{2k} \frac{A_1 A_2^*}{I_0} A_1^*\right),$$

$$\frac{dA_3}{dz} = -\gamma_t \frac{A_1 A_4^* + A_2^* A_3}{I_0} A_2 + v\left(\gamma_r \frac{A_1^* A_3 + A_2 A_4^*}{I_0} A_1 - \gamma_{2k'} \frac{A_3 A_4^*}{I_0} A_4\right),$$

$$\frac{dA_4^*}{dz} = -\gamma_t \frac{A_1 A_4^* + A_2^* A_3}{I_0} A_1^* + v\left(\gamma_r \frac{A_1^* A_3 + A_2 A_4^*}{I_0} A_2^* - \gamma_{2k'} \frac{A_3 A_4^*}{I_0} A_3\right), \quad (1)$$

and the boundary conditions are

$$A_1(0) = A_3(L) = 0, \text{ and } \frac{|A_4(0)|^2}{|A_2(L)|^2} = q, \quad (2)$$

where $I_0 = |A_1|^2 + |A_2|^2 + |A_3|^2 + |A_4|^2$ is the total intensity of all the beams, γ_t, γ_r, γ_{2k}, and $\gamma_{2k'}$ are the photorefractive coupling coefficients for transmission, reflection, and $2k$-reflection gratings, respectively, q is the intensity ratio of the pump beams, L is the interaction length. It is clear that when two pump beams are mutually incoherent, i.e., $v=0$, the coupled wave equations reduce to the conventional ones, where only the transmission grating is present [11].

Since strong beam couplings occur in photorefractive materials, pump depletion is common in most of the photorefractive phase-conjugation processes, especially in MPPC. Therefore, we have to solve the nonlinear coupled wave equation taking into account the depletion of the pump beams. The coupled wave equations are solved with numerical techniques. We use the conventional 4-th-order Runge–Kutta algorithm to solve the coupled equation in (1) first. We then fit the correct boundary conditions (2) and allow the program to iterate until the boundary conditions are satisfied. It is found that the iteration usually converges, although it may take much more iterations to converge for some parameter regions than the other. We investigate the transmission properties of the mutually pumped phase conjugator as

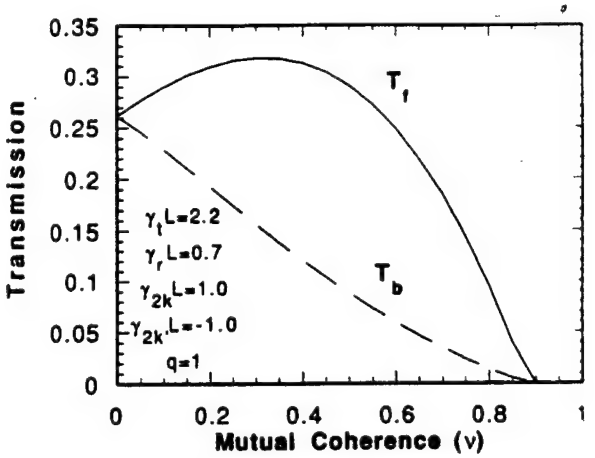

Fig. 2. Transmissions of a photorefractive mutually pumped phase conjugator as a function of mutual coherence of the two pump beams, where $\gamma_t L = 2.2$, $\gamma_r L = 0.7$, $\gamma_{2k} L = 1.0$, $\gamma_{2k'} L = -1.0$, $q = 1$.

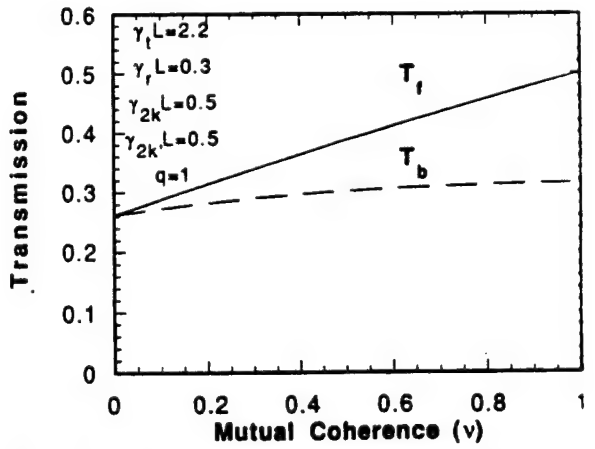

Fig. 3. Transmissions of a photorefractive mutually pumped phase conjugator as a function of mutual coherence of the two pump beams, where $\gamma_t L = 2.2$, $\gamma_r L = 0.3$, $\gamma_{2k} L = 0.5$, $\gamma_{2k'} L = 0.5$, $q = 1$.

a function of the degree of mutual coherence of the pump beams. The transmissions are defined as the ratio of the phase-conjugate intensity and the pump intensity, i.e., $T_f = |A_1(L)|^2/|A_4(0)|^2$ for the forward transmission, and $T_b = |A_3(0)|^2/|A_2(L)|^2$ for the backward transmission. It has been shown theoretically that for the mutually pumped phase conjugators that have only transmission gratings, the forward and the backward transmissions are always identical [11]. This phenomenon can be interpreted by using the principle of reciprocity [12]. However, in the presence of reflection gratings, one of the distinct characteristics is that these two quantities, T_f and T_b, are no longer the same. Figure 2 shows the variation of the transmissions as functions of the degree of mutual coherence with $\gamma_t L = 2.2$, $\gamma_r L = 0.7$, $\gamma_{2k} L = 1.0$, $\gamma_{2k'} L = 1.0$, and $q = 1$. We note that these two transmissions have a quite different dependence on the degree of mutual coherence. Depending on the sign and the magnitude of the reflection-grating coupling strength ($\gamma_r L$, $\gamma_{2k} L$, $\gamma_{2k'} L$), the performance of the mutually pumped phase conjugators can be significantly enhanced or reduced due to the mutual coherence of the pump beams. Figure 3 shows an example where the phase conjugator has a weak reflection coupling ($\gamma_r L = 0.3$), and strong favored $2k$ couplings ($\gamma_{2k} L = 0.5$, $\gamma_{2k'} L = 0.5$). All other parameters remain the same as those in Fig. 2. Due to the contribution of the $2k$ gratings where the energy is coupled towards the directions of phase conjugation, the phase conjugator becomes more efficient when both beams are coherent. On the other hand, if we change the sign of the $2k$ coupling coefficients, the phase conjugator will cease oscillating when the pump beams become coherent. This example is illustrated in Fig. 4. We find that the degree of mutual coherence between two pump beams could significantly affect the performance of the mutually pump phase conjugators especially when the crystal has strong reflection-coupling coefficients.

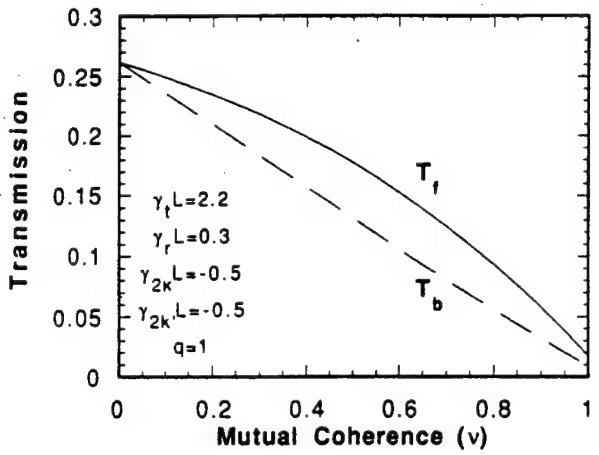

Fig. 4. Transmissions of a photorefractive mutually pumped phase conjugator as a function of mutual coherence of the two pump beams, where $\gamma_t L = 2.2$, $\gamma_r L = 0.3$, $\gamma_{2k} L = -0.5$, $\gamma_{2k'} L = -0.5$, $q = 1.0$

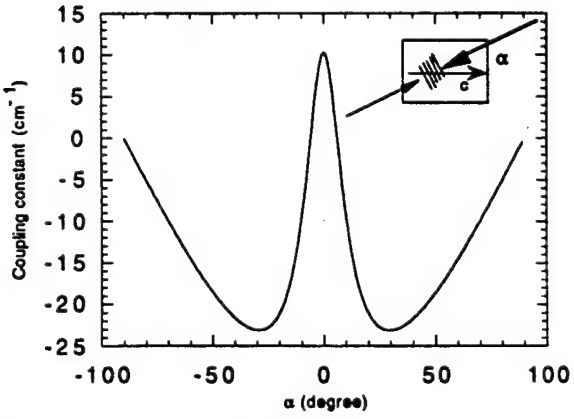

Fig. 5. Coupling constant via $2k$ grating in the $BaTiO_3$ crystal as a function of the angle between the pump beam and the c-axis

In a practical system, the coupling directions and the coupling strength of the reflection and $2k$ gratings are mainly dependent on the specific configuration used. We now discuss the coherence effect of some of the most common mutually pumped phase-conjugator geometries. For the case of DPCM geometry and the bridge phase-conjugator geometry in $BaTiO_3$ crystals, two pump beams are usually incident from two sides of the crystal with a small intersection angle. The c-axis of the crystal has an acute angle with one phase-conjugate beam and an obtuse angle with the other phase-conjugate beam [1, 13]. As a result, the $2k$-coupling coefficients in the directions of the two pump beams always have opposite signs in these configurations. This fact becomes more clear if we plot the coupling constant of a $2k$ grating in $BaTiO_3$ crystals, as shown in Fig. 5 [3]. From Fig. 5 we notice that in $BaTiO_3$ crystals the energy is coupled toward the positive c-axis via the $2k$ grating occurs only in a relatively narrow range of angles, (i.e., $\alpha < 6°$). In ploting Fig. 5 we assumed the trap density of the $BaTiO_3$ crystal $N_A = 8 \times 10^{16}/cm^3$. Furthermore, since the two pump beams in the DCPM geometry are directly overlapped with each other, the reflection grating formed by the interference of the pumps is also very strong. Therefore, according to our analysis, it is expected that the DPCM and the bridge phase-conjugator (in $BaTiO_3$) geometries are very susceptible to the mutual coherence of the pump beams. Their performance would generally decrease as the pump beams become coherent. This is similar to the case shown in Fig. 2. For the Bird-Wing Phase Conjugator (BWPC) [14] and the Mutually Incoherent-Beam Coupler (MIBC) [15] configurations, the performance could be much less susceptible to the coherence than in DPCM configuration and should even be enhanced with the coherent pump beams. The reason is that in these two geometries, pump beams are not directly overlapped in space, instead they are interconnected by the fanning via total internal reflections. Therefore, they usually have weak reflection gratings written by the pump beams. Most importantly, they have the same coupling directions (same sign) for the $2k$ gratings and the energy coupling is also towards the phase-conjugate directions. Taking the BWPC in the $BaTiO_3$

crystal for example, as shown in Fig. 1b, two pump beams are incident in the two sides of the a-face of the crystal, where the positive c-axis is codirectional with both pump beams. From the characteristics of the $2k$-coupling coefficient in the $BaTiO_3$ crystals as shown in Fig. 5, we know that once the angle between the $2k$-grating wavevector and the c-axis direction is larger than approximately 6°, the energy-coupling direction is always opposite to the c-axis. The two pump beams have angles larger than 6° with respect to the c-axis in both the bird-wing and the MIBC configurations. In these two geometries, the phase conjugate transmissions or reflectivities should be increased when pump beams become mutually coherent. This is similar to the case as shown in Fig. 3. It is also reasonable to predict that the MIBC geometry will gain more than the bird-wing because the MIBC geometry tends to have longer beam path inside the crystal thus a higher gain-length product for the $2k$ gratings. Although our theory is based on the one-interactive-region model, two-interactive-region geometries will have similar behaviors since they may be treated as a generalized version of the one-region process. These results are also consistent with the experimental measurement [7, 10]. For the case of complex coupling constants, the dynamic behavior of the phase conjugator could be much more complicated especially when the conjugator is seeded. It may be very unstable, even chaotic in these situations. More detailed studies and comparison between the theory and the experiment are under current investigation.

In conclusion, we have developed a theoretical model for mutually pumped phase conjugation with partially coherent pump beams. The analysis shows that the performance of the phase conjugator can be decreased or enhanced depending on the contribution of the reflection gratings. This also provides us a guide line in taking advantage of the reflection-grating couplings for enhanced phase conjugators.

Acknowledgements. Q.B. He is supported by NASA's Resident Research Associateship, administrated by the National Research Council. The work, performed at UC Santa Barbara, was supported, in part, by a grant from the US Air Force Office for Scientific Research.

References

1. S. Weiss, S. Sternklar, B. Fischer: Opt. Lett. **12**, 114 (1987)
2. P. Yeh, T.Y. Chang, M.D. Ewbank: J. Opt. Soc. Am. B **5**, 1743 (1988)
3. See, for example, P. Yeh: *Introduction to Photorefractive Nonlinear Optics* (Wiley, New York 1993)
4. Q.C. He, J. Shamir, J.G. Duthie: Appl. Opt. **306**, (1989)
5. M. Segev, S. Weiss, B. Fischer: Appl. Phys. Lett. **50**, 1397 (1987) and M.A. Kramer, S. Sifuentes, C.M. Clayton: Appl. Opt. **27**, 1371 (1988)
6. H.J. Caulfield, J. Shamir, Q.C. He: Appl. Opt: **26**, 2291 (1987)
7. M.T. Gruneisen, E.D. Seeberger, J.F. Mileski, K. Koch: Opt Lett. **16**, 596 (1991)
8. W. Krolikowiski, M.R. Belic: Opt. Lett. **13**, 150 (1987)
9. M.R. Belic, W. Krolikowiski: J. Opt. Soc. Am. B **6**, 901 (1989)
10. S.-C. De La Cruz, S. MacCormack, J. Feinberg: Tech. Digest CLEO'93, 532 (1993)
11. M. Cronin-Golomb, B. Fischer, J.O. White, A. Yariv: IEEE J QE-**20**, 12 (1984)
    Q.C. He: IEEE J. QE-**24**, 2507 (1988)
12. C. Gu, P. Yeh: Opt. Lett. **16**, 455 (1991)
13. D. Wang, Z. Zhang, Y. Zhu, S. Zhang, P. Ye: Opt. Commun **73**, 495 (1989)
14. M.D. Ewbank: Opt. Lett. **13**, 47 (1988)
15. A.M. Smout, R.W. Eason: Opt. Lett. **12**, 498 (1987)

2k-Grating-assisted self-pumped phase conjugation: theoretical and experimental studies

Shiuan Huei Lin,* Ying Wu Lian,† and Pochi Yeh

Electrical and Computer Engineering Department, University of California, Santa Barbara, California 91306

Ken Y. Hsu

Institute of Electro-Optical Engineering, National Chiao Tung University, Hsinchu, Taiwan

Zhu Yong

Institute of Physics, Chinese Academy of Sciences, Beijing, China

Received November 1, 1995

We investigated 2k-grating-assisted self-pumped phase conjugation in photorefractive Ce:$BaTiO_3$ crystals. The phase-conjugation process involves a combination of four-wave mixing and stimulated photorefractive backscattering. An approximation involving separate interaction regions is used to theoretically calculate the reflectivity of phase conjugation as a function of the coupling strength of four-wave mixing and stimulated photorefractive backscattering. In our experiments, grating-erasure techniques are employed at the interaction regions to investigate the dependence of phase-conjugate reflectivity on the coupling strength of four-wave mixing and stimulated photorefractive backscattering. The experimental results are in good agreement with the theoretical prediction.

Key words: Self-pumped phase conjugate, stimulated photorefractive backscattering, four wave mixing.

1. INTRODUCTION

In self-pumped phase conjugators the counterpropagating beams needed in a four-wave-mixing process are generated by the incident beam itself. By a process that is not entirely understood, the self-generated pump beams are often formed in a configuration tending to optimize the phase-conjugated beam. Self-pumped phase conjugators have been demonstrated in a variety of configurations. Two classes of self-pumped phase conjugator have been proposed and demonstrated: the passive self-pumped phase conjugator, which needs externally aligned mirrors,[1] and the true self-pumped phase conjugator, which uses a single crystal without external elements.[2] The true self-pumped phase conjugator is of potential interest because of its convenience for practical applications.[3] The first true self-pumped configuration was observed in 1982 by Feinberg in a single $BaTiO_3$ photorefractive crystal.[4] There are three different models to explain the origin of self-pumped phase conjugators in a signal photorefractive crystal (as shown in Fig. 1). In 1983, based on the experimental observation of the beam path in $BaTiO_3$ crystals, MacDonald and Feinberg[5] proposed a model that involved both four-wave mixing and total internal reflection (FWM-TIR) [see Fig. 1(a)]. In the model the phase conjugation is a result of FWM in two regions that are connected by TIR's from a corner of the crystal. Hence, a closed optical path loop is often observed inside the crystal. In 1985, Chang and Hellwarth[6] were the first to point out the close analogy between backward-stimulated Brillouin scattering and some configurations of self-pumped phase conjugation (SPPC) in $BaTiO_3$ and suggested that stimulated photorefractive backscattering (SPB) or stimulated two-wave mixing may be responsible for the generation of the SPPC [as shown in Fig. 1(b)]. It has been shown theoretically that the backward-scattered wave is dominated by the phase conjugate of the incident beam.[7,8] Recently we[9,10] proposed an alternative model of FWM-SPB (four-wave mixing and SPB, in which the SPB is produced by the formation of 2k gratings) to explain the SPPC observed in KTN:Fe and $BaTiO_3$:Ce crystals [as shown in Fig. 1(c)]. In this case the SPPC formation relies on both four FWM and SPB interactions. The phase-conjugate beam is generated by a four-wave-mixing process involving the incident beam, the forward-propagating beam (the fanning beam), and its backward-stimulated scattering beam. The backward-stimulated scattering beam is generated by the SPB process involving 2k gratings. Hence instead of a closed loop inside the crystal, filaments representing counter propagating beams are often observed.

In a typical SPPC experimental configuration, an extraordinarily polarized input beam is incident on the *a* face of a regular-cut $BaTiO_3$ photorefractive crystal. The SPPC formation mechanism is usually determined by the fanning pattern and the boundary conditions.[11] Generally speaking, SPPC is often generated by the SPB or the FWM-SPB mechanisms in some doped crystals but by the FWM-TIR mechanism in undoped crystals. This is mainly due to a significantly stronger fanning and larger coupling coefficients for 2k gratings in doped crystals. Changing the dopant concentration or the operat-

0740-3224/96/080000-08$10.00

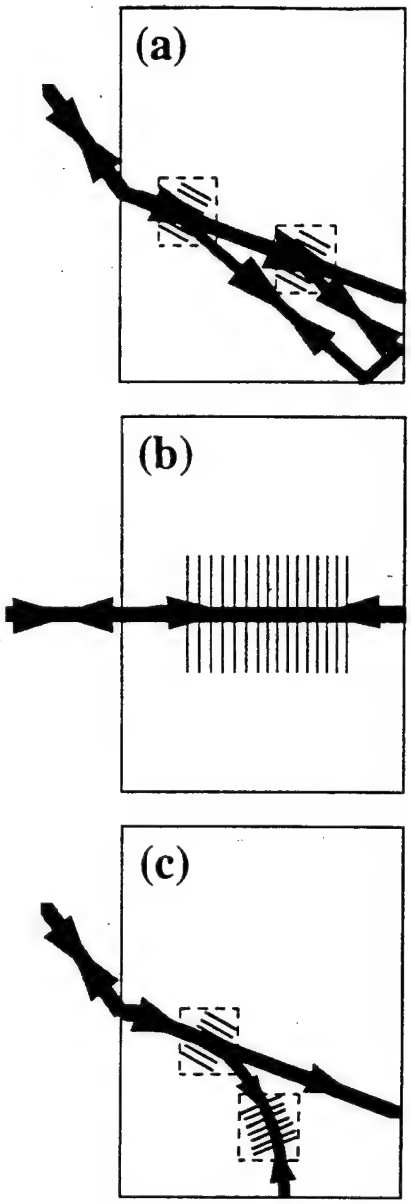

Fig. 1. Different modes of SPPC: (a) FWM-TIR, (b) SPB, and (c) FWM-SPB.

ing wavelength can cause a reconfiguration of the initial fanning pattern that leads to a change of the physical mechanism and the reflectivity of SPPC. Recently, we observed that the formation mechanism of SPPC was transformed from FWM-SPB to FWM-TIR when the wavelength of the input beam increased or the dopant concentration decreased.[12,13] We also observed that the mechanism transformation during SPPC and an enhancement of phase-conjugate reflectivity could be obtained by the variation of the polarization state of the input beam.[14] In a typical experiment an extraordinarily polarized input beam produces SPPC by FWM-SPB in a Ce:$BaTiO_3$ crystal. As the input polarization varies, the ordinary component, which serves as an erasing beam, decreases the effective coupling constant. This leads to a weaker fanning pattern. Depending on the boundary conditions, the fanned beam may reach the corner of the crystal cube, leading to SPPC by FWM-TIR. In this paper we theoretically and experimentally study the role of the $2k$ grating of SPB and the coupling strength of FWM in the FWM-SPB mode of self-pumped phase conjugators. A two-interaction-region approximation is used to theoretically calculate the reflectivity of phase conjugation and the threshold. We then present the results of our experimental studies, which validate the theoretical predictions. To vary the coupling constant, we also use an ordinarily incoherent erasing beam to reduce the index grating in the FWM and the SPB regions. The theoretical and the experimental results show that the reflectivity of phase conjugation depends strongly on the coupling strength of both the FWM and the SPB regions. In addition, the temporal dynamics of the phase-conjugate signal buildup process indicates that the $2k$ grating plays an important role in the FWM-SPB model. The paper can be organized as follows. In Section 2 we discuss a theoretical model of this new mode of SPPC. A closed-form solution of coupled-wave equations is obtained by use of an approximation. In Section 3 we discuss the experimental investigation using grating-erasure techniques at the two interaction regions to validate the theoretical predictions regarding the role of the $2k$ grating and the coupling strength of FWM during SPPC.

2. THEORETICAL ANALYSIS

Figure 2(a) shows a photograph of a typical optical beam path in the FWM-SPB mode of SPPC in Ce:$BaTiO_3$ crystals. Based on our experimental observation, the model of the FWM-SPB phase conjugator can be divided into two interactions regions, i.e., SPB and FWM interaction regions [as shown in Fig. 2(b)]. In the SPB interaction region there are two counterpropagating beams coupled by self-induced $2k$ gratings. The stimulated-backscattering beam A_2 is initially seeded by backscattering of fanned light from imperfection (pits) at the surface of the crystal. The backscattered light is amplified by SPB interaction with fanning beam A_1. These two beams provide the counterpropagating pump beams needed in the FWM for the generation of a phase-conjugate wave. Thus the SPB interaction region mainly acts as a feedback mirror (the SPB mirror, defined as the combination of the $2k$ grating gain region plus the scattering center) that provides one of the pump beams for the FWM interaction region. In the FWM interaction region, incident beam A_3, fanning beam A_1, and backscattering beam A_2 are coupled by a FWM interaction to generate a phase-conjugated beam A_4. For the phase-conjugation process to be sustained, the reflectivity of SPB region must be large enough to generate a self-oscillation between the SPB mirror and the FWM interaction region. Thus this phase conjugator is similar to a semilinear phase conjugator,[15] in which the mirror is replaced by a SPB mirror. The threshold and the reflectivity of a FWM-SPB phase conjugator are related to the net reflectivity of the SPB mirror.

We now treat this phase conjugator by using both optical FWM and contradirectional two-wave mixing in two separate regions. Referring to Fig. 2(b), we consider the interactions of all beams by using the following two sets of coupled equations. We consider only the transmission grating in the FWM region and the $2k$ grating in the SPB region. For the FWM interaction region the coupled

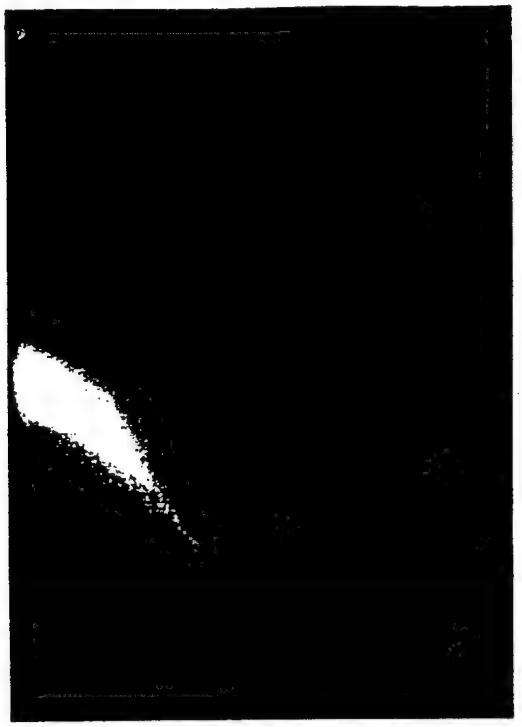

(a)

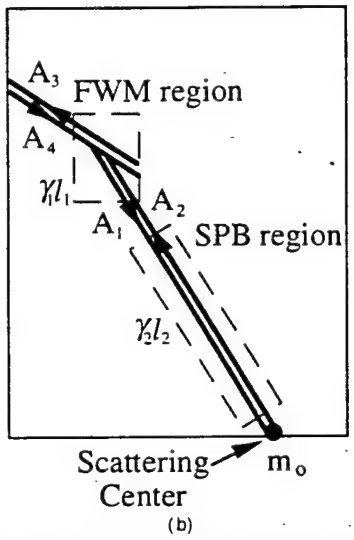

(b)

Fig. 2. FWM-SPB phase conjugator with a two-interaction region: (a) photograph of the optical beam path in a Ce:$BaTiO_3$ FWM-SPB phase conjugator; (b) theoretical model in which the forward-going fanning beam A_1 overlaps well with its backward-going scattering beam A_2 to form a SPB region. The amplified backscattering beam A_2 enters the FWM regions, mixes with A_1 and A_4, and generates the phase conjugate A_3.

equations are written as

$$\frac{dA_1}{dz} = \frac{\gamma_1}{2I_0}(A_1A_4^* + A_2^*A_3)A_4 - \frac{\gamma_2}{2I_0}A_1A_2^*A_2,$$

$$\frac{dA_2}{dz} = \frac{\gamma_1}{2I_0}(A_1^*A_4 + A_2A_3^*)A_3 - \frac{\gamma_2}{2I_0}A_1^*A_2A_1,$$

$$\frac{dA_3}{dz} = \frac{\gamma_1}{2I_0}(A_1A_4^* + A_2^*A_3)A_2,$$

$$\frac{dA_4}{dz} = \frac{\gamma_1}{2I_0}(A_1^*A_4 + A_2A_3^*)A_1, \qquad (1)$$

and for the SPB interaction region, the coupled equations are written as

$$\frac{dA_1}{dz'} = -\frac{\gamma_2}{2I_0'}A_1A_2^*A_2,$$

$$\frac{dA_2}{dz'} = -\frac{\gamma_2}{2I_0'}A_1^*A_2A_1, \qquad (2)$$

where γ_1 and γ_2 are the coupling constants of the transmission grating in the FWM region and the $2k$ grating in the SPB region, respectively. They are real and positive without the external electrical field in diffusion-dominant crystals, such as $BaTiO_3$, SBN, and KTN crystals. $I_0 = \sum_{j=1}^{4}|A_j|^2$ is the total intensity in the FWM region, and $I_0'(z') = \sum_{j=1}^{2}I_j(z') = \sum_{j=1}^{2}|A_j(z')|^2$ is the total intensity in the SPB region. The coordinate axis of the FWM region is defined as z, and that of the SPB region is defined as z'. These two regions are connected at $z' = 0$ or $z = l_1$, where l_1 is the interaction length of the FWM region and l_2 is the interaction length of the SPB region. In a typical FWM-SPB mode of self-pumped phase conjugation [as shown in Fig. 2(a)] the interaction length of the FWM region (l_1) is much smaller than that of the SPB region (l_2), but the γ_1 is much larger than γ_2 (in our case, $l_2 \approx 6l_1$ and $\gamma_1 \approx 5\gamma_2$). Hence these two sets of equations can be analytically solved by neglecting the $2k$ grating in the FWM region. In what follows, we first obtain the reflection generated by the SPB interaction by solving Eqs. (2). We then solve the coupled-mode equations in the FWM region by neglecting the $2k$-grating terms of Eq. (1). The phase-conjugate threshold and reflectivity of the FWM-SPB phase conjugator are obtained in terms of the coupling strength ($\gamma_2 l_2$) of SPB and that ($\gamma_1 l_1$) of FWM interaction.

A. Stimulated Photorefractive Backscattering Interaction Region

To examine the reflectivity of the SPB mirror, we first solve the coupled equations [Eqs. (2)] by following the procedure of contrapropagating two-wave mixing in Ref. 16 and by using the boundary condition $I_2(l_2)/I_1(l_2) = m_0$ at the surface of crystal (at $z' = l_2$), where m_0 is the backscattering coefficient of the imperfection on the surface of crystal. The solutions of Eqs. (2) are

$$I_1(z') = |A_1(z')|^2 = -C + \sqrt{C^2 + B\exp(-\gamma_2 z')},$$

$$I_2(z') = |A_2(z')|^2 = C + \sqrt{C^2 + B\exp(-\gamma_2 z')}, \qquad (3a)$$

where B and C are integration constants given by

$$B = I_1(l_2)I_2(l_2)\exp(-\gamma_2 l_2), \qquad C = \frac{I_2(l_2) - I_1(l_2)}{2}. \qquad (3b)$$

The effective intensity reflectivity of the SPB mirror, R, at $z' = 0$ (or $z = l_1$) can therefore be written

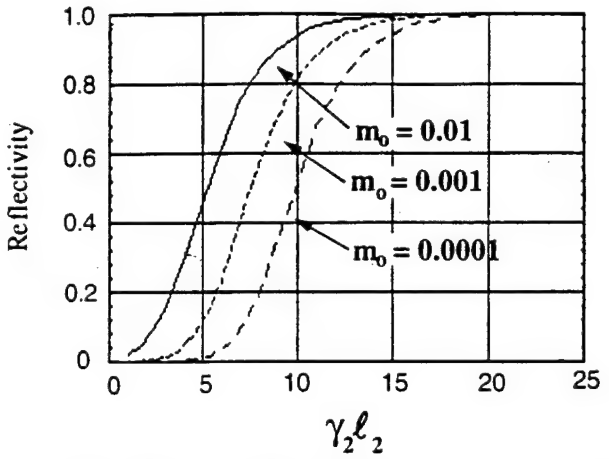

Fig. 3. Reflectivity of the SPB mirror as a function of $\gamma_2 l_2$ with various m_0.

$$R = \left|\frac{A_2(0)}{A_1(0)}\right|^2 = \frac{(1-m_0)^2 + 2m_0\exp(\gamma_2 l_2) - (1-m_0)\sqrt{(1-m_0)^2 + 4m_0\exp(\gamma_2 l_2)}}{2m_0\exp(\gamma_2 l_2)}. \quad (4)$$

When $m_0 \ll 1$, the reflectivity R can be written approximately as

$$R = \frac{1 + 2m_0\exp(\gamma_2 l_2) - \sqrt{1 + 4m_0\exp(\gamma_2 l_2)}}{2m_0\exp(\gamma_2 l_2)}. \quad (5)$$

We note that R depends strongly on the product of m_0 and exponential factor $\exp(\gamma_2 l_2)$. According to Eq. (5), the presence of an efficient $2k$ grating ($\gamma_2 l_2 \gg 1$) is sufficient to achieve a high reflectivity even through the initial seeding m_0 from crystal-surface imperfection is very weak. The reflectivity of the SPB mirror reaches 100% when $\gamma_2 l_2$ approaches infinity. By use of Eq. (4), Fig. 3 plots the reflectivity of the SPB mirror as a function of $\gamma_2 l_2$ for various m_0. It can be seen that for a given small $\gamma_2 l_2$, the reflectivity R of the SPB mirror is very different for different m_0. When $\gamma_2 l_2$ increases, the difference is diminished and R reaches almost 100% when $\gamma_2 l_2 > 5$, while m_0 varies from 10^{-5} to 10^{-1}. This means that the amplification of a $2k$ grating provides an efficient mechanism to retroreflect the fanning beam into the FWM region to facilitate the phase-conjugation process.

B. Four-Wave-Mixing Interaction Region

With the reflectivity of the SPB mirror available we can now solve the coupled equations (1) in the FWM region by neglecting the $2k$ grating. Following a procedure similar to the one used in Ref. 1, we obtain the following expression for the phase-conjugate reflectivity:

$$\eta = \frac{|A_3(z=0)|^2}{|A_4(z=0)|^2} = \left(\frac{1+\sigma}{1-\sigma}\right)^2 \frac{1}{R}, \quad (6)$$

where R again is reflectivity of the SPB mirror, σ is the net power flow in this region, given by

$$\sigma = \frac{-1 \pm \sqrt{R^2 s^2 + R s^2 - R}}{1+R}, \quad (7)$$

and s can be obtained from the following transcendental equation, which is related to the coupling strength $\gamma_1 l_1$ of the FWM region:

$$\tanh\frac{\gamma_1 l_1}{4} s = s. \quad (8)$$

Equations (7) and (8) provide some constraints on $\gamma_1 l_1$ and s. We note that nontrivial solutions of the transcendental equation exist only when $\gamma_1 l_1 > 4$. Once s is solved, σ is determined by Eq. (7). Being a new power flow, σ has to be real. This requires $s^2 > 1/(1+R)$. Thus if s or $\gamma_1 l_1$ are too small, there would be no phase conjugation. These constraints lead to a threshold coupling strength $(\gamma_1 l_1)_{\text{th}}$ and a threshold SPPC reflectivity η_{th} of the FWM-SPB phase conjugator, according to Eqs. (6) and (8), of

$$(\gamma_1 l_1)_{\text{th}} = 2\sqrt{1+R}\,\ln\left(\frac{\sqrt{1+R}+1}{\sqrt{1+R}-1}\right), \quad (9)$$

$$\eta_{\text{th}} = \frac{R}{(1+R)^2}. \quad (10)$$

We note that the phase-conjugate reflectivity is finite at threshold. Equation (9) shows that $(\gamma_1 l_1)_{\text{th}}$ is a decreasing function of R, reaching a minimum of 4.98 at $R = 1$. In order to further understand the concept, we plot $(\gamma_1 l_1)_{\text{th}}$ as a function of $\gamma_2 l_2$ for various scattering-center reflectivities m_0 (shown in Fig. 4). The SPPC reflectivity at threshold η_{th} is also plotted as a function of $\gamma_2 l_2$ for various m_0 (shown in Fig. 5). It can be seen that both m_0 and $\gamma_2 l_2$ influence greatly the threshold of the FWM-SPB phase conjugator. The threshold value of $(\gamma_1 l_1)_{\text{th}}$ decreases with m_0 and $\gamma_2 l_2$. The minimum value of 4.98 is almost the same as the threshold of the FWM-TIR phase conjugator (4.68 without loss, in which we should note that there is a factor of 2, according to our definition of the coupling constant).[17] It is also interesting to note that the reflectivity of SPPC at the threshold η_{th} is a decreasing function of $(\gamma_1 l_1)_{\text{th}}$. In general, the reflectivity of scattering center m_0 in the crystals is $\sim 10^{-3}$. An effective method to obtain a large SPB-mirror reflectivity R is to increase the coupling strength of the $2k$ grating $\gamma_2 l_2$

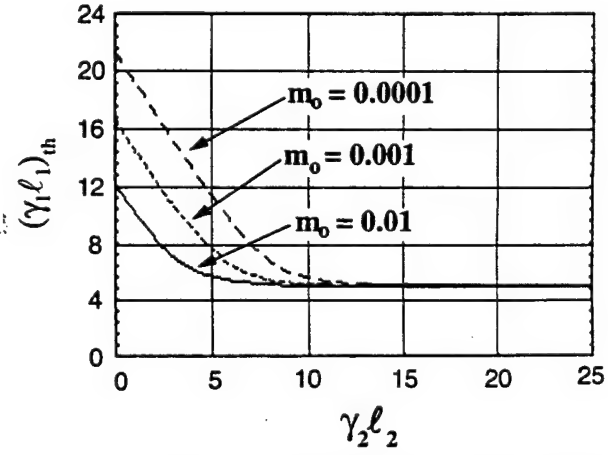

Fig. 4. Threshold coupling strength $(\gamma_1 l_1)_{\text{th}}$ of the FWM-SPB phase conjugator versus the coupling strength of the $2k$ grating $\gamma_2 l_2$ for various m_0.

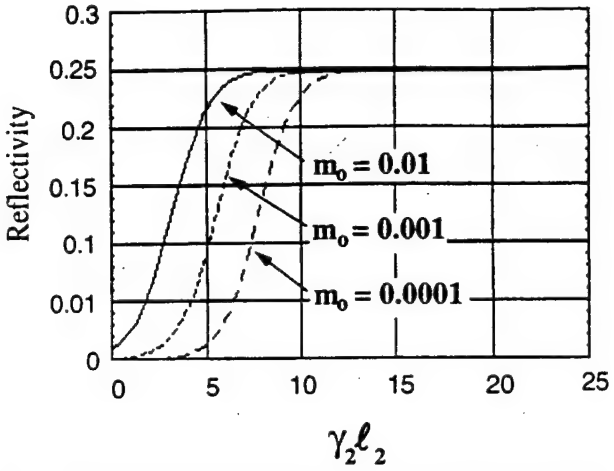

Fig. 5. SPPC reflectivity at threshold versus $\gamma_2 l_2$ for various m_0.

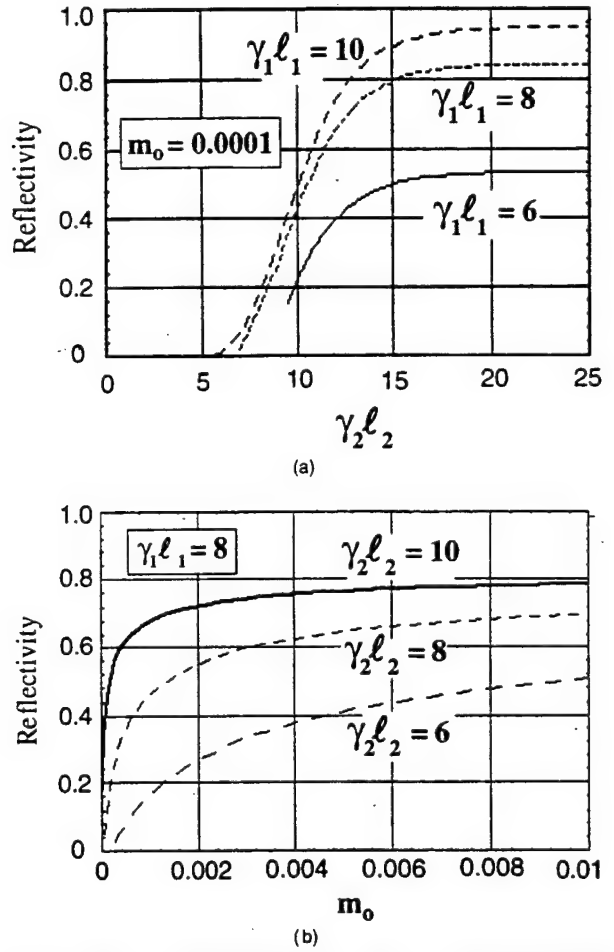

Fig. 6. Phase-conjugate reflectivity versus coupling strength of the $2k$ grating $\gamma_2 l_2$: (a) at different coupling strengths of the transmission grating $\gamma_1 l_1$ and (b) for various m_0.

(as shown in Fig. 3). This can be achieved by properly doping the crystals (e.g., Ce:$BaTiO_3$).

For $\gamma_1 l_1 > (\gamma_1 l_1)_{th}$ the reflectivity of the FWM-SPB phase conjugator η can be plotted as a function of $\gamma_2 l_2$ for the various $\gamma_1 l_1$ and m_0 [as shown in Figs. 6(a) and 6(b)]. We note that the reflectivity η obviously increases with $\gamma_2 l_2$ and behaves very differently for different $\gamma_1 l_1$. The reflectivity approaches a saturation value for a given $\gamma_1 l_1$, corresponding to a SPB-mirror reflectivity of $R = 100\%$ (at $\gamma_2 l_2 = \infty$). Referring to Fig. 3, we recall that SPB-mirror reflectivity R is an increasing function of $\gamma_2 l_2$, reaching $R = 100\%$ when $\gamma_2 l_2 = \infty$. We also note that all curves of different m_0 will approach the same saturation value when $\gamma_2 l_2 = \infty$. These figures confirm that the presence of a SPB $2k$ grating is essential to enhance the phase-conjugate reflectivity during SPPC. In order to increase the SPB-mirror reflectivity R, we can insert a retroreflecting screen into the path of the beam after the fanning beam leaves the crystal or use an artificial scattering center on the crystal face to increase m_0. We can also increase the coupling constant of $2k$ gratings by choosing an appropriate dopant and a proper wavelength. However, when the reflectivity of backscattering center m_0 is large enough, the phase-conjugate reflectivity is insensitive to the coupling strength of a $2k$ grating. For example, in the case of FWM-TIR, the corner cube is already providing a near 100% retroreflection regardless of the presence of $2k$ gratings. A small decrease of phase-conjugate reflectivity of ~20% was reported when the $2k$ grating was erased by an erasure beam in Ref. 18.

4. EXPERIMENT

In this section we report the results of our experiments to verify theoretical predictions based on the model of the FWM-SPB phase conjugator. The schematic diagram of the experimental arrangement is shown in Fig. 7. Our Ce-doped $BaTiO_3$ crystal has a red-orange color and a dopant concentration of approximately 30 parts in 10^6. The crystal is poled and 0° cut with dimensions 6.15 mm × 5.20 mm × 8.2 mm ($a \times b \times c$). An extraordinarily polarized beam from an argon laser (wavelength of 514.5 nm) is incident upon the crystal on the a face at an external angle of $\theta = 60°$. The phase conjugation was monitored by a calibrated photodiode (PD1). In order to investigate the buildup process of $2k$ gratings, the fanning beam was also monitored by another photodiode (PD2), and the optical path in the crystal was observed by imaging through the top of the crystal into a CCD camera. Figure 2(a) shows a photograph of the optical beam path inside the crystal during a typical mode of FWM-SPB SPPC. The input beam is depleted almost completely after propagating through a short distance and bends to the bottom surface of the crystal owing to the fanning effect. At steady state the end of the beam is characterized by a filament that is sustained through the SPB

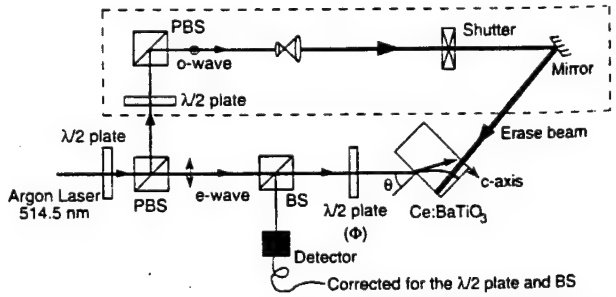

Fig. 7. Experimental setup used to demonstrate SPPC in the FWM-SPB mode: PBS's, polarizing beam splitters; BS's, beam splitters.

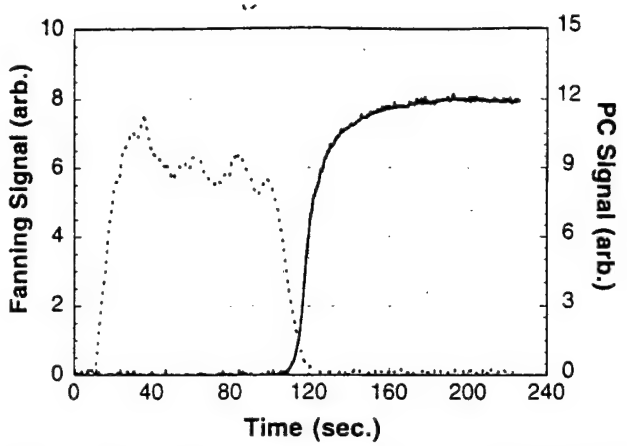

Fig. 8. Time evolution of the reflectivity of SPPC (solid curve) and intensity of the fanning beam (dashed curve).

process by $2k$ gratings. This SPPC formation is significantly different from the traditional FWM-TIR mechanism. There is no closed optical loop involving a corner inside the crystal.

Figure 8 shows the time evolution of the phase-conjugate signal (the solid curve) and the fanning signal (the dotted curve) during the buildup of the phase conjugation. At the first stage (t of 0–110 s, where $t = 0$ corresponds to the time when the incident beam is turned on), the fanning signal grows to a steady state, but the phase-conjugation signal only begins to start, as indicated by the recording at PD1. It indicates that at this moment, only the fanning beam is produced by the fanning grating in the FWM region, but the $2k$ grating has not been established in the SPB region. The forward fanning beam cannot be retroreflected into the FWM region to generate the phase conjugation. When $t > 110$ s, the phase-conjugation signal appears suddenly, while the fanning signal decreases significantly. This indicates the buildup of the $2k$ grating. After the fanning beam is produced by the incident beam, a backscattering can be generated by some defects on the surface of crystal, and the $2k$ grating can be written by the fanning beam and the retroreflected scattering beam. Once the $2k$ grating is formed, energy will be transformed from the fanning beam to the backscattering beam. With the increase of the backscattering, the amplitude of $2k$ grating also increases. This leads to more energy transfer from the fanning beam to the backscattering beam. The positive feedback provides the stimulated photorefractive backscattering and leads to some filaments at steady state. At the same time the backscattering beam will generate the phase conjugation by the FWM region and rewrite a new in-phase version of the fanning grating with the phase-conjugate beam to enhance the coupling in the FWM region. This explains the sharp rise of the phase conjugation as indicated in Fig. 8.

To further study the characteristics of the $2k$ grating in our model, we use an ordinarily polarized beam (see Fig. 7) that is incoherent with the input beam to illuminate the filaments uniformly in the SPB region. Since the refractive-index change of a photorefractive crystal is proportional to the modulation depth of the input light, the coupling coefficient of the $2k$ grating, $\gamma_2(I_r)$, can be written to incorporate the reduction in the modulation that results from the erasing beam,

$$\gamma_2(I_r) = \frac{\gamma_{2o}}{1 + I_r/I}, \tag{11}$$

where I is the total intensity in the filament, and γ_{2o} is the coupling-coefficient constant in the absence of the erasure beam I_r. According to the above equation, the coupling strength of the photorefractive grating can be easily controlled. Figure 9 shows the time evolution and the reflectivity of the phase-conjugate signal as the erasure beam is turned on. The signal decreases to different steady-state values depending on the intensity of erasure beams I_r. Figure 9 also shows that the reflectivity of the phase-conjugation signal decreases with the intensity of the erasing beam and exhibits a sharp threshold at $I_r = 4$ W/cm^2. To further illustrate the concept, we replot the phase-conjugate reflectivity as a function of $\gamma_2 l_2$, in which the intensity of the erasure beam can be calculated in terms of the coupling strength by use of Eq. (10). We also present the theoretical results by the dashed line in the figure for the purpose of comparison. The results are shown in Fig. 10, in which we estimate an average of I as 4 W/cm^2, a value of $\gamma_{2o} l_2$ as 11.5, a value of $\gamma_1 l_1$ as 7.0, and a reflectivity of scattering center m_0 as 0.001.

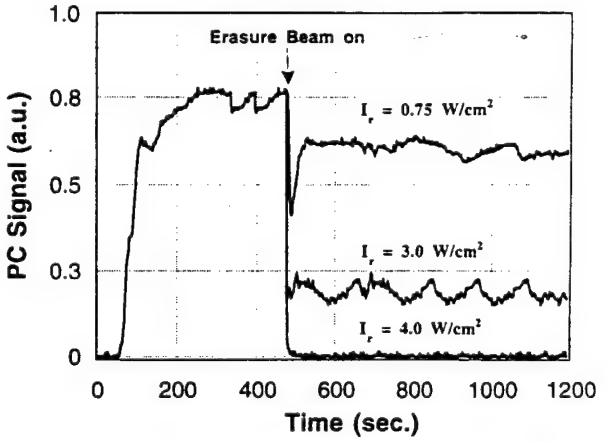

Fig. 9. Time-evolution of the phase-conjugate signal when the different erasing beams are applied.

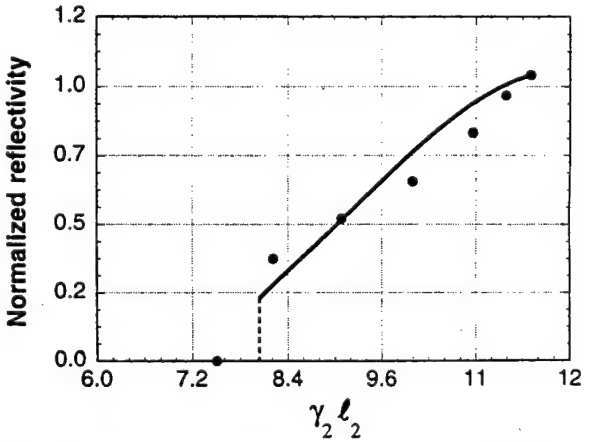

Fig. 10. Experimental phase-conjugate reflectivity versus $\gamma_2 l_2$. Note the phase-conjugate threshold at $\gamma_2 l_2 \approx 7.5$ (corresponding to $I_r = 4$ W/cm^2). The solid curve is from a theoretical calculation.

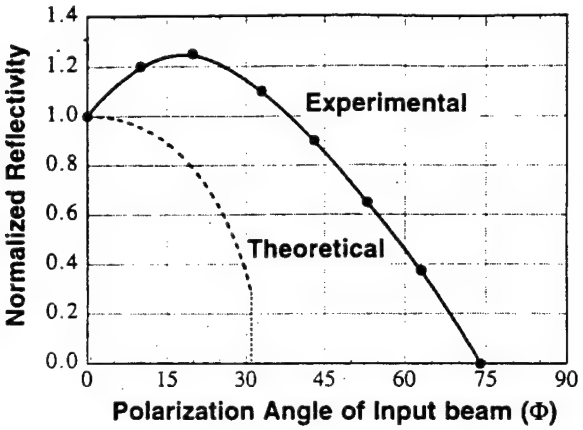

Fig. 11. Normalized phase-conjugation reflectivity as a function of the polarization angle, Φ, of the input beam. These experimental data are not corrected for Fresnel reflections. The dashed curve is from a theoretical calculation for a pure FWM-SPB mode of SPPC.

This curve is in agreement with the experimental results. Thus we note again that the presence of a $2k$-grating significantly affects the reflectivity of the backscattering beam and the SPPC in this model.

In a different experiment, to study the characteristic of the FWM region in this model, we block the erasing beam and introduce a general linear polarized input beam by inserting a half-wave plate in the path of the input beam (as shown in Fig. 7). The plane of polarization of the input beam could now be changed by rotating the half-wave plate. This leads to the presence of an ordinarily polarized component of the input beam. It is known that the coupling coefficient in Ce:$BaTiO_3$ crystal for an ordinarily polarized beam is much less than that of an extraordinarily polarized beam, and the cross coupling is negligible. Thus the extraordinarily polarized beam will contribute significantly to the fanning and the phase conjugation, whereas the ordinarily polarized beam will serve only to erase the gratings in the interaction regions. In this case the effective coupling coefficient of the grating, $\gamma_1(\phi)$, can be written as

$$\gamma_1(\phi) = \frac{\gamma_{1o}}{1 + \tan^2 \phi}, \qquad (12)$$

where γ_{1o} is the coupling coefficient at $\phi = 0°$, where ϕ is the state of polarization of the input beam. It is defined (as shown in Fig. 7) as $\phi = 0°$ for the extraordinarily polarized direction and $\phi = 90°$ for the ordinarily polarized direction. The experimental (solid curve) and the theoretical (dashed curve) results of the reflectivity of phase conjugation are shown in Fig. 11. Here, we note that the phase-conjugate output is always extraordinarily polarized regardless of the input polarization state. The reflectivity of phase conjugation is therefore defined as the ratio of the conjugated signal and the extraordinary component of the incident beam. In other words, the reflectivity is normalized to that of a totally extraordinarily polarized state of the input beam ($\phi = 0°$). According to the theoretical prediction, the reflectivity will decrease with the ordinarily component of input beam. On the contrary, the experimental results show an improvement over the theoretical prediction. The reflectivity of phase conjugation exceeds the value at $\phi = 0°$ in the range $\phi < 35°$. The increase in phase-conjugate reflectivity can be caused by a mechanism transformation during SPPC.[14] In addition, the presence of an ordinarily polarized component in the input beam can restrain the self-generated fanning pattern. Thus the energy loss caused by fanning can be limited.

5. CONCLUSION

We have carried out a theoretical analysis of a FWM-SPB self-pumped phase conjugator by using two-interaction-region approximation. The phase-conjugate wave is generated by four-wave mixing with the assistance of $2k$ gratings by SPB. From our results, we find that the coupling strength $\gamma_2 l_2$ of the $2k$ grating in the SPB region and the feedback reflectivity m_0 of scattering centers play very important roles in the generation of the phase-conjugate wave. We have also presented the results of a comprehensive experimental investigation of a FWM-SPB phase conjugator by using two different types of erasing beam. We find that the phase conjugation of the FWM-SPB model relies on both the FWM and the SPB interactions.

ACKNOWLEDGMENT

This work is supported, in part, by the U.S. Office of Naval Research and the Air Force Office of Scientific Research. Pochi Yeh is also a principal technical advisor at Rockwell International Science Center, Thousand Oaks, California.

*Permanent address, Institute of Electro-Optical Engineering, National Chiao Tung University, Hsinchu, Taiwan.

†Current address, Lambda Research Optics, Inc., 17605 Fabrica, Suites A and B, Cerritos, California 90703.

REFERENCES

1. See, for example, P. Yeh, *Introduction to Photorefractive Nonlinear Optics* (Wiley, New York, 1993).
2. M. Cronin-Golomb, B. Fisher, J. O. White, and A. Yariv, "Theory and applications of four-wave mixing in photorefractive media," IEEE J. Quantum Electron. **QE-20,** 12 (1984).
3. See, for example, P. Gunter and J.-P. Huignard, eds., *Photorefractive Materials and Their Applications* (Springer-Verlag, Berlin, 1988), Vols. I and II.
4. J. Feinberg, "Self-pumped, continuous-wave phase conjugator using internal reflections," Opt. Lett. **42,** 919 (1983).
5. K. R. Macdonald and J. Feinberg, "Theory of a self-pumped phase conjugator with two coupled interaction regions," J. Opt. Soc. Am. **73,** 548 (1983).
6. T. Y. Chang and R. W. Hellwarth, "Optical phase conjugation by backscattering in barium titanate," Opt. Lett. **10,** 408 (1985).
7. J. F. Lam, "Origin of phase conjugate waves in self-pumped photorefractive mirrors," Appl. Phys. Lett. **46,** 909 (1985).
8. G. C. Valley, "Evolution of phase-conjugate waves in stimulated photorefractive backscattering," J. Opt. Soc. Am. B **9,** 1440 (1992).
9. Y. W. Lian, H. Gao, P. Ye, Q. Guan, and J. Wang, "Self-pumped phase conjugation with a new mechanism in $KTa_{1-x}Nb_xO_3$:Fe crystals," Appl. Phys. Lett. **63,** 1754 (1993).
10. Y. W. Lian, S. X. Dou, H. Gao, Y. Zhu, X. Wu, C. Yang, and P. Ye, "Mechanism transformation with wavelength of self-pumped phase conjugation in $BaTiO_3$:Ce," Opt. Lett. **19,** 610 (1994).

11. A. A. Zozulya, M. Saffman, and D. Z. Anderson, "Propagation of light beams in photorefractive media: fanning, self-bending, and formation of self-pumped four-wave-mixing phase conjugation geometries," Phys. Rev. Lett. **73,** 818 (1994).
12. Y. W. Lian, S. X. Dou, J. Zhang, H. Gao, Y. Zhu, X. Wu, C. Yang, and P. Ye, "Variation of mechanism transition wavelength of self-pumped phase conjugation with Ce-content in $BaTiO_3$:Ce crystals," Opt. Commun. **110,** 192 (1994).
13. Y. W. Lian, H. Gao, S. X. Dou, H. Wang, P. Ye, Q. Guan, and J. Wang, "Mechanism transition of self-pumped phase conjugation in $KTa_{1-x}Nb_xO_3$:Fe crystals," Appl. Phys. B **59,** 655 (1994).
14. Y. W. Lian, S. H. Lin, S. Campbell, K. Y. Hsu, P. Yeh, and Y. Zhu, "Polarization-dependent mechanism transformation during self-pumped phase conjugation in $BaTiO_3$:Ce," Opt. Lett. **20,** 1683 (1995).
15. M. Cronin-Golomb, B. Fisher, J. O. White, and A. Yariv, "Passing (self-pumped) phase conjugate mirror: theoretical and experimental investigation," Appl. Phys. Lett. **41,** 689 (1982).
16. P. Yeh, "Two-wave mixing in nonlinear media," IEEE J. Quantum Electron. **25,** 484 (1989).
17. Q. He, "Theory and applications of four-wave mixing in photorefractive media," IEEE J. Quantum Electron. **QE-24,** 2507 (1988).
18. G. L. Wood, E. J. Sharp, and G. J. Salamo, "Performance of photorefractive self-pumped phase conjugators," Proc. SPIE **1626,** 21 (1992).

Contradirectional two-wave mixing with partially coherent waves in photorefractive crystals

Xianmin Yi, Shiuan Huei Lin, and Pochi Yeh

Department of Electrical and Computer Engineering, University of California, Santa Barbara, Santa Barbara, California 93106

Ken Yuh Hsu

Institute of Electro-Optical Engineering, National Chiao Tung University, 1001 Ta Hsueh Road, Hsinchu, Taiwan

Received January 31, 1996

We investigate contradirectional two-wave mixing with partially coherent waves in photorefractive crystals in the nondepleted pump regime. Equations governing the propagation of the self-coherence function and the mutual-coherence function of the signal wave and the pump wave are derived and simulated numerically. Numerical solutions of these equations are in excellent agreement with the experimental measurements.

Two-wave mixing in photorefractive crystals is an interesting and useful nonlinear-optical phenomenon for many applications such as image amplification, laser wave cleanup, spatial light modulators, thresholding, and power-limiting devices. Most of the theoretical study in this area has addressed wave mixing with monochromatic waves. Two-wave mixing with partially coherent waves has been studied for the case of transmission grating interaction,[1–3] in which the optical path difference between the two interacting waves remains approximately the same as the two waves propagate codirectionally through the photorefractive medium, especially when the incident angles of the two waves are close. In the case of reflection grating interaction the optical path difference between the two interacting waves varies significantly as the two waves propagate contradirectionally through the photorefractive medium. As a result, the latter case is quite different from the former and is much more complicated to analyze. In this Letter we present a theoretical analysis and experimental investigation for the case of reflection grating interaction in the nondepleted pump regime. The absorption effect is also included.

In the case of contradirectional two-wave mixing in a purely diffusive photorefractive medium the coupled-wave equations for the slowly varying amplitudes $\mathbf{E}_1(z,t)$ and $\mathbf{E}_2(z,t)$ can be written as[1]

$$\frac{\partial \mathbf{E}_1}{\partial z} + \frac{1}{v}\frac{\partial \mathbf{E}_1}{\partial t} = \frac{\gamma}{2}\frac{\mathbf{Q}\cdot\mathbf{E}_2}{\mathbf{I}_1+\mathbf{I}_2} - \frac{\alpha}{2}\mathbf{E}_1, \tag{1}$$

$$\frac{\partial \mathbf{E}_2}{\partial z} - \frac{1}{v}\frac{\partial \mathbf{E}_2}{\partial t} = \frac{\gamma}{2}\frac{\mathbf{Q}^*\cdot\mathbf{E}_1}{\mathbf{I}_1+\mathbf{I}_2} + \frac{\alpha}{2}\mathbf{E}_2, \tag{2}$$

where γ is the intensity coupling constant, α is the intensity absorption coefficient, v is the group velocity, and $\mathbf{E}_1 \exp(-i\omega t + ikz)$ and $\mathbf{E}_2 \exp(-i\omega t - ikz)$ are the coupled quasi-monochromatic waves that interact through a dynamic photorefractive grating $\delta n(z,t) \propto \mathbf{Q}\exp(2ikz) + \text{c.c.}$ The dynamics of the photorefractive grating can be written as

$$\tau\frac{\partial \mathbf{Q}}{\partial t} + \mathbf{Q} = \mathbf{E}_1\mathbf{E}_2^*, \tag{3}$$

where τ is the relaxation time constant.

The temporal behavior of each wave's complex amplitude can be modeled with a stationary random process, with coherence time $\delta\omega^{-1}$ being substantially less than the relaxation time of the material, i.e., $\delta\omega\tau \gg 1$.[4] When the optical path difference of the two waves is smaller than the coherence length of the source laser wave, a dynamic photorefractive grating is recorded in the medium. Its position and profile are nearly temporally constant. Then, as an approximation, we can replace the dynamic grating amplitude $\mathbf{Q}$ in Eqs. (1) and (2) with its ensemble average $\mathbf{Q} \approx \langle\mathbf{Q}\rangle = \langle\mathbf{E}_1\mathbf{E}_2^*\rangle$.

Since the complex amplitudes $\mathbf{E}_1(z,t)$ and $\mathbf{E}_2(z,t)$ are stationary random processes, we can define some of their ensemble averages as $\Gamma_{12}(z,\Delta t) \equiv \langle\mathbf{E}_1(z,t_1)\mathbf{E}_2^*(z,t_2)\rangle$, $\Gamma_{11}(z,\Delta t) \equiv \langle\mathbf{E}_1(z,t_1)\mathbf{E}_1^*(z,t_2)\rangle$, and $\Gamma_{22}(z,\Delta t) \equiv \langle\mathbf{E}_2(z,t_1)\mathbf{E}_2^*(z,t_2)\rangle$, where $\Delta t = t_1 - t_2$. We refer to Γ_{11} and Γ_{22} as the self-coherence of the signal wave $\mathbf{E}_1(z,t)$ and the pump wave $\mathbf{E}_2(z,t)$, respectively, and Γ_{12} as the mutual coherence between the signal wave and the pump wave. With this notation we can immediately write $\mathbf{Q} = \Gamma_{12}(z,0)$, $I_1 = \Gamma_{11}(z,0)$, and $I_2 = \Gamma_{22}(z,0)$. Equations (1)–(3) can therefore be reduced to a system for these average values[5]:

$$\frac{\partial\Gamma_{12}(z,\Delta t)}{\partial z} = -\frac{2}{v}\frac{\partial\Gamma_{12}(z,\Delta t)}{\partial\Delta t} + \frac{\gamma}{2}\frac{\Gamma_{12}(z,0)}{I_1+I_2} \times [\Gamma_{11}(z,\Delta t) + \Gamma_{22}(z,\Delta t)], \tag{4}$$

$$\frac{\partial\Gamma_{11}(z,\Delta t)}{\partial z} = \frac{\gamma}{2}\frac{\Gamma_{12}(z,0)}{I_1+I_2}\Gamma_{12}^*(z-\Delta t) + \frac{\Gamma_{12}^*(z,0)}{I_1+I_2} \times \Gamma_{12}(z,\Delta t) - \alpha\Gamma_{11}(z,\Delta t), \tag{5}$$

0146-9592/96/151123-03$10.00/0

$$\frac{\partial \Gamma_{22}(z,\Delta t)}{\partial z} = \frac{\gamma}{2}\frac{\Gamma_{12}(z,0)}{I_1+I_2}\Gamma_{12}^{*}(z,-\Delta t) + \frac{\gamma}{2}\frac{\Gamma_{12}^{*}(z,0)}{I_1+I_2} \times \Gamma_{12}(z,\Delta t) + \alpha\Gamma_{22}(z,\Delta t). \quad (6)$$

Note that Eqs. (4)–(6) are a set of self-consistent partial differential equations governing the propagation of the mutual-coherence and self-coherence functions of the two waves. We can solve them numerically as an initial-value problem, if we have the complete boundary conditions at either one of the two boundaries that the two waves are incident upon. In general, we know only the self-coherence functions and the mutual-coherence function of the two waves before they enter the medium. In the case of pump depletion, either wave has changed significantly as it reaches the second boundary. Therefore the complete boundary conditions are unavailable at either boundary. In the case of the nondepleted pump, we can assume that the pump wave passes through the photorefractive medium unaffected by the weak signal wave. In this case we obtain the complete boundary conditions at the boundary where the signal wave enters the medium. We then can solve Eqs. (4)–(6) for the self-coherence function of the signal wave and the mutual-coherence function of the two waves.

To determine the boundary conditions in the nondepleted pump regime, we assume that both the signal wave and the pump wave are derived from the same source wave, as is shown in Fig. 1. If the source wave has a Gaussian line shape with a linewidth of Δv, then the normalized self-coherence function of the source wave can be written as

$$\Gamma_s(\delta t) = \exp\left[-\left(\frac{\pi\Delta v\delta t}{2\sqrt{\ln 2}}\right)^2\right]. \quad (7)$$

At the signal-wave incident plane $z = 0$ the intensity ratio between the signal wave and the pump wave is assumed to be β. In our simulation the intensity of the pump wave is taken to be 1. Then the boundary conditions at $z = 0$ can be written as

$$\Gamma_{12}(z=0,\Delta t) \equiv \sqrt{\beta}\,\Gamma_s(\Delta t+\delta t), \quad (8)$$

$$\Gamma_{11}(z=0,\Delta t) \equiv \beta\,\Gamma_s(\Delta t), \quad (9)$$

$$\Gamma_{22}(z=0,\Delta t) \equiv \Gamma_s(\Delta t), \quad (10)$$

where δt is the time delay between the two waves.

In Fig. 2 we show the mutual-coherence function $\Gamma_{12}(z,0)$ of the two waves and the self-coherence function $\Gamma_{11}(z,0)$ of the signal wave as a function of the position z inside the photorefractive medium for two coupling constants γ of 3 and 7. At the signal entrance plane $z = 0$ the time delay δt is 0 s, and the input intensity ratio β is 10^{-4}. The linewidth Δv of the source is 10 GHz, and the index refraction of the photorefractive medium is 2.3. As a result of the coupling, part of the pump wave branches off in the direction of the signal wave, retaining its temporal profile. Therefore the mutual-coherence function will increase with coupling constant γ. For a small coupling constant the mutual-coherence function eventually decreases to zero as z increases because of the relatively rapid increase of the time delay of the two waves. Thus, as z increases, the coupling between the two waves decreases, and the signal intensity approaches a certain limit that is much less than the pump intensity. For a large coupling constant the mutual-coherence function increases as z increases because of relatively strong coupling. Thus, as z increases, the coupling between the two waves increases, and the signal intensity increases exponentially. In other words, for a large coupling constant the interaction length of the two waves can be much longer than the coherent length of the source wave.

The above theory is validated experimentally. Referring to Fig. 1, we consider two partially coherent waves, obtained by splitting an argon laser wave with a linewidth of 1.83 GHz. The signal and pump waves are contradirectionally incident upon a $KNbO_3$:Co crystal ($\gamma = 3.3\ \mathrm{cm}^{-1}$, $\alpha = 0.5\ \mathrm{cm}^{-1}$, and thickness $d = 0.72$ cm). The optical path difference of the two waves at the signal-wave incident plane $z = 0$ was set to be $\Delta L = L_2 - L_1$. To monitor the mutual coherence between the signal wave and the pump wave at the output plane $z = d$, we employ another reference

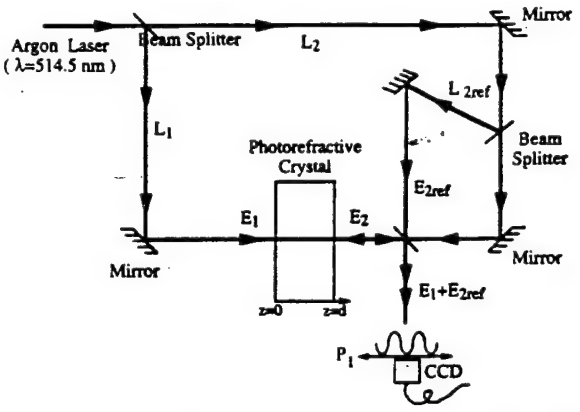

Fig. 1. Schematic of the two-wave-mixing configuration used in our calculations and experiments. The distances L_1 and L_2 are the optical path lengths of the signal wave and the pump wave from the laser source to the signal-wave incident plane $z = 0$, respectively. L_{2ref} is the optical path length of reference wave E_{2ref} from the laser source to the signal output plane $z = d$.

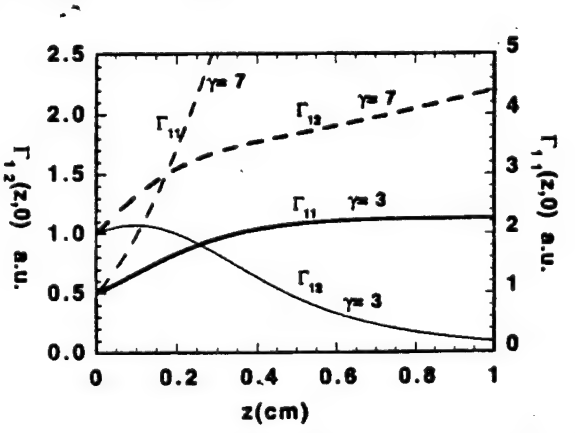

Fig. 2. Mutual-coherence function $\Gamma_{12}(z,0)$ and the self-coherence function of the signal wave $\Gamma_{11}(z,0)$ as a function of z for coupling constants $\gamma = 3$ (solid curves) and $\gamma = 7$ (dashed curves).

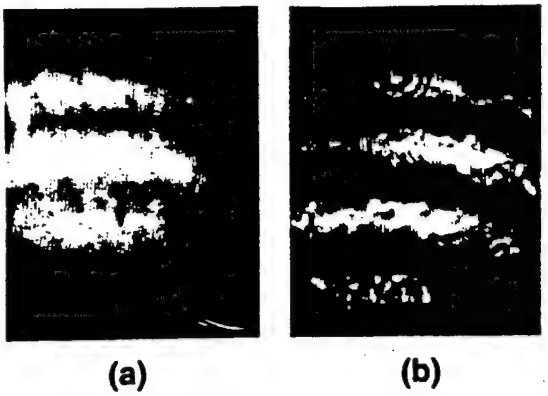

Fig. 3. Interference patterns of the signal wave and the reference wave at the output plane P1 (a) without and (b) with coupling. Note the increase of fringe visibility owing to the coupling.

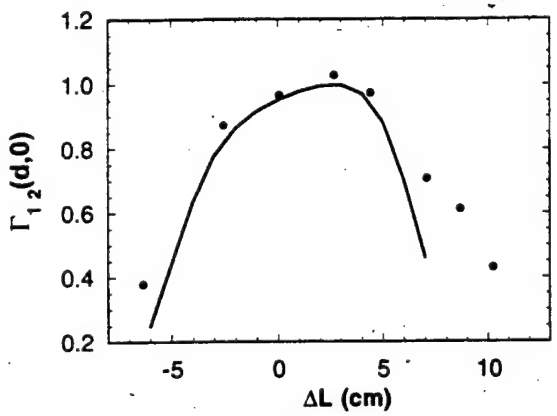

Fig. 4. Mutual coherence $\Gamma_{12}(d,0)$ as a function of the optical path difference ΔL.

wave $E_{2\mathrm{ref}}$ that was split from the pump wave E_2. The optical path difference of waves E_1 and $E_{2\mathrm{ref}}$ was adjusted to be the same as that of waves E_1 and E_2 at the output plane $z = d$. Using a simple homodyne technique, we observed the interference fringes generated by waves E_1 and $E_{2\mathrm{ref}}$ with a CCD camera at the output plane P1. The normalized mutual coherence $\Gamma_{12}(d,0)/[\Gamma_{11}(d,0)\Gamma_{22}(d,0)]^{1/2}$ can be estimated as $(I_{\max} - I_{\min})/(4\sqrt{I_1 I_2})$, where $(I_{\max} - I_{\min})$ is the amplitude of the fringes. In our experiment we monitored the interference pattern with and without pump beam E_2. Figure 3 shows photographs taken with a normalized mutual coherence $\Gamma_{12}(0,0) \approx 0.43$ at $z = 0$ ($\Delta L = 4$ cm) and an intensity ratio $\beta = 0.00151$. The measured normalized mutual coherence increases from 0.19 to 0.7 at $z = d$. We then measured the normalized mutual coherence as a function of the optical path difference. Figure 4 shows the data

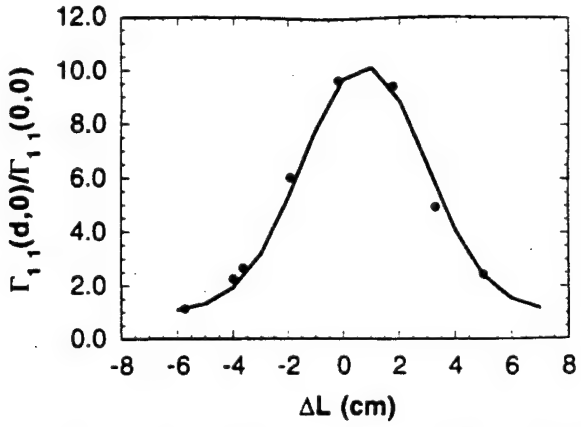

Fig. 5. Intensity gain of the signal wave at $z = d$ plane as a function of the path difference ΔL.

obtained from this measurement (filled circles) and the theoretical curve for the same parameters. Note that the normalized mutual coherence is close to 1 for small optical path differences and decreases quickly to zero as the optical path difference increases beyond certain values. The intensity gain of the signal wave was also measured. Figure 5 shows the measurement of the intensity gain (filled circles) of the signal wave at the $z = d$ plane as a function of the optical path difference ΔL, along with the theoretical curve for the same parameters. Excellent agreement between theory and experiment has been achieved in the case of the signal-wave intensity gain.

In conclusion, we have studied contradirectional two-wave mixing with partially coherent waves in photorefractive crystals both theoretically and experimentally. A set of partial differential equations has been derived to describe the propagation of the mutual-coherence and self-coherence functions of the two waves in the nondepleted pump regime. Excellent agreement has been achieved between theory and experiment.

This research was supported by the U.S. Office of Naval Research and the U.S. Air Force Office of Scientific Research.

References

1. N. V. Bogodaev, L. I. Ivleva, A. S. Korshunov, N. M. Polozkov, and V. V. Shkunov, J. Opt. Soc. Am. B **10,** 2287 (1993).
2. M. Cronin-Golomb, H. Z. Kong, and W. Krolikowski, J. Opt. Soc. Am. B **9,** 1698 (1992).
3. H. Z. Kong, C. K. Wu, and M. Cronin-Golomb, Opt. Lett. **16,** 1183 (1991).
4. P. Yeh, Appl. Opt. **26,** 602 (1987).
5. See, for example, J. W. Goodman, *Statistical Optics* (Wiley, New York, 1985), Chap. 5.

General solution of contradirectional two-wave mixing with partially coherent waves in photorefractive crystals

Xianmin Yi, Changxi Yang, and Pochi Yeh

Department of Electrical and Computer Engineering, University of California, Santa Barbara, California 93106

Shiuan-Huei Lin and Ken Yuh Hsu

Institute of Electro-Optical Engineering, National Chiao Tung University, 1001 Ta Hsueh Road, Hsinchu, Taiwan

Received June 13, 1996; revised manuscript received November 20, 1996

We investigate contradirectional two-wave mixing with partially coherent waves in photorefractive crystals. By use of a statistical theory on linear systems, a general formulation of the problem in the space and frequency domain is derived and implemented numerically. We obtain results on beam intensity and mutual coherence. The results on the enhancement of mutual coherence are compared with previous theoretical results on simpler cases and with experimental measurements. Excellent agreements are achieved. The results also indicate that the effective interaction length can be significantly longer than the coherence length of the waves. © 1997 Optical Society of America [S0740-3224(97)01906-1]

1. INTRODUCTION

Two-wave mixing in photorefractive crystals has been investigated extensively for many applications including image amplification, laser-beam cleanup, spatial light modulators, thresholding, and power-limiting devices.[1,2] Most of the theoretical works in this area are based on wave-mixing with mutually coherent waves.[1,2] However, in some applications, such as self-pumped and mutually pumped phase-conjugate mirrors[3–6] and photorefractive filters,[7] the effect of partial temporal coherence in a two-wave-mixing process cannot be ignored. Two-wave mixing with partially coherent waves has been studied previously for the case of transmission-grating interaction.[8] In the case of transmission-grating interaction the optical path difference between the two interacting waves remains approximately the same as the two waves propagating codirectionally through the photorefractive medium, especially when the incident angles of the two waves are close to each other.[9] In the case of reflection-grating interaction the optical path difference between the two interacting waves varies significantly as the two waves propagate contradirectionally through the photorefractive medium. Thus for the case of transmission-grating interaction, only one free variable for the position is needed to describe in a self-consistent way the second-order statistical properties of the two optical waves, i.e., their intensities and mutual coherence, while at least two free variables, one for the position and one for the optical path difference, will be needed for the case of reflection-grating interaction. Another difficulty in studying the reflection-grating interaction of partially coherent waves is to find a way to incorporate the complete boundary conditions into the theoretical formulation as a result of the two-point boundary-value problem. In such a problem a complete set of boundary conditions includes both the second-order self-statistical properties (e.g., self-coherence) of each wave at its entrance boundary and the second-order mutual statistical properties (e.g., mutual coherence) of the two waves at their respective entrance boundaries. In a recent work we provided a theoretical formulation of the problem in the space and time domain for the reflection-grating interaction in the nondepleted-pump regime.[9] By using the nondepleted-pump approximation, we reduced the two-point boundary-value problem to an initial value problem. In this paper we present a general formulation of the problem in the space and frequency domain based on the standard statistical theory on linear systems. The general formulation is also implemented numerically. Specifically, we investigate the signal-intensity gain and the mutual coherence in the contradirectional wave mixing of two partially coherent waves. Contrary to conventional belief, we discover that the effective interaction length (or grating length) can be significantly longer than the coherence length of the incident waves. The results are also compared with previous theoretical results on simpler cases and with experimental measurements.

2. THEORETICAL MODEL

Photorefractive two-wave mixing is a nonlinear optical process. Because of the mutual coherence of the two waves, a dynamic holographic grating is formed in the medium. Its position and index profile are nearly stationary under the condition of a cw illumination. Both waves are scattered into each other by the presence of this index grating. Scattering of partially coherent waves by a stationary grating can be modeled with a statistical theory on linear systems.[10] An iterative procedure can subsequently be devised to obtain the final pho-

0740-3224/97/0601396-11$10.00

torefractive grating profile from an initially arbitrary grating profile.

As is shown in Fig. 1, two counter propagating waves with partial coherence enter a photorefractive medium at $z = 0$ and $z = L$, respectively. The electric field in the photorefractive medium can be written as

$$\mathbf{E}(z, t) = \mathbf{E}_1(z, t)\exp(-i\omega_0 t + i\mathbf{k}_0 z) + \mathbf{E}_2(z, t)\exp(-i\omega_0 t - i\mathbf{k}_0 z), \quad (1)$$

where ω_0 is the center frequency of the two partially coherent waves, $\mathbf{k}_0 = n\omega_0/c$ is the corresponding wave vector, and n is the refractive index of the photorefractive medium. Reflecting the partial coherence, $\mathbf{E}_1(z, t)$ and $\mathbf{E}_2(z, t)$ are stationary random variables. They represent the random fluctuation of the amplitudes of the two waves. For the convenience of our later discussion we will now briefly describe some notations and definitions for the second-order statistical properties of the two optical waves. Let $\Gamma_{11}(z, \tau) \equiv \langle \mathbf{E}_1(z, t_1)\mathbf{E}_1^*(z, t_2)\rangle$ and $\Gamma_{22}(z, \tau) \equiv \langle \mathbf{E}_2(z, t_1)\mathbf{E}_2^*(z, t_2)\rangle$ denote the self-coherence functions of $\mathbf{E}_1(z, t_1)$ and $\mathbf{E}_1(z, t_1)$, respectively, and $\Gamma_{12}(z, \tau) \equiv \langle \mathbf{E}_1(z, t_1)\mathbf{E}_2^*(z, t_2)\rangle$ be the mutual-coherence function between $\mathbf{E}_1(z, t_1)$ and $\mathbf{E}_2(z, t_2)$, where $\tau = t_1 - t_2$ is the time delay and $\langle\ \rangle$ means ensemble average. Let $\mathbf{E}_{11}(z, \Delta\omega)$ and $\mathbf{E}_{22}(z, \Delta\omega)$ denote the self-spectral-density functions of $\mathbf{E}_1(z, t)$ and $\mathbf{E}_2(z, t)$, respectively, and $\mathbf{E}_{12}(z_1, z_2, \Delta\omega)$ be the cross-spectral-density function between $\mathbf{E}_1(z_1, t)$ and $\mathbf{E}_2(z_2, t)$. The spectral-density functions and the corresponding coherence functions are Fourier-transform pairs, i.e.,

$$\Gamma_{11}(z, \tau) = \int \mathbf{E}_{11}(z, \Delta\omega)\exp(-i\Delta\omega\tau)\mathrm{d}\Delta\omega, \quad (2)$$

$$\Gamma_{22}(z, \tau) = \int \mathbf{E}_{22}(z, \Delta\omega)\exp(-i\Delta\omega\tau)\mathrm{d}\Delta\omega, \quad (3)$$

$$\Gamma_{12}(z, \tau) = \int \mathbf{E}_{12}(z, z, \Delta\omega)\exp(-i\Delta\omega\tau)\mathrm{d}\Delta\omega, \quad (4)$$

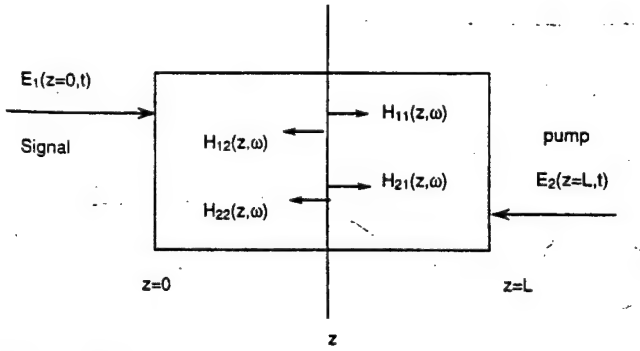

Fig. 1. Two-wave mixing in photorefractive crystals modeled as a linear system with the signal-wave entrance plane and the pump-wave entrance plane as two input planes and any arbitrary plane inbetween as the output plane.

where $\Delta\omega = \omega - \omega_0$, with ω being a general frequency component of the waves. With the above notations and relations the intensity of the two waves can be expressed as

$$I_1(z) \equiv \Gamma_{11}(z, 0) = \int \mathbf{E}_{11}(z, \Delta\omega)\mathrm{d}\Delta\omega, \quad (5)$$

$$I_2(z) \equiv \Gamma_{22}(z, 0) = \int \mathbf{E}_{22}(z, \Delta\omega)\mathrm{d}\Delta\omega, \quad (6)$$

and the mutual coherence of the two waves can be expressed as

$$\Gamma_{12}(z, 0) = \int \mathbf{E}_{12}(z, z, \Delta\omega)\mathrm{d}\Delta\omega. \quad (7)$$

With these equations the intensity of the waves as well as the mutual coherence can be obtained as soon as the spectral-density functions are obtained. In what follows we will derive the spectral-density functions by using the statistical approach.

Using the above notations and definitions, we now begin our discussion on the photorefractive interaction. Inside the photorefractive medium, a dynamic index grating is generated. It can be written as

$$\delta n = -i\frac{\gamma}{2}\frac{c}{\omega_0}\left[\frac{\mathbf{Q}(z, t)}{I_0(z)}\exp(2i\mathbf{k}_0 z) + \text{c.c.}\right], \quad (8)$$

where $\mathbf{Q}(z, t)$ is a measure of the index grating, γ is the intensity coupling coefficient, and $I_0(z) = I_1(z) + I_2(z)$ is the total intensity at position z. For the purpose of our discussion we will call $\mathbf{E}_1$ the signal wave and $\mathbf{E}_2$ the pump wave. Thus for a photorefractive grating with a positive γ, the signal wave $\mathbf{E}_1$ can be amplified. If the photorefractive effect is based purely on carrier diffusion (e.g., $BaTiO_3$,) the dynamics of the index grating is described by the following equation:

$$\tau_{\text{ph}}\frac{\partial \mathbf{Q}(z, t)}{\partial t} + \mathbf{Q}(z, t) = \mathbf{E}_1(z, t)E_2^*(z, t), \quad (9)$$

where τ_{ph} is the relaxation-time constant. By virtue of photoexcitations, photorefractive processes are usually slow at low intensities. It is reasonable to assume that the coherence time $\delta\omega^{-1}$ of the two partially coherent waves is much smaller than the relaxation time τ_{ph} of the photorefractive medium, i.e., $\delta\omega\tau_{\text{ph}} \gg 1$. Since $\mathbf{E}_1(z, t)$ and $\mathbf{E}_2(z, t)$ are stationary random variables, we can make the following approximation (see Appendix A)[8]:

$$\mathbf{Q}(z, t) \cong \langle \mathbf{Q}(z, t)\rangle = \Gamma_{12}(z, 0). \quad (10)$$

In other words, two partially coherent waves with their complex amplitudes fluctuating randomly with time can actually write a stationary grating in a photorefractive medium under the appropriate conditions. For simplicity we will denote $\mathbf{Q}(z, t)$ with $\mathbf{Q}(z)$ from now on. Note that $\mathbf{Q}(z)$ is also the mutual coherence of the two waves at position z. We note that the approximation is also valid when $\delta\omega\tau_{\text{ph}} \ll 1$.

Given arbitrary functions of $\mathbf{Q}(z)$ and $I_0(z)$, Eq. (8) yields an index grating. The propagation of a monochromatic wave through such an index grating can be described by the coupled wave equations. The coupled monochromatic waves can be written as

$$\tilde{\mathbf{E}} = \tilde{\mathbf{E}}_1(z, \omega)\exp(-i\omega t + i\mathbf{k}z) + \tilde{\mathbf{E}}_2(z, \omega)\exp(-i\omega t - i\mathbf{k}z), \quad (11)$$

where $\tilde{\mathbf{E}}_1$ and $\tilde{\mathbf{E}}_2$ are the amplitudes of the monochromatic components, ω is the optical wave frequency, and $\mathbf{k} = n\omega/c$ is the optical wave vector. The coupled wave equations can be written as

$$\frac{\partial\tilde{\mathbf{E}}_1(z, \omega)}{\partial z} = \frac{\gamma}{2I_0(z)}\mathbf{Q}(z)\tilde{\mathbf{E}}_2(z, \omega)\exp(-2i\Delta\mathbf{k}z) - \frac{\alpha}{2}\tilde{\mathbf{E}}_1(z, \omega), \quad (12)$$

$$\frac{\partial\tilde{\mathbf{E}}_2(z, \omega)}{\partial z} = \frac{\gamma}{2I_0(z)}\mathbf{Q}^*(z)\tilde{\mathbf{E}}_1(z, \omega)\exp(2i\Delta\mathbf{k}z) + \frac{\alpha}{2}\tilde{\mathbf{E}}_2(z, \omega), \quad (13)$$

where $\Delta\mathbf{k} = \mathbf{k} - \mathbf{k}_0$ is the phase mismatch between the optical waves and the index grating and α is the intensity absorption coefficient. With sufficient boundary conditions, Eqs. (12) and (13) can be solved either analytically in some special cases or numerically in general. When the boundary conditions are $\tilde{\mathbf{E}}_1(z = 0, \omega) = 1$ and $\tilde{\mathbf{E}}_2(z = L, \omega) = 0$, the solutions (output) are denoted as $\tilde{\mathbf{E}}_1(z, \omega) = \mathbf{H}_{11}(z, \omega)$ and $\tilde{\mathbf{E}}_2(z, \omega) = \mathbf{H}_{12}(z, \omega)$. When the boundary conditions are $\tilde{\mathbf{E}}_1(z = 0, \omega) = 0$ and $\tilde{\mathbf{E}}_2(z = L, \omega) = 1$, the solutions (output) are denoted as $\tilde{\mathbf{E}}_1(z, \omega) = \mathbf{H}_{21}(z, \omega)$ and $\tilde{\mathbf{E}}_2(z, \omega) = \mathbf{H}_{22}(z, \omega)$. As a linear system, the general solutions are linear combinations of $\mathbf{H}_{11}$, $\mathbf{H}_{12}$, $\mathbf{H}_{21}$, and $\mathbf{H}_{22}$.

In each of the iterations an arbitrary stationary index grating can be considered as a linear system. Referring to Fig. 1, we consider a given stationary index grating in the photorefractive medium as a linear system with the optical waves at the boundary planes $z = 0$ and $z = L$ as the input and the optical waves at an arbitrary plane z as the output. According to the theory on the statistical properties of linear systems, the second-order statistical properties of the optical waves at the output plane can be expressed in terms of the second-order statistical properties of the optical waves at the input planes and the frequency response of the linear system. To be specific, the input at the $z = 0$ plane is $\mathbf{E}_1(z = 0, t)$, the input at $z = L$ plane is $\mathbf{E}_2(z = L, t)$, and the outputs at the z plane are $\mathbf{E}_1(z, t)$ and $\mathbf{E}_2(z, t)$. The frequency response of this linear system can be expressed in terms of the solutions of Eqs. (12) and (13). With the notations described in the previous paragraph, the frequency responses from the input $\mathbf{E}_1(z = 0, t)$ to the outputs $\mathbf{E}_1(z, t)$ and $\mathbf{E}_2(z, t)$ are

$$\mathbf{H}_{11}'(z, \omega) = \mathbf{H}_{11}(z, \omega)\exp(i\Delta\mathbf{k}z), \quad (14)$$

$$\mathbf{H}_{12}'(z, \omega) = \mathbf{H}_{12}(z, \omega)\exp(-i\Delta\mathbf{k}z), \quad (15)$$

respectively. Similarly, the frequency responses from the input $\mathbf{E}_2(z = L, t)$ to the outputs $\mathbf{E}_1(z, t)$ and $\mathbf{E}_2(z, t)$ are

$$\mathbf{H}_{21}'(z, \omega) = \mathbf{H}_{21}(z, \omega)\exp(i\Delta\mathbf{k}L)\exp(i\Delta\mathbf{k}z), \quad (16)$$

$$\mathbf{H}_{22}'(z, \omega) = \mathbf{H}_{22}(z, \omega)\exp(i\Delta\mathbf{k}L)\exp(-i\Delta\mathbf{k}z), \quad (17)$$

respectively. The additional phase terms in Eqs. (14)–(17) account for the difference $\Delta\mathbf{k} = \mathbf{k} - \mathbf{k}_0$ owing to a finite $\Delta\omega = \omega - \omega_0$. With these spectral-response functions we can express the spectral-density functions of the two outputs $\mathbf{E}_1(z, t)$ and $\mathbf{E}_2(z, t)$ in terms of the spectral-density functions of the two inputs $\mathbf{E}_1(z = 0, t)$ and $\mathbf{E}_2(z = L, t)$. Thus, according to their definitions and Eqs. (14)–(17), we obtain

$$\begin{aligned}\mathbf{E}_{11}(z, \Delta\omega) = {} & \mathbf{H}_{11}(z, \omega)\mathbf{H}_{11}^*(z, \omega)\mathbf{E}_{11}(z = 0, \Delta\omega) \\ & + \mathbf{H}_{21}(z, \omega)\mathbf{H}_{21}^*(z, \omega)\mathbf{E}_{22}(z = L, \Delta\omega) \\ & + \mathbf{H}_{11}(z, \omega)\mathbf{H}_{21}^*(z, \omega) \\ & \times \mathbf{E}_{12}(z = 0, z = L, \Delta\omega)\exp(-i\Delta\mathbf{k}L) \\ & + \mathbf{H}_{21}(z, \omega)\mathbf{H}_{11}^*(z, \omega) \\ & \times [\mathbf{E}_{12}(z = 0, z = L, \Delta\omega) \\ & \times \exp(-i\Delta\mathbf{k}L)]^*, \end{aligned} \quad (18)$$

$$\begin{aligned}\mathbf{E}_{22}(z, \Delta\omega) = {} & \mathbf{H}_{12}(z, \omega)\mathbf{H}_{12}^*(z, \omega)\mathbf{E}_{11}(z = 0, \Delta\omega) \\ & + \mathbf{H}_{22}(z, \omega)\mathbf{H}_{22}^*(z, \omega)\mathbf{E}_{22}(z = L, \Delta\omega) \\ & + \mathbf{H}_{12}(z, \omega)\mathbf{H}_{22}^*(z, \omega) \\ & \times \mathbf{E}_{12}(z = 0, z = L, \Delta\omega)\exp(-i\Delta\mathbf{k}L) \\ & + \mathbf{H}_{22}(z, \omega)\mathbf{H}_{12}^*(z, \omega) \\ & \times [\mathbf{E}_{12}(z = 0, z = L, \Delta\omega) \\ & \times \exp(-i\Delta\mathbf{k}L)]^*, \end{aligned} \quad (19)$$

$$\begin{aligned}\mathbf{E}_{12}(z, z, \Delta\omega) = {} & \exp(i2\Delta\mathbf{k}z)\{\mathbf{H}_{11}(z, \omega)\mathbf{H}_{12}^*(z, \omega) \\ & \times \mathbf{E}_{11}(z = 0, \Delta\omega) \\ & + \mathbf{H}_{21}(z, \omega)\mathbf{H}_{22}^*(z, \omega) \\ & \times \mathbf{E}_{22}(z = L, \Delta\omega) \\ & + \mathbf{H}_{11}(z, \omega)\mathbf{H}_{22}^*(z, \omega) \\ & \times \mathbf{E}_{12}(z = 0, z = L, \Delta\omega) \\ & \times \exp(-i\Delta\mathbf{k}L) + \mathbf{H}_{21}(z, \omega)\mathbf{H}_{12}^*(z, \omega) \\ & \times [\mathbf{E}_{12}(z = 0, z = L, \Delta\omega) \\ & \times \exp(-i\Delta\mathbf{k}L)]^*\}. \end{aligned} \quad (20)$$

Note that the spectral-density functions $\mathbf{E}_{11}(z = 0, \Delta\omega)$, $\mathbf{E}_{22}(z = L, \Delta\omega)$, and $\mathbf{E}_{12}(z_1 = 0, z_2 = L, \Delta\omega)$ of the two inputs $\mathbf{E}_1(z = 0, t)$ and $\mathbf{E}_2(z = L, t)$ are given as the boundary conditions.

Two physical processes happen simultaneously during two-wave mixing in a photorefractive medium. First, the two optical waves propagate through the photorefractive medium while being scattered into each other by the index grating. Second, the scattered waves modify the index grating through the photorefractive effect until a steady state is reached. We have provided above a mathematical model that describes these two physical processes separately. A steady state of the two-wave mixing in the photorefractive medium is reached when the two optical waves scattered by the photorefractive grating can

exactly sustain the same photorefractive grating. A steady-state solution of the two-wave mixing in a photorefractive medium can thus be obtained by use of the mathematical model described above through an iterative procedure. The procedure is outlined as follows:

Step 1: Give an initial guess on the function $\mathbf{Q}(z)/I_0(z)$.

Step 2: Solve Eqs. (12) and (13) for the functions $\mathbf{H}_{ij}(z, \omega)$ $(i, j = 1, 2)$ with the function $\mathbf{Q}(z)/I_0(z)$ provided in the last step.

Step 3: Obtain the spectral-density functions $\mathbf{E}_{11}(z, \Delta\omega)$, $\mathbf{E}_{22}(z, \Delta\omega)$, and $\mathbf{E}_{12}(z, z, \Delta\omega)$ by use of Eqs. (18)–(20).

Step 4: Obtain $I_1(z)$, $I_2(z)$, $\mathbf{Q}(z)$, and $\mathbf{Q}(z)/I_0(z)$ by use of Eqs. (5), (6), (7), and (10).

Step 5: Compare the new version of the index grating $\mathbf{Q}(z)/I_0(z)$ and the previous version. If they are close within a certain accuracy requirement, the solution has been obtained. Otherwise, the iteration continues by use of the new version of the index grating.

To determine the boundary conditions, we assume that both the input optical waves are derived from the same laser source. If the source laser wave has a Gaussian line shape with a FWHM linewidth of $\delta\omega$, then the normalized spectral-density function of the source laser wave can be written as

$$\mathbf{E}_{ss}(\Delta\omega) = \frac{4(\pi \ln 2)^{1/2}}{\delta\omega} \exp\left\{-\left[2(\ln 2)^{1/2}\frac{\Delta\omega}{\delta\omega}\right]^2\right\}. \tag{21}$$

Taking β as the incident-intensity ratio $I_1(z = 0)/I_2(z = L)$ of the two optical waves at their respective entrance boundary planes, we obtain the boundary conditions as

$$\mathbf{E}_{11}(z = 0, \Delta\omega) = \beta\mathbf{E}_{ss}(\Delta\omega), \tag{22}$$

$$\mathbf{E}_{22}(z = 0, \Delta\omega) = \mathbf{E}_{ss}(\Delta\omega), \tag{23}$$

$$\mathbf{E}_{12}(z_1 = 0, z_2 = L, \Delta\omega) = \sqrt{\beta}\mathbf{E}_{ss}(\Delta\omega)\exp(-i\mathbf{k}_0 L) \times \exp(-i\omega t_d), \tag{24}$$

where t_d is the time delay between the optical waves when they reach their respective entrance planes. In deriving the above boundary conditions, we have assumed that the laser source has a Gaussian line shape. There is no loss of generality in this assumption. Similar results can be obtained with a different line shape.

This completes the general formulation to model contradirectional two-wave mixing in photorefractive crystals.

3. DISCUSSIONS AND SIMULATIONS

To clarify the complicated formulation described above, we consider some simple cases first before presenting the numerical and experimental results.

In the absence of coupling ($\gamma = 0$) in a lossless medium ($\alpha = 0$) with $\beta = 1$ the above formulation describes the interference of two counterpropagating optical waves in a dielectric medium. In this case it takes only one iteration to obtain the solution, which is

$$\mathbf{E}_{12}(z, z, \Delta\omega) = \mathbf{E}_{ss}(\Delta\omega)\exp(-i\mathbf{k}L) \times \exp(-i\omega t_d)\exp(2i\Delta\mathbf{k}z). \tag{25}$$

Fourier transforming the above equation over ω and taking into account the extra phase term $\exp(2i\mathbf{k}_0 z)$ resulted from the definition of $\mathbf{E}_1(z, t)$ and $\mathbf{E}_2(z, t)$ in Eq. (1), we obtain the mutual coherence of the two waves as a function of position z,

$$\Gamma_{12}(z, \tau) = \Gamma_s\left(\tau + t_d + \frac{nL - 2nz}{c}\right)\exp(-i\omega_0 t_d), \tag{26}$$

where $\Gamma_s(\tau)$ is the normalized self-coherence function of the source laser wave and n is the index of refraction of the medium. The result has been well established in the literature. This example can also help us see more clearly the subtle contribution of the phase terms in the above formulation. In our definition, $t_d = 0$ if $z = L/2$ is the plane of zero path difference.

When the coherence time $\delta\omega^{-1}$ is much larger than the time delay involved in the above formulation, i.e., $\delta\omega t_d \ll 1$ and $\delta\omega nL/c \ll 1$, the normalized spectral-density function of the source laser wave can be written as $\mathbf{E}_{ss}(\omega) = \delta(\omega - \omega_0)$. From the above formulation we can obtain the set of equations governing the intensities of the two optical waves,

$$\frac{\mathrm{d}}{\mathrm{d}z} I_1 = \gamma\frac{I_1 I_2}{I_1 + I_2} - \alpha I_1, \tag{27}$$

$$\frac{\mathrm{d}}{\mathrm{d}z} I_1 = \gamma\frac{I_1 I_2}{I_1 + I_2} + \alpha I_1. \tag{28}$$

These two equations are exactly the same as those obtained for two-wave mixing of monochromatic waves. We note that $\delta\omega t_d \ll 1$ is a condition for partially coherent waves to be treated as monochromatic waves in contradirectional two-wave mixing in a photorefractive medium. We also recall that the upper limit on the coherence time, i.e., $\delta\omega\tau_{ph} \gg 1$, still needs to be satisfied to reach Eqs. (27) and (28) from the above general formulation. This is the main difference between the results of Eqs. (27) and (28) in this paper and those obtained directly for monochromatic waves. Note that we did not use the iterative procedure in obtaining Eqs. (27) and (28). The complete boundary conditions for Eqs. (27) and (28) are simply $I_1(z = 0)$ and $I_2(z = L)$.

We now use the above general formulation to obtain the solution in the nondepleted-pump regime (for $\gamma \neq 0$), which has been obtained previously by a different method. Using Eqs. (12) and (13) and the following three definitions,

$$\mathbf{E}_{11}(z, \Delta\omega) = \langle\tilde{\mathbf{E}}_1(z, \omega)\tilde{\mathbf{E}}_1^*(z, \omega)\rangle, \tag{29}$$

$$\mathbf{E}_{22}(z, \Delta\omega) = \langle\tilde{\mathbf{E}}_2(z, \omega)\tilde{\mathbf{E}}_2^*(z, \omega)\rangle, \tag{30}$$

$$\mathbf{E}_{12}(z, z, \Delta\omega) = \langle\tilde{\mathbf{E}}_1(z, \omega)\tilde{\mathbf{E}}_2^*(z, \omega)\rangle\exp(2i\Delta\mathbf{k}z), \tag{31}$$

we can obtain a set of equations governing the propagation of the spectral-density functions as

$$\frac{\partial \mathbf{E}_{11}(z, \Delta\omega)}{\partial z} = \frac{\gamma}{2I_0(z)}[\mathbf{Q}(z)\mathbf{E}_{12}^*(z, z, \Delta\omega) + \mathbf{Q}^*(z)\mathbf{E}_{12}(z, z, \Delta\omega)] - \alpha\mathbf{E}_{11}(z, \Delta\omega), \quad (32)$$

$$\frac{\partial \mathbf{E}_{22}(z, \Delta\omega)}{\partial z} = \frac{\gamma}{2I_0(z)}[\mathbf{Q}(z)\mathbf{E}_{12}^*(z, z, \Delta\omega) + \mathbf{Q}^*(z)\mathbf{E}_{12}(z, z, \Delta\omega)] + \alpha\mathbf{E}_{22}(z, \Delta\omega), \quad (33)$$

$$\frac{\partial \mathbf{E}_{12}(z, z, \Delta\omega)}{\partial z} = 2i\Delta\mathbf{k}\mathbf{E}_{12}(z, z, \Delta\omega) + \frac{\gamma}{2I_0(z)}\mathbf{Q}(z) \times [\mathbf{E}_{11}(z, \Delta\omega) + \mathbf{E}_{22}(z, \Delta\omega)] - \alpha\mathbf{E}_{12}(z, z, \Delta\omega). \quad (34)$$

$\tilde{\mathbf{E}}_1(z, \omega)$ and $\tilde{\mathbf{E}}_2(z, \omega)$ in Eqs. (29)–(31) are related to the Fourier-transform coefficients of the two optical waves as defined in Eq. (11). Strictly speaking, a stationary random process cannot be Fourier transformed over the time variable t. However, we can truncate it into a finite duration T and Fourier transform the truncated process. After that, we can first obtain a set of equations similar to Eqs. (32)–(34) for the truncated process, then let T go to infinity to obtain Eqs. (32)–(34). This is a standard procedure in statistical optics.[10] Fourier transforming the above relation over $\Delta\omega$, we obtain a set of equations governing the propagation of the self and mutual coherence of the two optical waves as

$$\frac{\partial \Gamma_{12}(z, \tau)}{\partial z} = -\frac{2n}{c}\frac{\partial \Gamma_{12}(z, \tau)}{\partial \tau} + \frac{\gamma}{2}\frac{\Gamma_{12}(z, 0)}{I_1 + I_2} \times [\Gamma_{11}(z, \tau) + \Gamma_{22}(z, \tau)], \quad (35)$$

$$\frac{\partial \Gamma_{11}(z, \tau)}{\partial z} = \frac{\gamma}{2}\frac{\Gamma_{12}(z, 0)}{I_1 + I_2}\Gamma_{12}^*(z, -\tau) + \frac{\gamma}{2}\frac{\Gamma_{12}^*(z, 0)}{I_1 + I_2}\Gamma_{12}(z, \tau) - \alpha\Gamma_{11}(z, \tau), \quad (36)$$

$$\frac{\partial \Gamma_{22}(z, \tau)}{\partial z} = \frac{\gamma}{2}\frac{\Gamma_{12}(z, 0)}{I_1 + I_2}\Gamma_{12}^*(z, -\tau) + \frac{\gamma}{2}\frac{\Gamma_{12}^*(z, 0)}{I_1 + I_2}\Gamma_{12}(z, \tau) + \alpha\Gamma_{22}(z, \tau). \quad (37)$$

When there is no absorption in the photorefractive medium (i.e., $\alpha = 0$), we can obtain, from Eqs. (36) and (37),

$$\frac{\partial}{\partial z}[\Gamma_{11}(z, \tau) - \Gamma_{22}(z, \tau)] = 0. \quad (38)$$

Further, letting $\tau = 0$ in Eq. (38), we obtain

$$\frac{\partial}{\partial z}[I_1(z) - I_2(z)] = 0. \quad (39)$$

Equation (39) shows that, when there is no absorption in the photorefractive medium, the intensity difference between the signal wave and the pump wave is a constant of integration (conservation of power flow).

Note that, although Eqs. (35)–(37) are general and self-consistent, they contain only the mutual coherence of the two optical waves at the same locations. They are not compatible with the kind of boundary conditions as given by Eq. (24), which gives the mutual statistical properties of the two waves at two different points in space. Therefore they are useful only in the nondepleted-pump regime, where we can assume that the pump wave passes through the photorefractive medium without changing its statistical properties. Under this assumption we can obtain from Eqs. (22)–(24) the self- and mutual-coherence functions of the two waves at the signal-wave entrance boundary plane ($z = 0$) as

$$\Gamma_{12}(z = 0, \tau) \equiv \sqrt{\beta}\Gamma_{ss}(\tau + \delta t)\exp(-i\omega_0\delta t), \quad (40)$$

$$\Gamma_{11}(z = 0, \tau) \equiv \beta\Gamma_{ss}(\tau), \quad (41)$$

$$\Gamma_{22}(z = 0, \tau) \equiv \Gamma_{ss}(\tau), \quad (42)$$

where $\delta t = t_d + nL/c$ is the time delay between the two optical waves at the signal-wave entrance plane and

$$\Gamma_{ss}(\tau) = \exp\left\{-\left[\frac{\delta\omega\tau}{4(\ln 2)^{1/2}}\right]^2\right\} \quad (43)$$

is the coherence function of the source laser wave. We can use Eqs. (40)–(42) as the boundary conditions and integrate Eqs. (35)–(37).

Equations (35)–(37) are simple not only in the sense that they can be implemented easily numerically, but also that they can be used to obtain approximate analytical solutions to some special cases within the nondepleted regime. One such case is that the coherence length of the source laser wave is much longer than the two-wave-mixing interaction length and the coupling constant is large. This occurs when we use a multimode argon laser and a $KNbO_3$:Co crystal for the two-wave-mixing experiment. In this case we can neglect the term that contains the partial derivative on τ in Eq. (35) and reduce the set of partial differential equations, i.e., Eqs. (35)–(37), to a set of ordinary differential equations that can be solved analytically under the nondepleted-pump approximation. Remember that Eq. (35) is derived directly from Eq. (34). We can see from Eq. (34) that the approximation of neglecting the term that contains the partial derivative on τ in Eq. (35) implies that the wave-vector difference $\Delta\mathbf{k}$ of the different frequency components of the two partially coherent waves are negligible with respect to the thickness of the photorefractive medium (i.e., $\Delta\mathbf{k}L \ll 1$). Similar approximation has been made previously by Saxena *et al.* in the study of multiple-beam interaction by transmission gratings in the photorefractive media.[12,13] Therefore under the nondepleted-pump approximation and the approximation of $\Delta\mathbf{k}L \ll 1$ the signal-wave intensity gain and the normalized mutual coherence of the two waves can be obtained as

$$\frac{I_1(z)}{I_1(0)} \equiv \frac{\Gamma_{11}(z, 0)}{\Gamma_{11}(0, 0)} = \frac{\Gamma_{12}(0, 0)\Gamma_{12}^*(0, 0)}{\Gamma_{11}(0, 0)\Gamma_{22}(0, 0)} \times [\exp(\gamma z) - 1]\exp(-\alpha z) + \exp(-\alpha z), \quad (44)$$

$$\gamma_{12}(z) \equiv \frac{\Gamma_{12}(z, 0)}{[\Gamma_{11}(z, 0)\Gamma_{22}(z, 0)]^{1/2}} = \frac{1}{\left\{\frac{\Gamma_{12}^{*}(0, 0)}{\Gamma_{12}(0, 0)}[1 - \exp(-\gamma z)] + \frac{\Gamma_{11}(0, 0)\Gamma_{22}(0, 0)}{\Gamma_{12}^{2}(0, 0)}\exp(-\gamma z)\right\}^{1/2}}. \quad (45)$$

In most photorefractive crystals with $\exp[(\gamma - \alpha)z] \gg 1$ the signal-intensity gain is affected primarily by $(\gamma - \alpha)$. We also note that the normalized mutual coherence of the two waves is affected only by the photorefractive coupling constant γ.

As a comparison of the general formulation, the simplified formulation and the approximate analytical solutions, we show in Figs. 2 and 3 the signal-intensity gain and the normalized mutual coherence of the two waves at the signal-wave exit plane ($z = L$) as a function of the optical path difference between the two optical waves at the signal-wave entrance plane ($z = 0$). The parameters are $\gamma = 3.0\ \text{cm}^{-1}$, $\alpha = 0.0\ \text{cm}^{-1}$, $n = 2.3$, $L = 0.72$ cm, and $\delta\omega = 2\pi \times 1.8$ GHz, and $\beta = 10^{-4}$. These are typical parameters in our experiment when we use a multimode argon laser and a $KNbO_3$:Co crystal to implement the two-wave-mixing experiment. In this case the coherence length of the source laser wave is much longer than the thickness of the photorefractive medium. The general formulation and the simplified formulation produce the same results within the numerical accuracy in the nondepleted regime. The results of these two formulations are represented by the dashed curves in Figs. 2 and 3. We notice that the approximate analytical solution retains the major characteristics of the exact solution and provides a good understanding of the interaction. The results of the approximate analytical solution are represented by the solid curves in the figures. Note that the curves obtained from the approximate analytical solution are symmetric about $z_0 = 0$ owing to the approximation of neglecting the partial derivative over τ in Eq. (35), while the curves obtained from the general formulation are shifted to the right side (see Figs. 2 and 3). Here, z_0 is defined as the path difference. The difference between the results of the approximate analytical solution and those of the general formulation will decrease as the ratio between the coherence length of two waves and the thickness of the photorefractive medium increases.

Now let us consider the case of the depleted pump. Numerical simulation with the general formulation is the only means to analyze this case. We first consider the case in which the coherence length of the source laser wave is finite but much longer than the thickness of the photorefractive medium. Again, we use the following set of parameters: $\gamma = 3.0\ \text{cm}^{-1}$, $\alpha = 0.0\ \text{cm}^{-1}$, $n = 2.3$, $L = 0.72$ cm, and $\delta\omega = 2\pi \times 1.8$ GHz. The solid curves in Fig. 4 show the signal intensity $I_1(z)$, the pump intensity $I_2(z)$, and the normalized mutual coherence $\gamma(z) = \Gamma_{12}(z, 0)/[\Gamma_{11}(z, 0)\Gamma_{22}(z, 0)]^{1/2}$ as functions of the position z in the photorefractive medium. The optical path difference between the signal wave and the pump wave at the signal-wave entrance boundary ($z = 0$) is chosen to be zero. The incidence intensity ratio β of the two waves is chosen to be one. We also show in Fig. 4 with dashed curves the signal intensity $I_1(z)$ and the pump intensity $I_2(z)$ for two-wave mixing with monochromatic waves for the purpose of comparison. We notice that the results of two-wave mixing with partially coherent waves are very close to those of two-wave mixing with

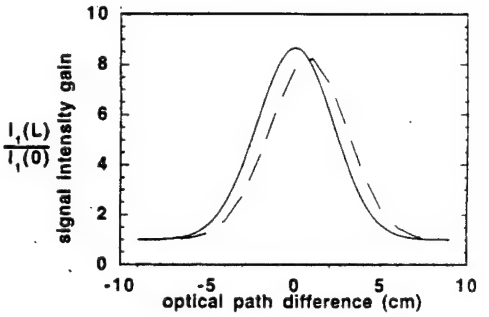

Fig. 2. Signal-wave intensity gain as a function of the optical-path difference at the signal-wave entrance plane in the nondepleted-pump regime. The dashed curve is the numerical solution. The solid curve is the approximate analytical solution.

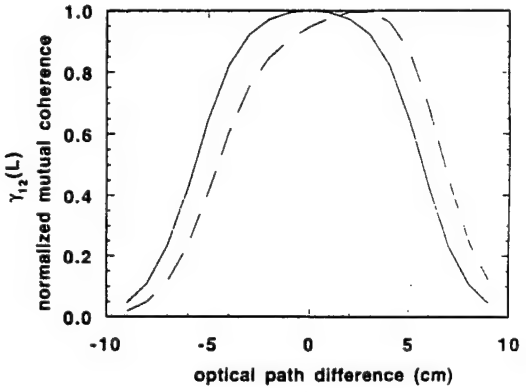

Fig. 3. Mutual coherence of the two waves at the signal-wave exit plane as a function of the optical path difference at the signal-wave entrance plane in the nondepleted-pump regime. The dashed curve is the numerical solution. The solid curve is the approximate analytical solution.

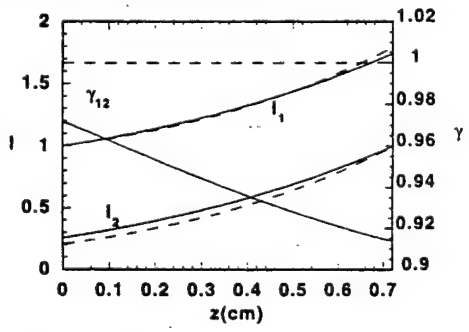

Fig. 4. Signal intensity, pump intensity, and the normalized mutual coherence as a function of position z in the photorefractive medium for partially coherent waves (solid curves) and monochromatic waves (dashed curves).

monochromatic waves when the optical path difference of the two waves is small compared with the coherence length of the source laser wave. The effect of partial coherence of the two waves in this case is significant only for a large optical path difference of the two waves. We show the signal-intensity gain in Fig. 5(a) and the mutual coherence between the signal wave and the pump wave at the pump-wave entrance plane ($z = L$) in Fig. 5(b) both as functions of the optical path difference between the two waves at the signal-wave entrance plane ($z = 0$) for various intensity ratios β. Figure 5(a) shows that the signal-intensity gain decreases as the optical path difference of the two waves increases until there is no coupling between the two waves when the optical path difference of the two waves exceeds the coherent length of the source laser wave. The same figure also shows that the signal-intensity gain increases as the intensity ratio β decreases until the signal-intensity gain saturates as the nondepleted-pump regime is reached. Figure 5(b) shows that the normalized mutual coherence of the two waves at the pump-wave entrance plane ($z = L$) decreases as the intensity ratio β of the two waves increases. When β is much larger than one, the signal wave will pass through the photorefractive medium with its statistical properties almost unchanged by coupling. In this limit the normalized mutual coherence of the two waves at the pump-wave entrance plane ($z = L$) with coupling will be the same as that for an arbitrary β but without coupling. We note that the normalized mutual coherence of the two waves at the pump-wave entrance plane ($z = L$) is enhanced by coupling. Figure 5(b) also shows that the normalized mutual coherence decreases quickly as the optical path difference gets close to and larger than the coherence length of the source laser wave.

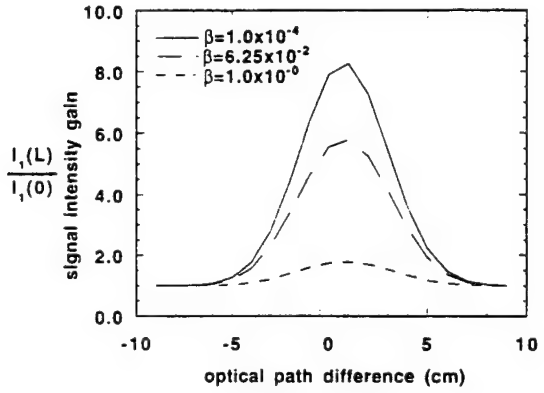

Fig. 5. (a) Signal-intensity gain and (b) the normalized mutual coherence of the two waves at the pump-wave entrance plane ($z = L$) as functions of the optical path difference at the signal-wave entrance plane ($z = 0$) for a coupling constant $\gamma = 3\ \mathrm{cm}^{-1}$ and various intensity ratios between the signal wave and the pump wave. Note that the curve for a coupling constant $\gamma = 3\ \mathrm{cm}^{-1}$ and $\beta \gg 1$ is the same as that for a coupling constant $\gamma = 0\ \mathrm{cm}^{-1}$ and an arbitrary β.

Second, we consider the case that the coherence length of the source laser wave is shorter than the thickness of the photorefractive medium. The following parameters are chosen in the simulation: $\alpha = 0.0\ \mathrm{cm}^{-1}$, $n = 2.3$, $L = 2.0$ cm, $\delta\omega = 2\pi \times 18$ GHz, and $t_d = -nL/c$. $t_d = -nL/c$ implies that the optical path difference between the signal wave and the pump wave is zero at the signal-wave entrance plane ($z = 0$). Since the spectral line shape of the source laser wave is assumed to be Gaussian, the coherence length of the source laser wave inside the photorefractive medium is $L_c = 2\pi \times 0.664c/(n\,\delta\omega) = 0.48$ cm. In Fig. 6 we show the signal intensity $I_1(z)$ and the grating profile $\mathbf{Q}(z)/I_0(z)$ as functions of the position z inside the photorefractive medium for an incident intensity ratio $\beta = 1$ and a coupling constant $\gamma = 20\ \mathrm{cm}^{-1}$. We note that the length of the photorefractive grating is limited by the partial coherence of the two interacting waves and that the pump depletion is moderate even for a very large coupling constant. In Figs. 7(a) and 7(b) we show the signal intensity $I_1(z)$ and the grating profile $\mathbf{Q}(z)/I_0(z)$ as functions of the position z inside the photorefractive medium for an incident intensity ratio $\beta = 10^{-4}$ and coupling constants $\gamma = 10\ \mathrm{cm}^{-1}$ and $\gamma = 20\ \mathrm{cm}^{-1}$, respectively. We note that the length of the photorefractive grating is increased but still primarily limited by the partial coherence of the two interacting waves for a small incident intensity ratio and a small coupling constant. Figure 7(b) shows that the length of the photorefractive grating is no longer limited by the partial coherence of the two interacting waves for a small incident intensity ratio and a large coupling constant. The length of the photorefractive grating in this case is limited by the length of the photorefractive medium, which is much longer than the coherence length of the interacting waves. The photorefractive grating is a temporally stationary index grating. When the incident intensity ratio is small, the amplified signal wave at its exit plane ($z = L$) is primarily the incident pump wave reflected by the photorefractive grating, and the depleted pump wave at its exit plane ($z = 0$) is primarily the incident pump wave transmitted through the photorefractive grating. When the length of the photorefractive grating is comparable to or longer than the coherence length of the source laser wave inside the photorefractive medium, the output waves $\mathbf{E}_1(L)$ and $\mathbf{E}_2(0)$ may have spectra different from those of the input waves $\mathbf{E}_1(0)$ and $\mathbf{E}_2(L)$ owing to the presence of the photorefractive grating, which acts as a spectral filter. In Figs. 8(a) and 8(b) we show the normalized spectra of the amplified signal wave and the depleted pump wave at their respective exit planes, using the same sets of parameters as those used to obtain Figs. 7(a) and 7(b), respectively. We note that the amplified signal wave has a bandwidth narrower than that of the

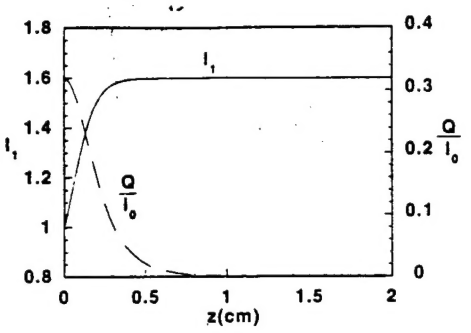

Fig. 6. Signal intensity $I_1(z)$ (solid curve) and the grating profile $Q(z)/I_0(z)$ (dashed curve) as functions of the position z inside the photorefractive medium for an incident intensity ratio $\beta = 1$ and a coupling constant $\gamma = 20\ \text{cm}^{-1}$.

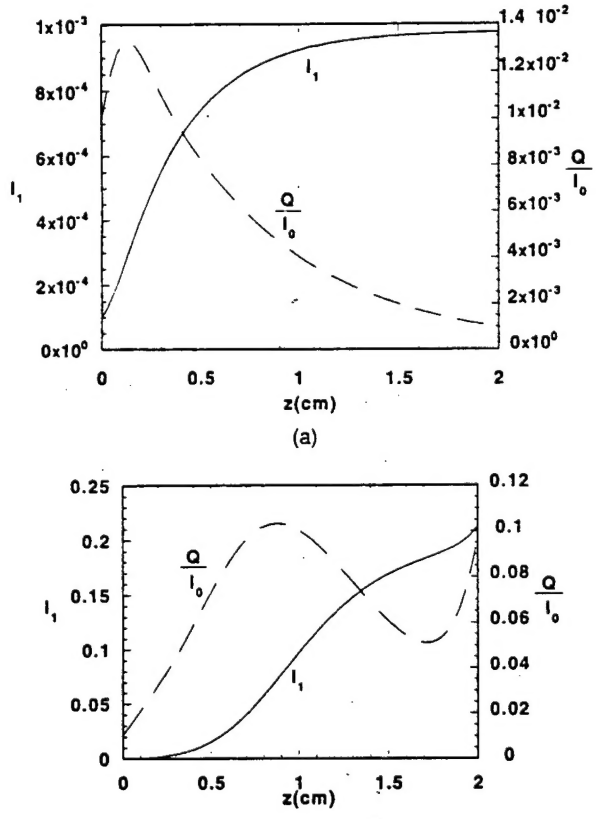

Fig. 7. Signal intensity $I_1(z)$ (solid curve) and the grating profile $Q(z)/I_0(z)$ (dashed curve) as functions of the position z inside the photorefractive medium for an incident intensity ratio $\beta = 10^{-4}$ and coupling constants (a) $\gamma = 10\ \text{cm}^{-1}$ and (b) $\gamma = 20\ \text{cm}^{-1}$.

incident pump wave. Furthermore, the bandwidth of the amplified signal wave decreases as the length of the photorefractive grating increases. In Fig. 8(a), since the coupling constant is small, the pump-wave depletion is small ($\gamma = 10\ \text{cm}^{-1}$) and the spectrum of the transmitted pump wave is almost the same as that of the incident pump wave. In Fig. 8(b), since the coupling constant is large ($\gamma = 20\ \text{cm}^{-1}$), the pump depletion is significant. The central part of the incident pump-wave spectrum is depleted most significantly, and therefore the transmitted pump wave has a different spectrum from the incident pump wave. According to the spectra shown in Fig. 8, the case considered in Fig. 7(a) and Fig. 8(a) is in the nondepleted-pump regime, and the case considered in Fig. 7(b) and Fig. 8(b) is in the depleted-pump regime, although both cases seem to be in the nondepleted-pump regime when we look only at the signal intensity. In Figs. 9(a) and 9(b) we show with solid curves the normalized mutual coherence of the two waves as a function of position z, again using the same sets of parameters as those used to obtain Figs. 7(a) and 7(b), respectively. For comparison we show in these two figures with dashed curves the normalized mutual coherence of the two waves as a function of position z without coupling. In Fig. 9(a) the normalized mutual coherence of the two waves is the same with coupling as that without coupling in the region $z < 0$ and is increased in the region $z > L$ owing to coupling; in Fig. 9(b) the normalized mutual coherence of the two waves is decreased in the region close to plane $z = 0$. The increase of mutual coherence in both Figs. 9(a) and 9(b) can be attributed to the reflection of the strong pump wave in the direction of the weak signal wave by the stationary photorefractive index grating. The decrease of mutual coherence in Fig. 9(b) can be attributed to the spectral-filtering effect of the photorefractive index grating on the pump wave. There is no decrease of mutual coherence in the region close to plane $z = 0$ in Fig. 9(a) because pump depletion and therefore the spectral-filtering effect on the pump wave are negligible in this case.

Third, when a laser beam enters a photorefractive crystal, scattering occurs because of surface pits, imperfec-

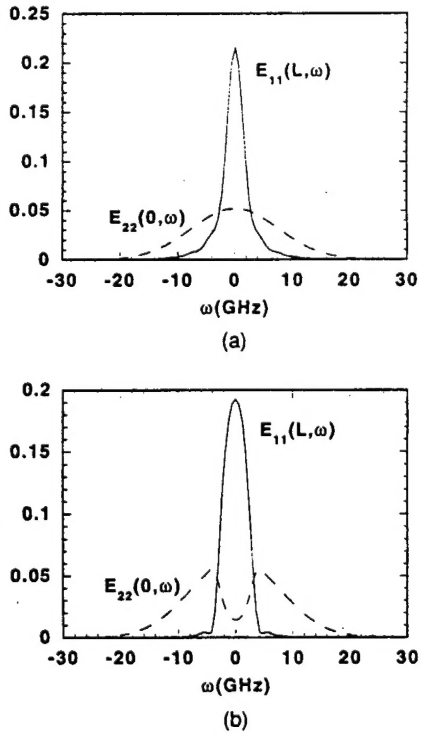

Fig. 8. Normalized spectra of the amplified signal wave (solid curve) and the depleted pump wave (dashed curve) at their respective exit planes for an incident intensity ratio $\beta = 10^{-4}$ and coupling constants (a) $\gamma = 10\ \text{cm}^{-1}$ and (b) $\gamma = 20\ \text{cm}^{-1}$.

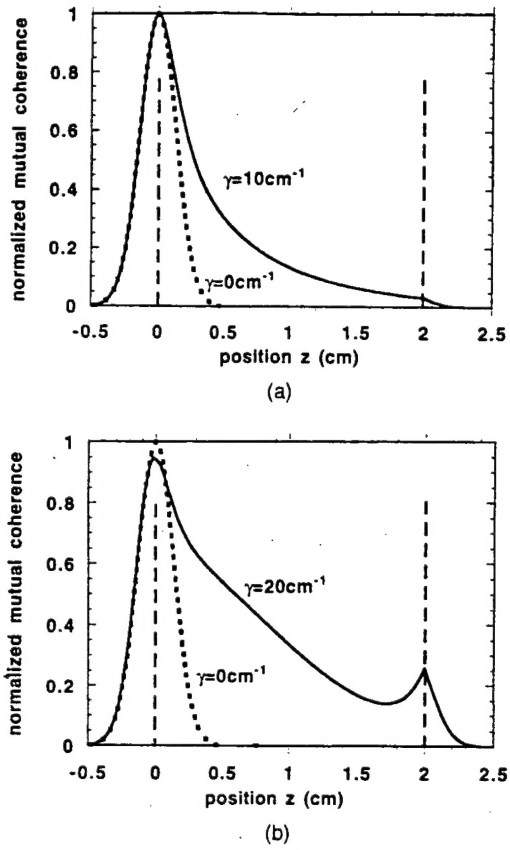

Fig. 9. Normalized mutual coherence of the two waves as functions of position z for an incident intensity ratio $\beta = 10^{-4}$ and for coupling constants (a) $\gamma = 10\ \mathrm{cm}^{-1}$ (solid curve) and $\gamma = 0\ \mathrm{cm}^{-1}$ (dashed curve) and (b) $\gamma = 20\ \mathrm{cm}^{-1}$ (solid curve) and $\gamma = 0\ \mathrm{cm}^{-1}$ (dashed curve).

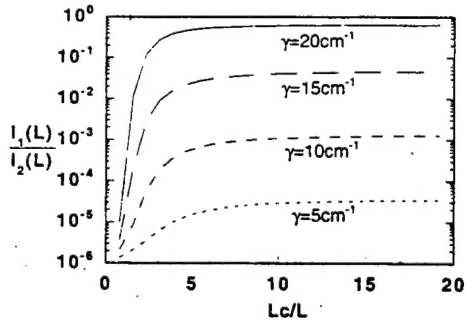

Fig. 10. Phase-conjugation reflectivity as a function of the coherence length of the incident beam for various value of the coupling constant γ.

tion, and defects in the crystal. The scattered light overlaps with the incident beam and they undergo two-wave mixing. Under the appropriate condition the scattered light can be amplified, leading to phenomena such as fanning and stimulated backscattering. In a manner very similar to stimulated Brillouin scattering the stimulated backward scattering in photorefractive media is a possible mechanism for self-pumped phase conjugation.[14,15] The general formulation developed in this paper can be employed to investigate the effect of coherence on self-pumped phase conjugation by 2**k** gratings. We show in Fig. 10 the phase-conjugation reflectivity as a function of the coherence length of the incident beams for various value of the coupling constant γ. The parameters in this simulation are $n = 2.3$, $L = 0.72$ cm, $\alpha = 0.0\ \mathrm{cm}^{-1}$, and $\beta = 1.0 \times 10^{-6}$. The time delay of the two waves is assumed to be zero at the signal-wave entrance plane ($z = 0$). The coherence length of the incident beams is related to the bandwidth as $L_c = 2\pi \times 0.664c/\delta\omega$. We note that the phase-conjugation reflectivity increases as the coherence length of the incident beam increases and reaches to a constant when the coherence length of the incident beam is much longer than the thickness of the photorefractive medium. We also note that the phase-conjugation reflectivity increases as the coupling constant increases.

4. EXPERIMENTS

The above theory is validated experimentally. The experimental setup is shown in Fig. 11. We utilized a 45°-cut $KNbO_3$:Co crystal (the c axis is in the horizontal plane leaning toward the $z = 0$ face of the crystal, and the b axis is in the vertical direction). The measured parameters of the crystal are $\gamma = 3.3\ \mathrm{cm}^{-1}$, $\alpha = 0.5\ \mathrm{cm}^{-1}$, $n = 2.3$, and $L = 0.72$ cm. A multimode argon laser operating at 514 nm is used as the laser source with a measured FWHM bandwidth of 1.83 GHz. The extraordinary polarization of the laser wave is used in the experiment. As illustrated in Fig. 11, the signal wave and the pump wave, obtained by splitting the argon laser wave, propagate contradirectionally into the $KNbO_3$:Co crystal. The incident intensity ratio of the two waves is $\beta = 0.00151$. The power of the pump wave is maintained at ~50 mW. The optical path difference of the two waves at the signal-wave incident plane $z = 0$ is denoted as $\Delta L = L_2 - L_1$. To monitor the mutual coherence between the signal wave and the pump wave at the output plane $z = L$, we employed another reference wave ($\mathbf{E}_{2\mathrm{ref}}$) that was split from the pump wave $\mathbf{E}_2$. The optical path difference of $\mathbf{E}_1$ and $\mathbf{E}_{2\mathrm{ref}}$ waves was adjusted to be the same as that of $\mathbf{E}_1$ and $\mathbf{E}_2$ waves at the output plane $z = L$. By a simple homodyne technique, the in-

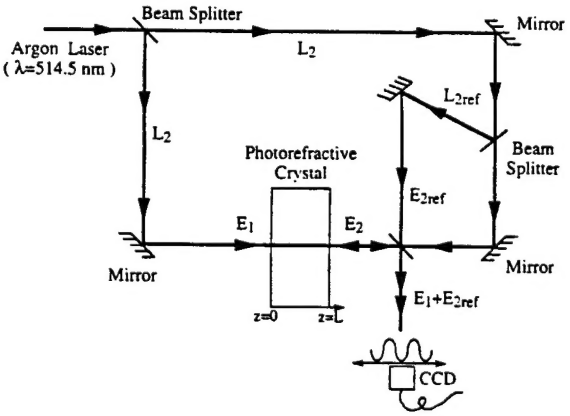

Fig. 11. Experimental setup. The distances L_1 and L_2 are the optical path length of the signal wave and the pump wave from laser source to the signal-wave incident plane $z = 0$, respectively. $L_{2\mathrm{ref}}$ is the optical path length of reference wave $E_{2\mathrm{ref}}$ from the laser source to the signal output plane $z = L$.

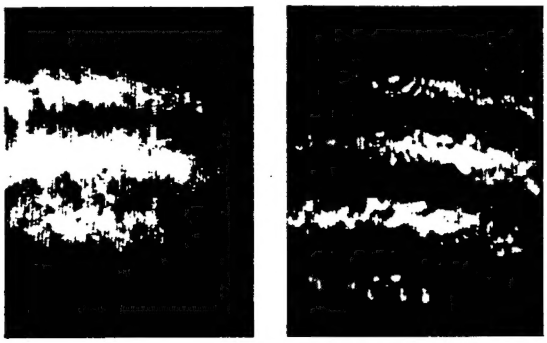

Fig. 12. Interference pattern of the signal wave and the reference wave at the output plane P1 (a) without photorefractive coupling and (b) with photorefractive coupling. Note the increase of fringe visibility that is due to the coupling.

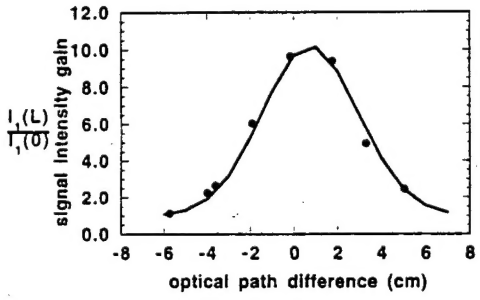

Fig. 13. Signal-intensity gain as a function of the optical path difference of the two waves at the signal-wave entrance plane ($z = 0$). The dots are experimental data, and the solid curve is the theoretical data.

terference fringes generated by $\mathbf{E}_1$ and $\mathbf{E}_{2\text{ref}}$ waves were observed by a CCD camera at the output plane $P1$. The normalized mutual coherence $\gamma_{12}(L)$ can be estimated as $(I_{\max} - I_{\min})/[4(I_1 I_2)^{1/2}]$, where $(I_{\max} - I_{\min})$ is the amplitude of the fringes. In our experiment we monitored the interference pattern with and without pump beam $\mathbf{E}_2$. Figure 12 shows the interference patterns with a normalized mutual coherence $\Gamma_{12}(0, 0) \approx 0.43$ at $z = 0$ ($\Delta L = 4$ cm). The measured normalized mutual coherence increases from 0.19 to 0.7 at $z = L$. The intensity gain of the signal wave was also measured. Figure 13 shows the measurement of the intensity gain (dots) of the signal wave at the $z = L$ plane as a function of the optical path difference ΔL. Along with the data is the theoretical curve for the same parameters. An excellent agreement between theory and experiment was achieved.

5. CONCLUSIONS

In conclusion, we have investigated theoretically contradirectional two-wave mixing with partially coherent waves in photorefractive crystals. A general formulation based on the theory of statistical properties of linear systems is provided.[16] Previous results on several simplified cases are rederived as special cases of the general formulation so that we can get more insight into the general formulation as well as into the simplified cases. Results of numerical implementation of the general formulation are also provided for various coupling constants and various incident intensity ratios between the signal wave and the pump wave. We found that the mutual coherence between the signal wave and the pump wave can be both increased and decreased owing to coupling. We also found that both the strength and the length of the photorefractive-index grating increases as the coupling constant increases. A photorefractive index grating much longer than the coherence length of the incident waves can be formed when the coupling constant is large and the incident intensity ratio is small. Owing to the spectral-filtering effect of the photorefractive-index grating, the spectra of the two interacting waves will be altered as they pass through the photorefractive medium. The general formulation is further used to model the effect of partial coherence on self-pumped phase conjugation by a **2k** grating. The theoretical predictions are in excellent agreement with experimental measurements.

APPENDIX A: ERGODICITY PROPERTY

In this appendix we provide the derivation of Eq. (10). Equation (9) gives the dynamics of the photorefractive index grating. It can be rewritten into an integration form as

$$\mathbf{Q}(z, t) = \frac{1}{\tau_{\text{ph}}} \int_{-\infty}^{t} \mathbf{E}_1(z, t')\mathbf{E}_2^*(z, t') \exp\left(\frac{t' - t}{\tau_{\text{ph}}}\right) dt'. \tag{A1}$$

Note that $1/\tau_{\text{ph}} \int_{-\infty}^{t} \exp[(t' - t)/\tau_{\text{ph}}]dt' = 1$. According to Eq. (A1), the grating amplitude $\mathbf{Q}(z, t)$ is approximately the average value of $\mathbf{E}_1(z, t')\mathbf{E}_2^*(z, t')$ over a time period τ_{ph}.

Since the optical wave amplitudes $\mathbf{E}_1(z, t)$ and $\mathbf{E}_2(z, t)$ are stationary random processes, the ensemble average $\langle \mathbf{E}_1(z, t)\mathbf{E}_2^*(z, t) \rangle$ is independent of the time variable t. Taking the ensemble average of Eq. (A1), we can obtain

$$\langle \mathbf{Q}(z, t) \rangle = \langle \mathbf{E}_1(z, t)\mathbf{E}_2^*(z, t) \rangle \equiv \Gamma_{12}(z, 0). \tag{A2}$$

Equation (A2) shows that the ensemble average of the grating amplitude $\mathbf{Q}(z, t)$ is equal to the mutual coherence of the two waves.

In general, the grating amplitude $\mathbf{Q}(z, t)$ is also a random variable. It fluctuates around its ensemble average. The mean square value of this random fluctuation, also called the variance of the random variable $\mathbf{Q}(z, t)$, can be written as

$$\langle |\mathbf{Q}(z, t) - \langle \mathbf{Q}(z, t) \rangle|^2 \rangle = \langle |\mathbf{Q}(z, t)|^2 \rangle - |\langle \mathbf{Q}(z, t) \rangle|^2. \tag{A3}$$

By using Eq. (A1), we can write the first term on the right side of Eq. (A3) explicitly as

$$\langle |\mathbf{Q}(z, t)|^2 \rangle = \frac{1}{\tau_{\text{ph}}^2} \int_{-\infty}^{t} \int_{-\infty}^{t} \langle \mathbf{F}(z, t')\mathbf{F}^*(z, t'') \rangle \times \exp\left(\frac{t' - t}{\tau_{\text{ph}}}\right) \exp\left(\frac{t'' - t}{\tau_{\text{ph}}}\right) dt' dt'', \tag{A4}$$

where $\mathbf{F}(z, t) \equiv \mathbf{E}_1(z, t)\mathbf{E}_2^*(z, t)$ is a shorthand notation. Since the optical wave amplitudes $\mathbf{E}_1(z, t)$ and $\mathbf{E}_2(z, t)$ are stationary random processes, $\mathbf{F}(z, t)$ is also a stationary random process. Therefore the ensemble average $\langle \mathbf{F}(z, t')\mathbf{F}^*(z, t'')\rangle$ is a function of only two variables z and $t' - t''$. We define $\mathbf{R}(z, t' - t'') \equiv \langle \mathbf{F}(z, t')\mathbf{F}^*(z, t'')\rangle$ as a shorthand notation. With this relation we can change the integration arguments in Eq. (A4) from t' and t'' to $t_1 = t' + t'' - 2t$ and $t_2 = t' - t''$ and rewrite Eq. (A4) as

$$\langle |\mathbf{Q}(z, t)|^2\rangle = \frac{1}{2\tau_{ph}^2}\int_{-\infty}^{0} dt_1 \exp\left(\frac{t_1}{\tau_{ph}}\right)\int_{t_1}^{-t_1} dt_2 \mathbf{R}(z, t_2). \tag{A5}$$

Note that $1/(2\tau_{ph}^2)\int_{-\infty}^{0} dt_1 \exp(t_1/\tau_{ph})\int_{t_1}^{-t_1} dt_2 = 1$. Substituting Eqs. (A2) and (A5) into Eq. (A3), we can rewrite the variance of the grating amplitude $\mathbf{Q}(z, t)$ as

$$\langle |\mathbf{Q}(z, t) - \langle \mathbf{Q}(z, t)\rangle|^2\rangle = \frac{1}{2\tau_{ph}^2}\int_{-\infty}^{0} dt_1 \exp\left(\frac{t_1}{\tau_{ph}}\right)\int_{t_1}^{-t_1} dt_2 [\mathbf{R}(z, t_2) - |\Gamma_{12}(z, 0)|^2]. \tag{A6}$$

Remember that $\mathbf{F}(z, t)$ is a stationary random process. Let Δt be the minimum time delay that is necessary for $\mathbf{F}(z, t)$ and $\mathbf{F}(z, t \pm \Delta t)$ to be uncorrelated. For $|t_2| \geq \Delta t$, $\mathbf{R}(z, t_2) - |\Gamma_{12}(z, 0)|^2$ is equal to zero. For $|t_2| \leq \Delta t$, $\mathbf{R}(z, t_2) - |\Gamma_{12}(z, 0)|^2$ is a function of t_2. Since both $\mathbf{R}(z, t_2)$ and $|\Gamma_{12}(z, 0)|^2$ are of the order of $I_1(z)I_2(z)$, the upper bound of $\mathbf{R}(z, t_2) - |\Gamma_{12}(z, 0)|^2$ can be written as $mI_1(z)I_2(z)$, where m is a constant factor of the order of unity. With these estimations we can obtain from Eq. (A6)

$$\langle |\mathbf{Q}(z, t) - \langle \mathbf{Q}(z, t)\rangle|^2\rangle < mI_1(z)I_2(z)\frac{\Delta t}{\tau_{ph}}. \tag{A7}$$

According to relation (A7), the fluctuation of the grating amplitude $\mathbf{Q}(z, t)$ decreases as the ratio $\Delta t/\tau_{ph}$ decreases. When $\Delta t/\tau_{ph} \ll 1$, we can neglect the fluctuation of the grating amplitude $\mathbf{Q}(z, t)$ and obtain Eq. (10), i.e.,

$$\mathbf{Q}(z, t) \approx \langle \mathbf{Q}(z, t)\rangle = \Gamma_{12}(z, 0). \tag{A8}$$

Usually Δt is of the order of the coherence time $(\delta\omega)^{-1}$ of the incident waves. In this case the condition for Eq. (A8) can also be written as $\delta\omega\tau_{ph} \gg 1$.

In this appendix we have shown that the time average of the random variable $\mathbf{E}_1(z, t)\mathbf{E}_2^*(z, t)$ is equal to the ensemble average of the random variable $\mathbf{E}_1(z, t)\mathbf{E}_2^*(z, t)$. This type of property is referred to as ergodicity in statistics.

ACKNOWLEDGMENTS

This research was supported by the U.S. Office of Naval Research and the U.S. Air Force Office of Scientific Research.

REFERENCES

1. See, for example, P. Yeh, *Introduction to Photorefractive Nonlinear Optics* (Wiley, New York, 1993).
2. See, for example, P. Gunter and J.-P. Huignard, eds., *Photorefractive Materials and Devices I and II*, Vols. 61 and 62 of Topics in Applied Physics (Springer-Verlag, Berlin, 1988, 1989).
3. B. Fischer, S. Sternklar, and S. Weiss, "Photorefractive oscillators," IEEE J. Quantum Electron. **25**, 550 (1989).
4. V. Wang, "Nonlinear optical phase conjugation for laser systems," Opt. Eng. **17**, 267 (1978).
5. S. C. De La Cruz, S. MacCormack, J. Feinberg, Q. B. He, H. K. Liu, and P. Yeh, "Effect of beam coherence on mutually pump phase conjugators," J. Opt. Soc. Am. B **12**, 1363 (1995).
6. Q. B. He and P. Yeh, "Photorefractive mutually pumped phase conjugation with partially coherent beams," Appl. Phys. B **60**, 47 (1995).
7. R. Hofmeister, A. Yariv, and S. Yagi, "Spectral response of fixed photorefractive grating interference filters," J. Opt. Soc. Am. A **11**, 1342 (1994).
8. N. V. Bogodaev, L. I. Ivleva, A. S. Korshunov, N. M. Polozkov, and V. V. Shkunov, "Increase of light-beam coherence by two-wave mixing in photorefractive crystals," J. Opt. Soc. Am. B **10**, 2287 (1993).
9. X. Yi, S. H. Lin, P. Yeh, and K. Y. Hsu, "Contradirectional two-wave mixing with partially coherent waves in photorefractive crystals," Opt. Lett. **21**, 1123 (1996).
10. See, for example, J. W. Goodman, *Statistical Optics* (Wiley, New York, 1985), Chap. 3.
11. P. Yeh, "Fundamental limit of the speed of photorefractive effect and its impact on device applications and material research," Appl. Opt. **26**, 602 (1987).
12. R. Saxena, F. Vachss, I. McMichael, and P. Yeh, "Diffraction properties of multiple-beam photorefractive gratings," J. Opt. Soc. Am. B **7**, 1210 (1990).
13. R. Saxena, C. Gu, and P. Yeh, "Properties of photorefractive gratings with complex coupling constants," J. Opt. Soc. Am. B **8**, 1047 (1991).
14. T. Y. Chang and R. W. Hellwarth, "Optical phase conjugation by backscattering in barium titanate," Opt. Lett. **10**, 108 (1985).
15. B. Ya. Zel'dovich, V. I. Popovichev, V. V. Ragul'skii, and F. S. Faizullov, "Connection between the wavefronts of the reflected and exciting light in SBS," Zh. Éksp. Teor. Fiz. **15**, 160 (1972).
16. A. W. Snyder, D. J. Mitchell, and Y. S. Kivshar, "Unification of linear and nonlinear wave optics," Mod. Phys. Lett. B **9**, 1479 (1995).